GEOLOGIC EVALUATION OF RADAR IMAGERY FROM DARIEN PROVINCE, PANAMA

by

Harold C. MacDonald

CRES Technical Report No. 133-6

Sponsored by
ADVANCED RESEARCH PROJECTS AGENCY, DEPARTMENT OF DEFENSE
Work Order No. 1079

Monitored for Advanced Research Projects Agency
by
U.S. ARMY ENGINEER TOPOGRAPHIC LABORATORIES
GEOGRAPHIC INFORMATION SYSTEMS BRANCH
GEOGRAPHIC SYSTEM DIVISION
FT. BELVOIR, VIRGINIA

Contract No. DAAK02-68-C-0089
and NASA Contract No. NAS 9-7175

CRES
THE UNIVERSITY OF KANSAS • CENTER FOR RESEARCH INC
ENGINEERING SCIENCE DIVISION • LAWRENCE, KANSAS

NASA CR 101971

AD _____

GEOLOGIC EVALUATION OF RADAR IMAGERY FROM DARIEN PROVINCE, PANAMA

by

Harold C. MacDonald

CRES Technical Report No. 133-6

Sponsored by
Advanced Research Projects Agency, Department of Defense
Work Order No. 1079

Monitored for Advanced Research Projects Agency
by
U. S. Army Engineer Topographic Laboratories
Geographic Information Systems Branch
Geographic System Division
Ft. Belvoir, Virginia

Contract No. DAAK02-68-C-0089
and NASA Contract No. NAS 9-7175

GEOLOGIC EVALUATION OF RADAR IMAGERY FROM DARIEN PROVINCE, PANAMA

ABSTRACT

The availability of extensive radar imagery covering approximately 17,000 sq. km. in eastern Panama and northwestern Colombia has provided geologic data for an area where previous geological investigations have been extremely limited because of inaccessibility and perpetual cloud cover. In previous radar-related geologic studies, most of the radar imagery was collected from areas within the continental United States where temperate climatic conditions prevail and where detailed geologic information was available. The radar imagery of eastern Panama, however, represents not only unique terrain information from the tropical environment, but the first practical mapping application of side-looking radar systems.

The primary objectives of this study were to 1) determine the utility of radar in the compilation of geological reconnaissance maps, 2) define and analyze radar-linears (joint systems and faults) and infer the nature of the tectonic forces responsible for certain types of local structures, 3) examine the effect of radar look-direction (direction orthogonal to ground track of the aircraft) and determine if there is a factor of directional dependency with radar systems, and 4) evaluate the potential of radar as a single geological reconnaissance tool in the tropical environment and what application these imaging systems may possess for future geological reconnaissance surveys in similar geographic areas.

As in aerial photographic interpretation, the analysis of tone, texture, shape, and pattern are recognition elements on radar imagery which contribute to the interpretation of geologic data. These recognition elements, as well as the distortions inherent to radar imagery are evaluated in this study.

ACKNOWLEDGEMENTS

This study was in large[illegible]nsored under Project THEMIS, funded by the Advanced Research Project Agency, Contract No. DAAK02-68-C-0089. The contract was monitored by U. S. Army Engineer Topographic Laboratories, Geographic Information Systems Branch, Geographic System Division, Ft. Belvoir, Virginia. NASA Contract No. NAS 9-7175 provided both funding and imagery for the initial phases of this study. The facilities and personnel of the Center for Research in Engineering Science, Remote Sensing Laboratory at the University of Kansas under the direction of Professors R. K. Moore, D. S. Simonett, and R. D. Ellermeier were an inestimable asset to this investigation. The logistical field support by U. S. Army Engineer Topographic Laboratory (USAETL), and the Inter-American Geodetic Survey, through the direct supervision of Col. Alexander Pearson, provided an indispensable phase of this study.

Special recognition is given to Professor Louis F. Dellwig, my advisor, whose impetus and ardent interest were responsible for securing the experimental data, and without his support and guidance the completion of this study would not have been possible.

The competence of the Remote Sensing Laboratory personnel were vital to this investigation; especially, Mr. Dwight Egbert whose photographic expertise is reflected in reproduction of illustrations, Mrs. Marilyn Morain whose meticulous drafting proficiency has provided all of the illustrations, and the secretaries Miss Donna Opperman, Mrs. Sharon McGeeney, and Mrs. Chris Jackson who have typed numerous revisions of the manuscript. Special appreciation is expressed to my colleague Mr. Anthony J. Lewis who provided assistance during field work in Panama and throughout all phases of the research connected with this study. I am deeply indebted to my colleague Mr. Richard Wing whose devoted interest and competence in geology have provided many hours of stimulating discussion pertinent to Isthmian geology. Appreciation is extended to D. S. Simonett, Mr. David Schwarz, and Mrs. Edith Oldfather who have critically reviewed the manuscript.

The cooperation and constructive criticism provided by my dissertation committee Professors Bickford, Ellermeier, Gillerman, and Ireland, have been exceedingly important to the revision of this manuscript. I am especially appreciative of my wife and five children, without whose encouragement and forebearance the completion of this research project would have been an impossibility.

TABLE OF CONTENTS

Chapter		Page
ACKNOWLEDGEMENTS		i
1. INTRODUCTION		
2. BACKGROUND		4
	2.1 Location	5
	2.2 Climate	9
	2.3 Field Reconnaissance	9
	2.4 History of Radar Geology	10
3. RADAR OPERATION		13
	3.1 Basic Case, Ground to Air	13
	3.2 Complex Case, Terrain-Signal Interaction	19
	3.3 Resolution and Detectability	23
	3.4 Radar Geometry	27
	3.5 Radar Shadow	34
	3.6 Radar Topographic Mapping	36
	3.7 Radar Mosaic	40
4. RADAR IMAGERY INTERPRETATION		43
	4.1 Tone	44
	4.2 Texture	45
	4.3 Shape	47
	4.4 Pattern	52
	4.5 Lithologic Interpretation - Igneous	52
	4.6 Lithologic Interpretation - Sedimentary	54
	4.7 Strike and Dip	55
	4.8 Faults and Joints	60

Analysis of single-strip radar imagery in combination with the radar mosaic have, for the first time, provided an accurate representation of the regional geologic relationships of eastern Panama and northwestern Colombia. A ready subdivision can generally be made between igneous and sedimentary rocks, and large scale structures can be synoptically studied, enabling the geologist to become quickly familiar with the essential features of structural provinces. On a more detailed scale, a relative stratigraphic sequence can be determined if the lithic units are topographically expressed. Where collateral field data have been used in conjunction with radar imagery interpretation, the geologic information interpretable from the radar imagery of eastern Panama far exceeds those data previously available.

At the present time, radar remote sensing offers the only practical technique for geological reconnaissance mapping in the tropical environment; however, to obtain the maximum benefit from such studies in poorly mapped areas it will be necessary to image a specific region from four orthogonal look-directions. Regardless of the inherent limitations of radar geological reconnaissance, the capability of obtaining topographic mapping data simultaneously with geologic information provides the geologist with an important exploration tool.

Chapter		Page
5.	LOOK-DIRECTION ANALYSIS	62
	5.1 Spanish Peaks, Colorado	63
	5.2 Central Humboldt Range, Nevada	65
	5.3 Trinity Range, Nevada and Seaview Area, Washington	66
	5.4 Boston Mountains, Arkansas	68
	5.5 Panama Imagery	69
	5.6 Look-Direction vs. Low Sun-Angle	75
6.	PANAMA STRATIGRAPHY	80
	6.1 Basement Rock Complex	80
	6.2 Sedimentary Strata	81
7.	GEOLOGICAL RECONNAISSANCE MAP INTERPRETATION	83
	7.1 Reconnaissance Mapping	84
	7.2 Igneous Rock Interpretation - Plate I	84
	7.3 Sedimentary Rocks - Plate I	85
	7.4 History of Sedimentation - Regional	92
	7.5 Structure - Background	94
	7.6 Structure - Plate I	96
	7.7 Geologic History - Eastern Panama	102
8.	CONCLUSIONS	104
APPENDIX A		108
BIBLIOGRAPHY		115
PLATE I		End of Report

LIST OF FIGURES

Figure		Page
Figure 2.1	Index map of Panama	6
Figure 2.2	Air photo coverage, Darien Province, Panama . . .	7
Figure 2.3	Radar mosaic, Darien Province, Panama.	8
Figure 3.1	Block diagram, typical airborne radar system . . .	15
Figure 3.2	Sketch diagram, typical side-looking airborne radar system (modified from Westinghouse, 1967) .	17
Figure 3.3	Letter code and frequency-wavelength bands. . . .	18
Figure 3.4	SLAR imaging system. (A) Ground coverage (after Moore and Simonett, 1967). (B) Hypothetical swath width and respective incidence angles for flat terrain from near to far range, (modified from McCoy, 1967). (C) Effect of terrain slopes on incidence angles	21
Figure 3.5	SLAR imaging system resolution. (A) Pulse length and beam width in relation to ground track (after Beatty and others, 1965). (B) Range resolution. (C) Azimuth resolution	26
Figure 3.6	Measurement of slant range and ground range . . .	28
Figure 3.7	Comparison of slant range and ground range. (A) Geometry of slant range and ground range presentation, (after Innes, 1968). (B) Graphical conversion from slant range to ground range for a single radar system (after McCoy, 1967)	30
Figure 3.8	Effect of near-range compression on geometric shape, La Palma Peninsula, Darien Province, Panama (prepared by A. J. Lewis)	31
Figure 3.9	Radar foreshortening. (A) Time measurements from transmitter, (modified from Kirk, et al., 1968). (B) Relationship between angle of incidence and terrain slope. (C) Variations in slant range measurements, (after McCoy, 1967)	33

Figure		Page
Figure 3.10	Radar layover, a function of the slant range to the transmitter	35
Figure 3.11	Shadowing characteristics assocaited with SLAR imaging systems	37
Figure 3.12	Radar topographic mapping. Interferometric model (modified from Levine, et. al., 1966) . . .	39
Figure 3.13	Documentation of errors incorporated in the radar mosaic (prepared by Anthony J. Lewis, CRES).	42
Figure 4.1	Virgin Mountains area, Arizona. (A) Radar imagery. (B) Aerial Photograph. (C) Radar imagery enlargement 2x	46
Figure 4.2	Topographic texture from radar imagery, Darien Province, Panama	48
Figure 4.3	Topographic texture from radar imagery, Darien Province, Panama	49
Figure 4.4	Central Humboldt Range, Nevada. (A) Look-direction, south. (B) Look-direction, north . . .	50
Figure 4.5	Mono Craters, California. (A) Look-direction, east. (B) Look-direction, west. (C) Look-direction, north	51
Figure 4.6	Spanish Peaks, Colorado. (A) Look-direction, north. (B) Look-direction, south	53
Figure 4.7	Viewing the terrain slope, α, from two different look-directions, resulting in two depression angles, Θ , and two slant range lengths, L (from McCoy, 1967).	57

Figure		Page
Figure 4.8	Nomogram based on equation (1) provides an easy solution of slope angle. The dashed vertical line is an example based on Figure 4.7 where $\Theta_1 = 50°$, $\Theta_2 = 50°$, $R_L = 0.38$, $\alpha = 20°$ (from McCoy, 1967)	59
Figure 5.1	Portion of the geologic map of the Spanish Peaks area, Colorado (after Johnson, 1968) . . .	64
Figure 5.2	Trinity Mountains area, Nevada; (A) Look-direction east, (B) Look-direction, south. Seaview area, Washington; (C) Look-direction south, (D) Look-direction, east	67
Figure 5.3	Multiple flight coverage, Boston Mountains, Arkansas, (A) Look-direction, west. (B) Look-direction, north, (C) Look-direction northwest . .	70
Figure 5.4	Illumination of a three-dimensional plaster terrain model from incidence angles of 90 - 20 degrees. (modified from R. J. Hackman, Personal Communication)	77
Figure 7.1	Major mountain ranges of eastern Panama and northwestern Colombia	93

LIST OF TABLES

Table		Page
Table 5.1	Analysis of look-direction, Panama Imagery	73
Table 6.1	Correlation data, Eastern Panama and Canal Zone	82

CHAPTER 1

INTRODUCTION

Geologic reconnaissance techniques, which in previous years were highly dependent upon exploitation of visible spectrum sensors, have recently been augmented by a new family of remote sensors. No longer is the geologist restricted to the analysis of aerial photography for reconnaissance studies, although cameras have by no means been displaced or abandoned. Aerial photography, while it provides both a photograph and valuable data for the compilation of highly accurate maps, is severely limited by light and weather conditions. Thus many regions of the world, especially the tropics, are poorly mapped because adequate photography cannot be obtained. Radar imaging systems provide the capability of obtaining terrain data independent of most weather conditions, and this information may be sufficient to provide a data base for geologic reconnaissance map construction.

Since the fall of 1965, interdisciplinary research on the geoscience value of side-looking radar systems (SLAR) has been conducted by geologists, geographers and electrical engineers at The University of Kansas, Center for Research, Inc., Engineering Science Division (CRES). Airborne systems of the SLAR type are remote sensors which operate in the microwave portion (wavelengths of 1 mm to several meters) of the electromagnetic spectrum. As a potential geological tool, radar has the capability of recording imagery of acceptable resolution, irrespective of most weather conditions and totally independent of daylight conditions. Initial studies have revealed that imaging radars can be a valuable adjunct to other remote sensors and have particular application in mapping and correlating geologic features on a regional scale. To date we have utilized radar imagery in studies which include hydrology, stratigraphy, lineament tectonics, geomorphology, vegetation analysis,and agriculture.

In previous radar studies, certain capabilities and limitations have been defined; however, the need for additional and expanded studies has become evident. Most of the radar imagery used in past and present work at CRES has been collected over areas in the U.S. where temperate climatic conditions prevail and where adequate geologic field data are available. The extension of our experience and knowledge to another climatic environment where geologic data are extremely limited has been made possible through the availability of extensive radar imagery covering 17,000 sq. km. in eastern Panama. This part of Central America serves adequately as an area typical of the tropical, cloudy environments with dense vegetal cover, so characteristic of most seriously underdeveloped countries in equatorial latitudes.

The primary objective of this study was to determine the utility of radar in the compilation of geological reconnaissance maps. That radar is useful in certain terrain studies is known, but the degree of geologic information radar will provide in the tropical terrain environment is as yet unknown. The answer to this question was sought by constructing and evaluating a geological reconnaissance map of Darien Province, a region that is characterized by areas where existing geologic maps have been compiled from such limited field data that they usually fail to delineate anything but gross features. The relatively larger scale (1:172,000) of the imagery, as compared with the smaller scale (1:500,000) of existing geologic maps, should allow the definition of geologic features at a lower level of generalization than has been previously available.

The mapping of photo-linears during the last decade has proven to be a valuable tool in regional and local stress analyses. Fractures or lineaments, which usually represent one of several structural features such as faulting, and joint systems can be expressed on the surface as differences in vegetation vigor, straight segments of streams, topographic alignments, or other features. Through the analysis of such linear features it should be possible to infer the nature of the tectonic forces responsible for certain types of local structures. Similarly, the definition of local tectonic forces should add some insight to the regional tectonic history of the area.

The Darien region has been imaged in such a manner that four orthogonal imaging passes are available for most areas, but in no case are there less than two imaging passes over any particular strip of terrain. This type of comprehensive coverage has provided a unique opportunity for an evaluation of a SLAR imagery that has not been previously available. Multiple-look coverage provides terrain and geologic data that can be systematically evaluated. This part of the study has examined the effect of look-direction on the detection of geologic features under a variety of different terrain conditions to determine if there is a factor of directional dependency with radar imaging systems.

The final objective of this investigation was to determine what potential radar may possess as a single geological reconnaissance tool in the tropical environment, and what applications SLAR systems may have for furture geological reconnaissance surveys in similar geographic areas.

CHAPTER 2

BACKGROUND[1]

Balboa discovered the Pacific Ocean 456 years ago, after a journey across the Darien area of Panama. The possibility of constructing an inter-oceanic canal in Central America was raised almost immediately, and since the 1530's, canal projects have been a matter of more or less serious pre-occupation of the Central America Republics, Colombia, England, France, and the United States (Rubinoff, 1968). Although the French Canal Company was the first to actually attempt construction, it was the United States which completed the project in 1914. Unfortunately, the present canal system is becoming increasingly inadequate because of both the increase in number and size of ships needing access.

The authorization of the Isthmian Canal studies by the 79th Congress initiated reconnaissance studies for a number of possible nuclear excavated, sea-level routes from the Isthmus of Tehuantepec in Mexico to northwestern Colombia. In conjunction with these studies Project RAMP (Radar Mapping in Panama) was undertaken by the U. S. Army Corps of Engineers. The objectives of Project RAMP were (1) to determine the overall feasibility of producing topographic maps from high resolution side-looking radar presentations, (2) to establish concepts and techniques for radar mapping data reduction and compilation, (3) to determine the performance characteristics of state-of-the-art radar equipment in a near operational environment, and (4) to obtain original mapping coverage over a geographic area with a known history of inclement weather.

---

[1] Spanish orthography, including accent marks is used for geographic names in Panama; however in the Canal Zone, many names of Spanish origin are anglicized, and for such names the accent marks are omitted (Woodring, 1957). In this study, because of the dependence on geologic studies within the Canal Zone, names of Spanish origin are anglicized.

Attempts to obtain complete aerial photographic coverage of the Darien area (Figure 2.1) have been notably unsuccessful for several decades because the region is perpetually cloud covered. A map illustrating the photography available for the Darien area (Figure 2.2) shows coverage to be available only on the edges of the study area. To exploit radar's capability to penetrate clouds, the Corps of Engineers successfully collected both data for a topographic map, and imagery of the entire Darien area during six separate days of flight operations. The radar imagery was used to construct an uncontrolled mosaic (Figure 2.3) which although not without error itself, provides a much more accurate configuration of Darien, and reveals numerous errors made by earlier cartographers (Bylinsky, 1968). The multiple imagery coverage obtained for Project RAMP was used for the data base in the present geological evaluation.

2.1 Location

The Republic of Panama is located between 7°9' and 9°34' north latitude and 77°9' and 83°1' west longitude (Figure 2.1). This very narrow, east-west trending land is bounded on the north by the Caribbean Sea and on the south by the Pacific Ocean. The maximum north-south extension of Panama is 272 km; however, the east-west extension measures 624 km, being bounded on the east by Colombia and on the west by Costa Rica. Although the width of Panama above sea level is only 272 km, the arch of the isthmus exceeds 320 km below the 1000 fathom line. Thus the ocean bottom physiography reflects a wide submarine swell flattened at the top by erosion and by the deposition of volcanic and marine material (Schuchert, 1935). Of the total land area of Panama which is approximately 46,400 square kilometers, less than half is permanently inhabited. One-half the country is above the 300 meter contour, but 90 per cent of the population live below it. All of the provincial capitals and also the national capital are below the 100 meter contour (Terry, 1956).

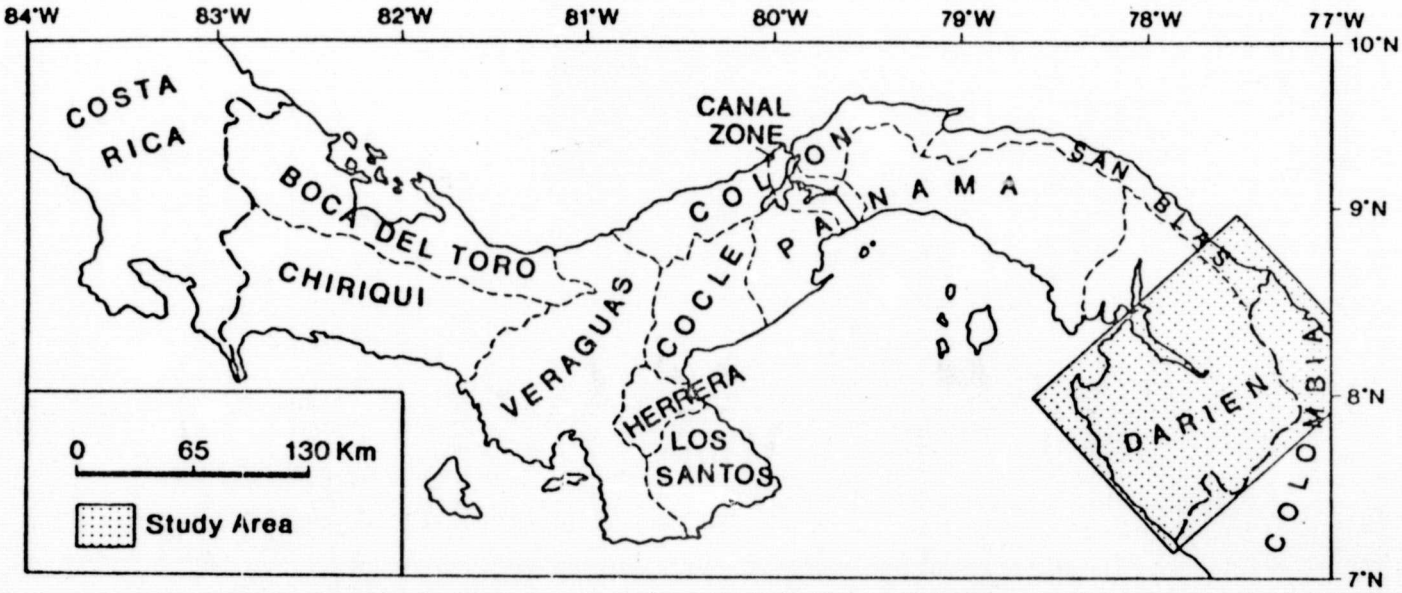

POLITICAL DIVISIONS OF PANAMA

Figure 2.1 Index map of Panama

AIR PHOTO COVERAGE

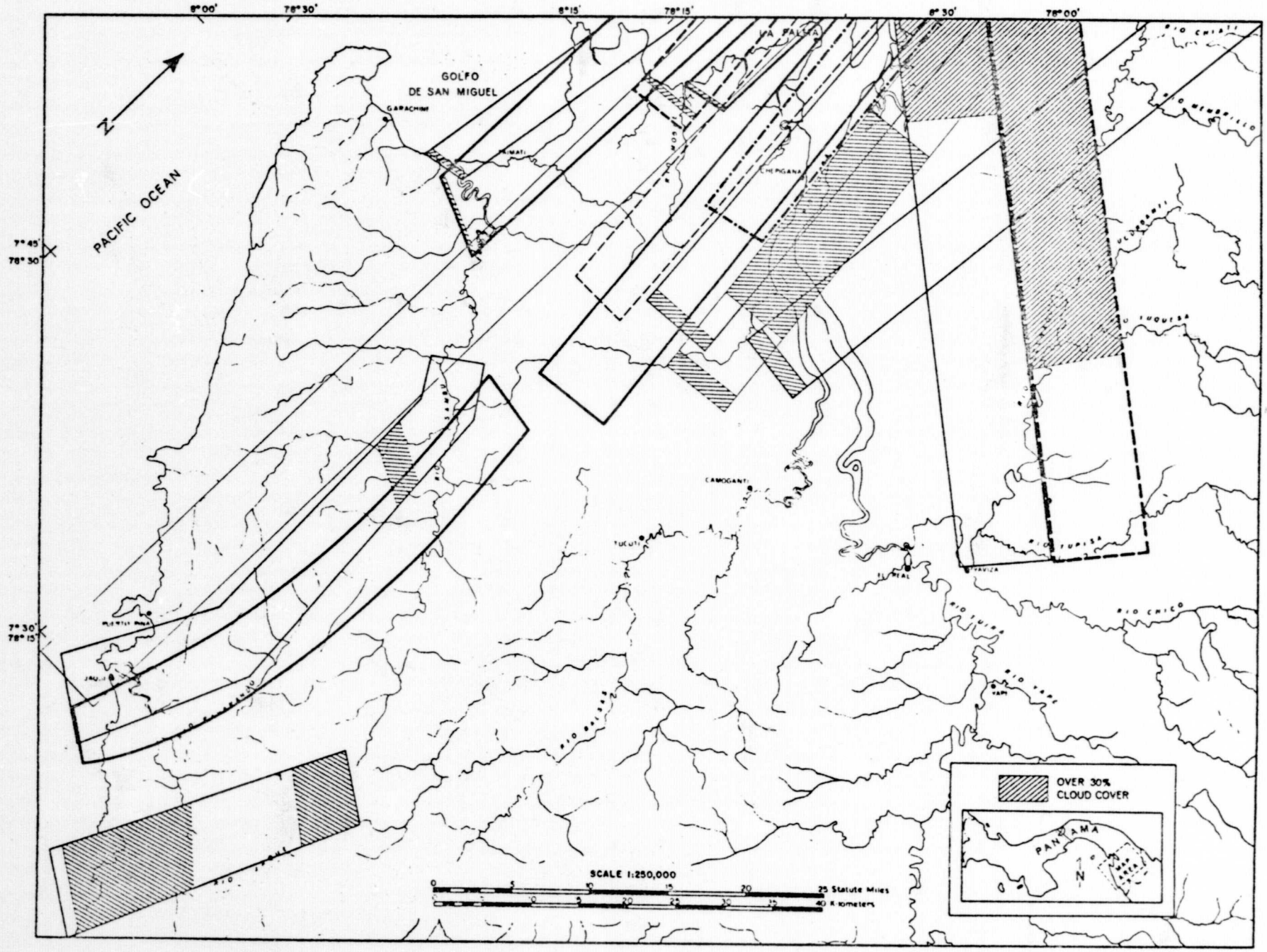

Figure 2.2 Air photo coverage, Darien Province, Panama

RADAR MOSAIC

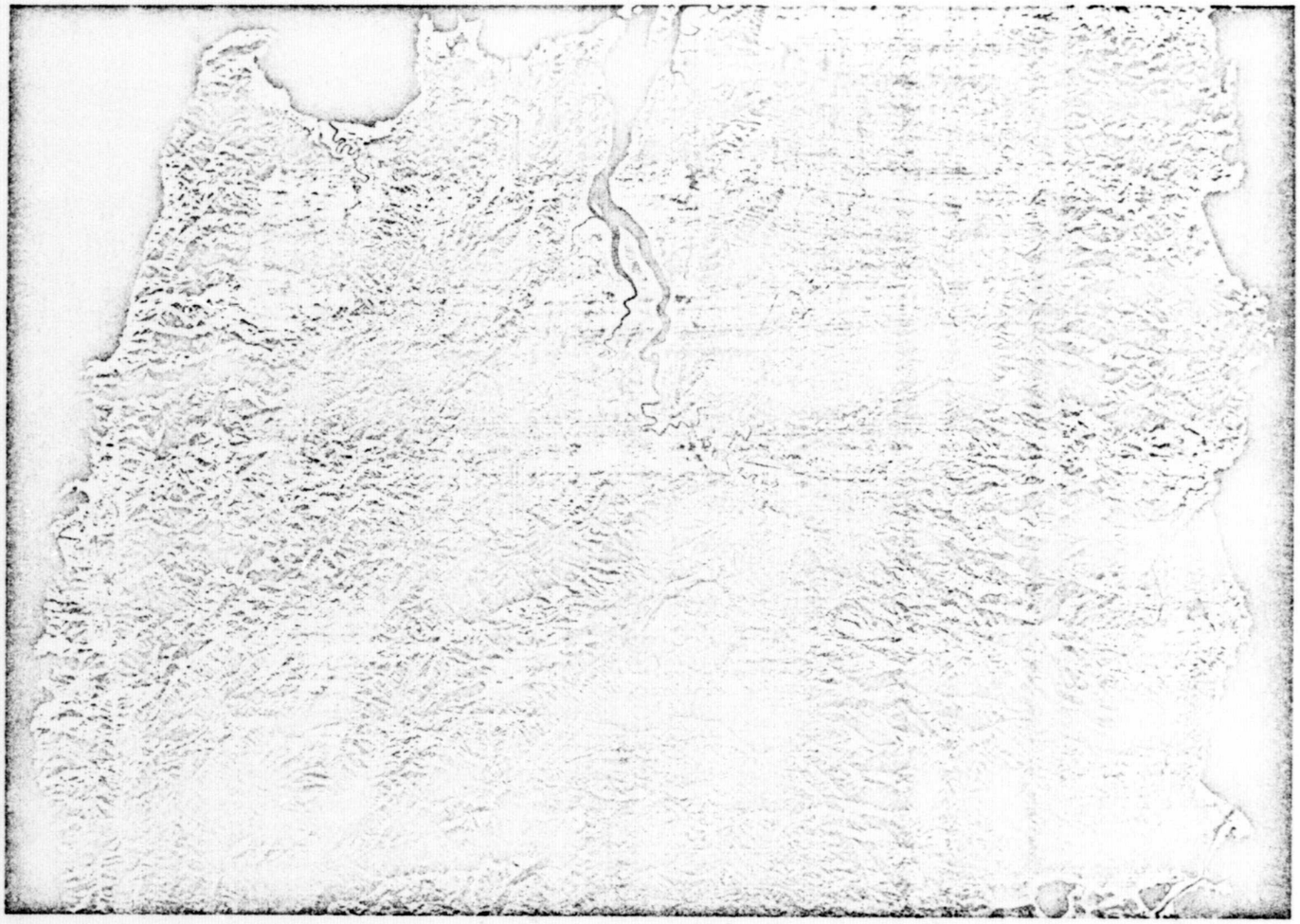

DARIEN PROVINCE, REPUBLIC OF PANAMA
AND
NORTHWEST COLOMBIA

Scale: 1:1,000,000

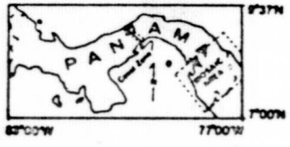

Figure 2.3

2.2 Climate

The climate of the Isthmus of Panama is marked by both a wet (eight months) and a dry (four months) season; however the "dry season" is a misleading term because in some years up to 30 cm of precipitation have been recorded. The Pacific coast of Darien receives more than 400 cm of rainfall each year and has no persistent dry season. La Palma (Plate I, 8° 24'N, 78° 09'W) receives 193 cm of rainfall annually and the village of Garachine (8° 04'N, 78° 22'W) receives slightly less than 169 cm. At sea level within the study area (El Real, 8° 08'N, 77° 44'W) the mean annual temperature is 26 8 degrees Celsius (80.2 degrees Fahrenheit) whereas in the surrounding mountains (Serrania de Pirre), the mean annual temperature is 16.0 degrees Celsius (60.8 degrees Fahrenheit) (Wilson, et al., 1964).

2.3 Field Reconnaissance

During March and April 1968 field reconnaissance (associated with this study) was accomplished through the cooperation of Geographic Sciences Division, U. S. Army Engineer Topographic Laboratory (USAETL). The USAETL personnel were in the Darien area to spot-field check twelve Geographic overlays constructed by the Autometrics Corporation of Alexandria, Virginia. The geologic reconnaissance was planned as follows: prior to departure into the jungle, the overlays were compared with the preliminary geologic map constructed for the present study to determine those areas which would yield the greatest data for the limited time and resources available. Sites were selected on the basis of (1) accessibility from the base camp, (2) compatibility for obtaining both geologic and geographic data, (3) uniqueness of features within a specific area, and (4) conformity of selected sties with other areas.

Aircraft support consisted of a U-1A (Otter) furnished by the Inter-American Geodetic Survey and a UH-1 (Huey) helicopter furnished by the Aviation Section, Headquarters, U. S. Army South. Water transportation was primarily by motor driven piraquas (an Indian canoe) rented from the local natives in the staging area of El Real. Travel through the jungle was

possible only where a trail was chopped through the tangled, dense undergrowth. All support equipment and supplies including drinking water were flown into El Real. The local diet of rice and beans was used to supplement the rations flown in from the Canal Zone. Two interpreters accompanied the party into the field, one from the U. S. Army and one from the Panamanian Instituto Cartigrafico. The Panamanian representative provided liaison with local government officials (National Guard) as well as local Indian groups encountered in the field.

2.4 History of Radar Geology

Prior to World War II the concept of using reflected radio waves for remote target location evolved with the development of radio frequency systems which transmitted from ground to airborne targets, and in some cases from airborne platforms to ground targets. The non-military applications of radar were first reported by Lt. H. P. Smith (1948) when the "ground clutter" that radar engineers had by tradition sought to suppress, appeared to have potential application in terrain studies. When Smith compared radar scope photographs of a PPI (Plan Position Indicator) presentation with existing charts of northwestern Greenland, he noted that the radar photographs contained terrain information exceeding that interpretable from available maps. Recognizing that the intensity of the returned signals from the ground were related to the character and configuration of the terrain, and the resemblance of the standard PPI display to a map, Smith recorded his observations and turned over these data (in the form of a classified report) to the Chart Service, which in turn submitted the information to the U. S. Geological Survey (Scheps, 1963). During World War II radar operation techniques had developed to a high degree; however, the development of radar technology was somewhat decelerated after the War. No appreciable advances in the state-of-the-art were accomplished until the early nineteen fifties, when the development of sophisticated components was required for the tracking of missiles and satellites. During this same period, the evolution of supersonic manned bombers necessitated the development of both complex naviga-

tional radars and precision bombing radars. Since then, radar technology has been continuously refined, and the nonmilitary applications of radar imaging systems have been recently investigated by the scientific community.

Feder (1957, 1960) was one of the pioneers and primary advocates of the potential application of radar interpretation to geologic investigations, even though his initial research embraced only those data from the low resolution PPI systems. Coincident with Feder's studies, the electromagnetic reflection properties of natural surfaces, and measurements of terrain backscattering were investigated for both static and airborne radar systems in important studies conducted by the Goodyear Corp. (1959) and Ohio State University (Cosgriff, et al., 1960). Although the concept of side-look airborne radar (SLAR) systems had been known in the late 1940's, it remained only a concept until the 1950's when modern techniques and components for the centimeter wavelength band were developed to the point of practical usefulness. Limited declassification of data concerning SLAR imagery in the early 1960's allowed the geoscience potential of such radar systems to be openly discussed in the literature (Rydstrom, 1961; Fisher, 1963). Probably the greatest catalyst for introduction of the earth scientists to the research fields of radar and remote sensing was the First Symposium on Remote Sensing of Environment held at the University of Michigan in 1962. The purpose of this symposium was to investigate the possible applications of remote sensing techniques to various earth science fields.

In the early stages of applied research on SLAR systems, emphasis was placed on the utilization of radar imagery for the study of volcanic terrains which were considered analogous to portions of the lunar surface. It was not long, however, before early researchers demonstrated the value of radar imagery in more typical terrestrial environments. Early studies conducted by the Autometric Corporation were oriented towards geological-engineering investigations, and a report by Bienvenu and Pascucci (1962) summarizes some of the initial phases of applied research utilizing SLAR imagery. A subsequent report by the Autometric Corporation "An Evaluation of Geoscience Applications of Side-Looking Airborne Mapping Radar" (Simons and Becassio, 1964) represents one of the first comprehensive

unclassified investigations oriented toward terrain and geologic analyses. Simons (1965) related the applicability of SLAR imagery for the interpretation of geological structure, the observation of geomorphologic features, and delineation cultural patterns. Although SLAR imagery was not used for a study conducted by Cameron (1965), radar scope photographs (PPI presentation) of the Gaspe Peninsula were reported to reveal radar linears and patterns suggesting a number of new geological features including two unmapped thrusts cutting across fold trends. A generalized summary of the application of radar imagery to geologic interpretations up to 1964 was revealed by Pierson, et al., (1964).

The first detailed, geoscientifically-oriented report on SLAR imagery interpretation was released by the National Aeronautics and Space Administration in 1965, (Beatty, et al., 1965). This report summarizes the state-of-the-art at that time, even though the imaging systems which collected the imagery were obsolete when the report was released. The publication of the NASA report coincides with the declassification and ultimate release of high-resolution SLAR imagery to a limited number of scientific personnel for government sponsored, geologically-oriented research projects. The primary investigators included: NASA, Cold Regions Research and Engineering Laboratory, USGS, Goodyear Aerospace Corp., Raytheon/Autometric Corp. and CRES, University of Kansas.

The more significant and recent results of the application of radar imagery to geologic investigations are summarized in: Pierson, et al., (1965), Ellermeier and Simonett (1965); Davis, et al., (1966), McCoy (1967); Dellwig, et al., (1968), Barr, (1968), and Rouse, et al., (in press). For the most recent and comprehensive bibliography concerning radar geology, the reader is referred to "Radar Bibliography for Geoscientists" by R. L. Walters, (1968).

CHAPTER 3

RADAR OPERATION

The design of imaging radars for geological reconnaissance requires an interdisciplinary effort which includes both a theoretical (provided by the radar engineer) and practical (provided by the geologist) understanding of the sensor's operation. Certainly the geologist utilizing the imagery need not be capable of system design; however, certain fundamentals of radar operation should be understood in order to provide optimum data retrieval for the interpretation. This chapter summarizes some of the fundamental parameters pertinent to radar operation; first, in the simpler case familiar to most geologists where the signal is sent from ground to air and target-signal interaction is ignored; and second, in the more complex case when the signal is sent air to ground, and where the terrain-signal interaction is of primary concern.

3.1 Basic Case, Ground to Air

A transmitter on the ground emits electromagnetic radiation in the form of RF (radio frequency) energy, and when the RF energy is interrupted by any object such as an aircraft, part of the energy is reflected back to a receiver. The reflection or reradiation of energy sent back to the receiver is referred to as an "echo," and the object reflecting or reradiating the signal is called the target. If, however, reradiation is returned from the surrounding terrain which makes it difficult to select the desired target, the unwanted return signals are termed "clutter" (Wheeler, 1967). The time duration from transmission of the original energy to the reception of the return signal is a measure of the range, or distance from the target. The velocity of electromagnetic waves in free space is 3×10^8 m/sec (1000 feet/microsecond), and therefore, if an object is one nautical mile away (1,853m or 6080 ft.) it will take slightly more than 12 microseconds for the transmitted energy to reach the target and return to the transmitter.

If the transmitter were in continuous operation, return signals from a specific target would be continuously received, and it would be difficult to determine which portion of the signal return was correlative with a particular transmitted signal. A common practice therefore is to pulse-modulate the transmitter so that the RF signal is emitted in short bursts or pulses, and then transmit another signal only after the previous transmission has been reradiated back to the receiver. Thus, the transmitter and receiver are not in use simultaneously, allowing a single antenna for both transmission and reception. Figure 3.1 is presented for those readers interested in the "black-box" components of a typical radar system, where the components perform the following functions:[2]

Pulse Generator: Produces short repetitive bursts of energy (called pulses) to drive the transmitter and to initiate a synchronous sweep on the CRT.

Transmitter: Converts each pulse from the pulse generator into a burst of RF (radio frequency) energy.

Duplexer: Acts as a switch that connects the antenna to the transmitter during the brief pulse period that the radio-frequency energy is generated, and then connects the antenna to the receiver for the rest of the time.

Antenna: Radiates the energy into space in a narrow shaped beam, and intercepts the reradiation from the terrain.

Receiver: The superheterodyne receiver consists of RF amplifier, mixer, local oscillator, IF amplifier, detector and video amplifier. The weak signal from the antenna is amplified by the RF amplifier. The mixer combines the RF frequency with the local oscillator frequency to produce the difference between the combined frequencies, called IF or intermediate

---

[2]For a more detailed explanation of radar theory and operation the reader is referred to Skolnik, (1962); Levine, et al., (1966); Moore, (1966); and Wheeler, (1967).

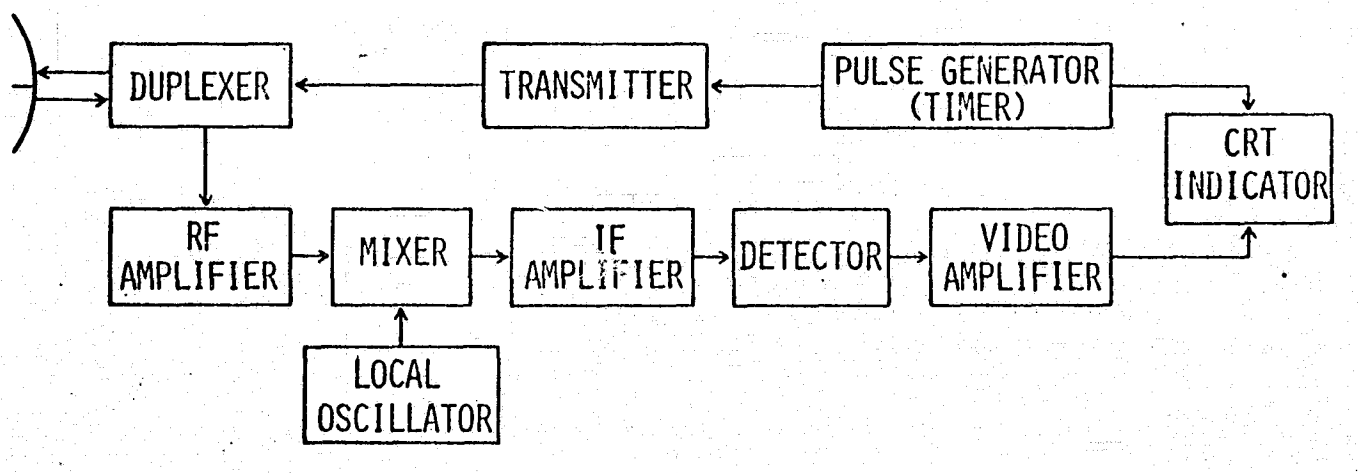

Figure 3.1 Block diagram, typical airborne radar system.

frequency. The IF signal is then amplified, and demodulated in the detector to produce a video signal which is amplified and sent to the CRT indicator.

3.1.1 Side-Looking Airborne Radar System (SLAR) Operation—Air to Ground[3]

Figure 3.2 shows an area being imaged by a typical SLAR system. The transmitter generates short bursts or pulses of radio frequency (RF) energy. These pulses are propagated into space by means of a directional antenna (A), and radiate from the antenna as a block of energy (B) at the velocity of light (3×10^8 m/sec.). Conventional radars utilize the frequency range from 230 to 40,000 MHz (Megahertz, MHz = Megacycles, Mc) although neither end of this range is truly definitive of the frequency limitation for radar operation. A letter code of frequency-wavelength bands, K, X, L, etc., was arbitrarily selected to ensure military security in the early developmental stages of radar, and has continued in use for convenience (Figure 3.3).

The RF energy is confined to a narrow path, as shown in Figure 3.2. At any one instant, the terrain illuminated by the transmitted pulse is limited in the range direction by the pulse duration and in the azimuth direction by the beam-width of the directional antenna (a more detailed discussion of these parameters will be given later in this chapter). Thus, the size of the illuminated patch on the terrain as indicated by the crosshatched area in Figure 3.2 is determined by the radar's resolving power.

If a terrain feature capable of intercepting RF energy is irradiated at point (a), a fraction of the transmitted energy will be reradiated back to the antenna (A). An object at (b) will also reradiate energy back at a later time when it is illuminated by the pulse packet of RF energy. The same is true for features at (c) and (d). The portion of energy returned to the antenna from the terrain features (a), (b), (c), and (d) is converted to a video signal by the receiver. The signal return from these features is displaced from the origin as a function of the range from the antenna to the target, whereas the amplitude of each return is a function of the scattering properties of the terrain.

---

[3]Summarized in part from Westinghouse (1967).

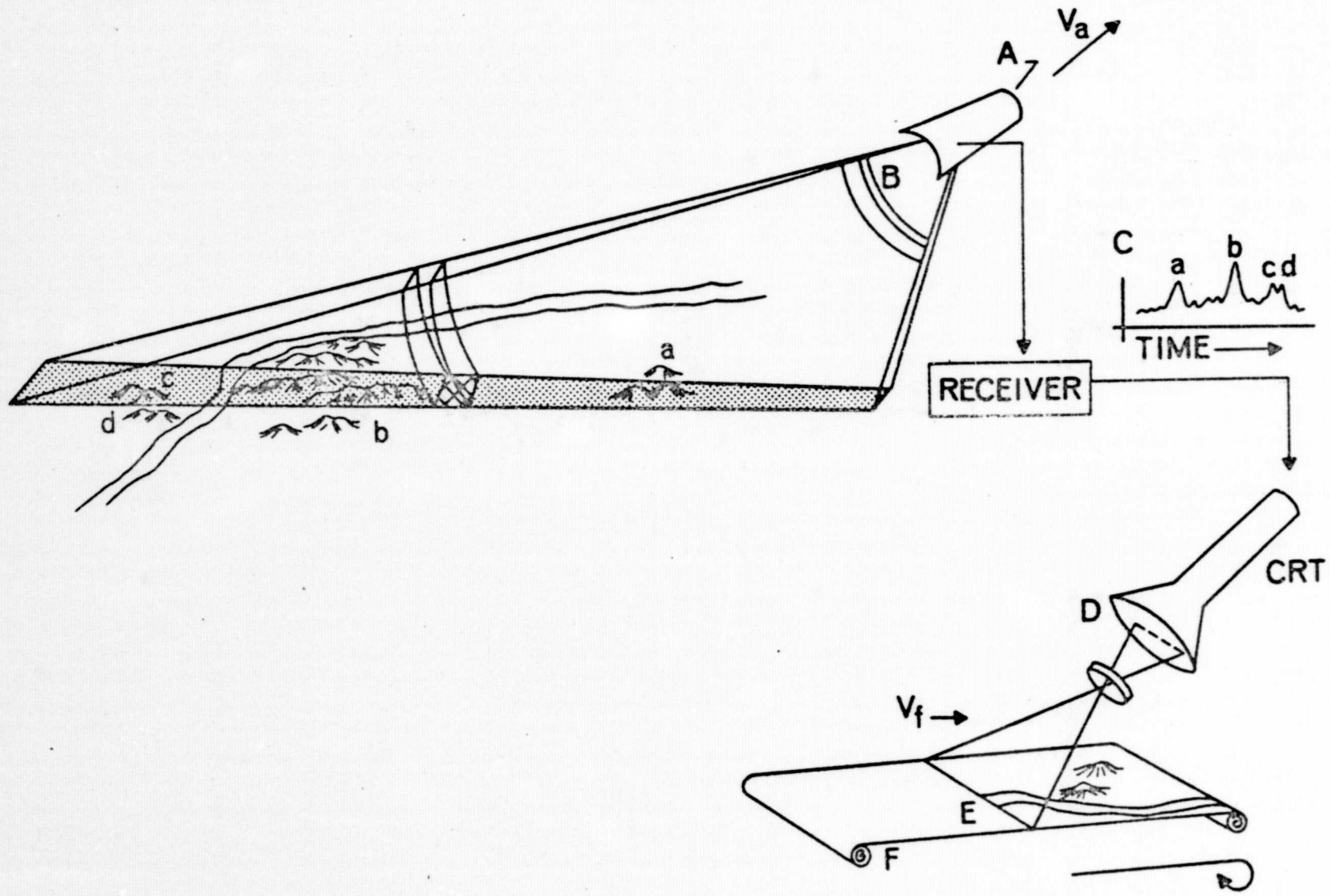

Figure 3.2 Sketch diagram, typical side-looking airborne airborne radar system (modified from Westinghouse, 1967).

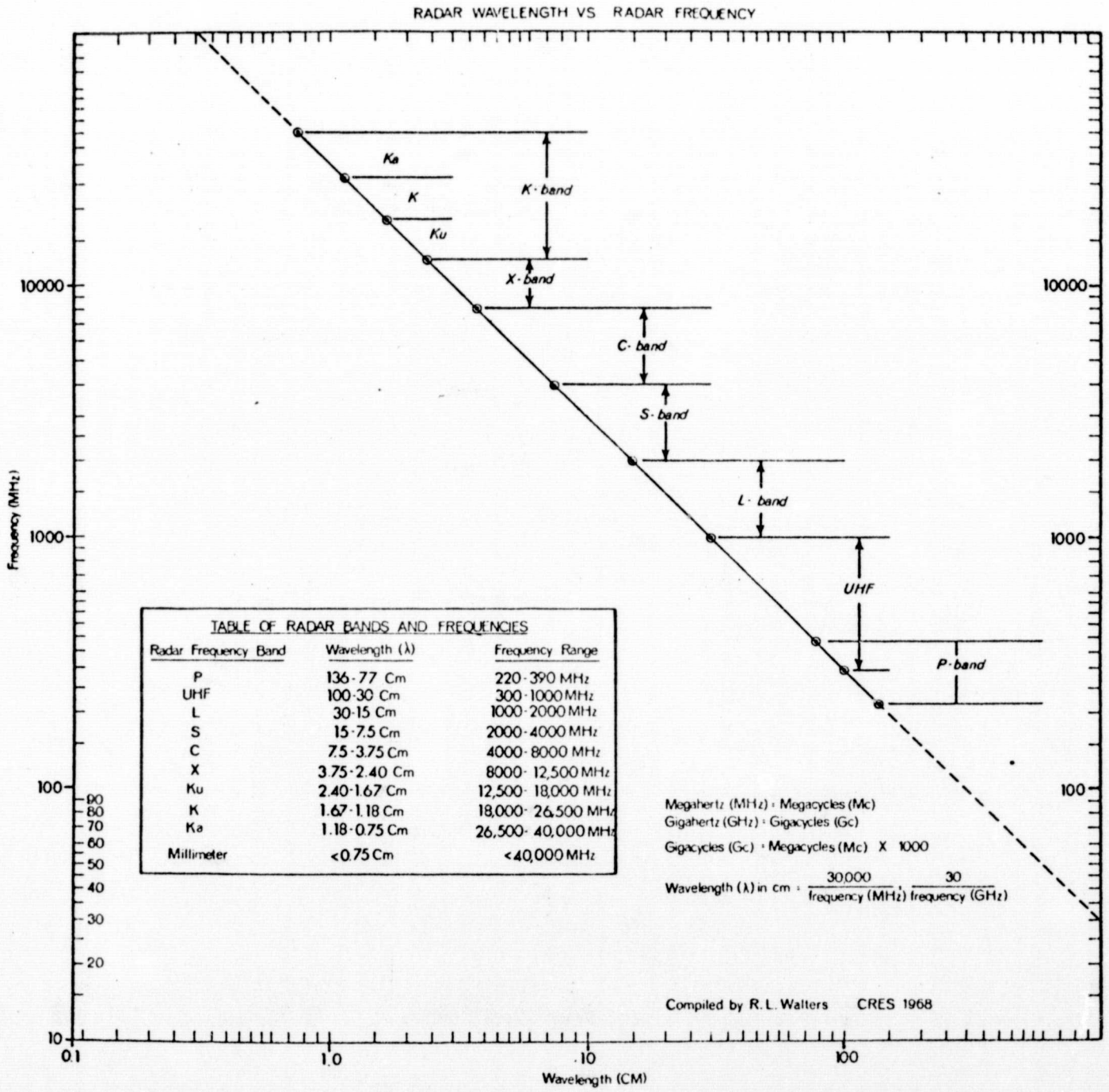

Figure 3.3 Letter code and frequency-wavelength bands.

The video signal is displayed by intensity modulating the beam of a cathode-ray tube (CRT) as the beam is swept across the face of the CRT. If the antenna is repositioned by translation to "look" at a new strip of terrain adjacent to the one just imaged, and each resultant line is displayed on the CRT in the same relative position, an image of the terrain can be generated on a continuous strip of film drawn across the face of the CRT.

In summary, the antenna (A) is repositioned laterally at the velocity of the aircraft (V_a). Each RF pulse transmitted (B) returns signals from the targets within the beamwidth. These target returns are converted to a time/amplitude video signal (C) which is imaged as a single line (E) on photographic film (F). Returns from subsequently transmitted pulses are displayed on the CRT at the same position (D) as the previous scan lines. By moving the photographic film past the CRT display line at a velocity (V_f) proportional to the velocity of the aircraft (V_a), an image of the terrain is recorded on the film (F) as a continuous strip map.

3.2 Complex Case-Terrain-Signal Interaction

Radar return is that portion of the transmitted radar energy which returns to the radar receiver. The appearance of radar imagery can be understood by considering some of the characteristics RF energy shares with light waves. When electromagnetic waves strike a boundary or surface, some of the waves are transmitted into the new material and are either absorbed or transmitted through it. On the surface of the material, waves are reflected specularly (similar to light reflection from a mirror) or scattered in all directions (diffusely). The significant difference between light waves and RF energy is the respective wavelength involved (visible light .4 - .76 microns; radar 1 mm to several meters).

Radar signals are normally returned from the terrain, to the receiver, by a scattering process (reradiation). The signal strength (or intensity of this terrain return) received at the antenna determines the relative degree of brightness of a resolution cell on the imagery. Taylor (1959) measured the backscatter from many different types of terrain (using three frequencies with

vertical and horizontal polarization), and concluded that the fundamental parameters which affect terrain return are: surface roughness, incidence angle, polarization, frequency, and complex dielectric constant.

Surface roughness and dielectric properties are functions directly related to the terrain and may be collectively expressed as the scattering coefficient, (scattering cross-section per unit target area per unit solid angle in the direction of the receiver). The scattering coefficient contains a major part of the geoscience information about the illuminated terrain that the radar is capable of sensing, except for location (Rouse, et al., 1966). Frequency is a function of the transmitted signal and the frequency dependence of the electromagnetic properties of the terrain. Incidence angle depends in part on the position of the transmitter and in part on the geometry of the local terrain, while polarization is both a function of polarization of the incident signal and the depolarizing effects of the terrain (Ellermeier, et al., 1966).

3.2.1 Angle of Incidence

The angle of incidence, Θ, is the angle formed by an impinging beam of radar energy and a perpendicular to the incident surface at the point of incidence. The angle between a line from the transmitter to a point on the terrain, and a horizontal line passing through the transmitter is the depression angle (Figure 3.4C). The geometric parameters of SLAR imaging systems are such that along the swath width of an area imaged (near to far-range), there is a continuous change in the angle of incidence (Figure 3.4A-B). When imaging homogeneous flat terrain, for any constant depression angle along the flight path, the angle of incidence will remain constant. Under more typical natural terrain conditions, however, local variations in terrain slope can change the effective angle of incidence. The consequence of terrain slope on the incidence angle, at a constant depression angle, is shown in Figure 3.4C. The slope of the terrain is expressed in the measurement of the aspect angle; the complement of the incidence angle. Note on Figure 3.4C that if the terrain is flat, the aspect angle equals the depression angle.

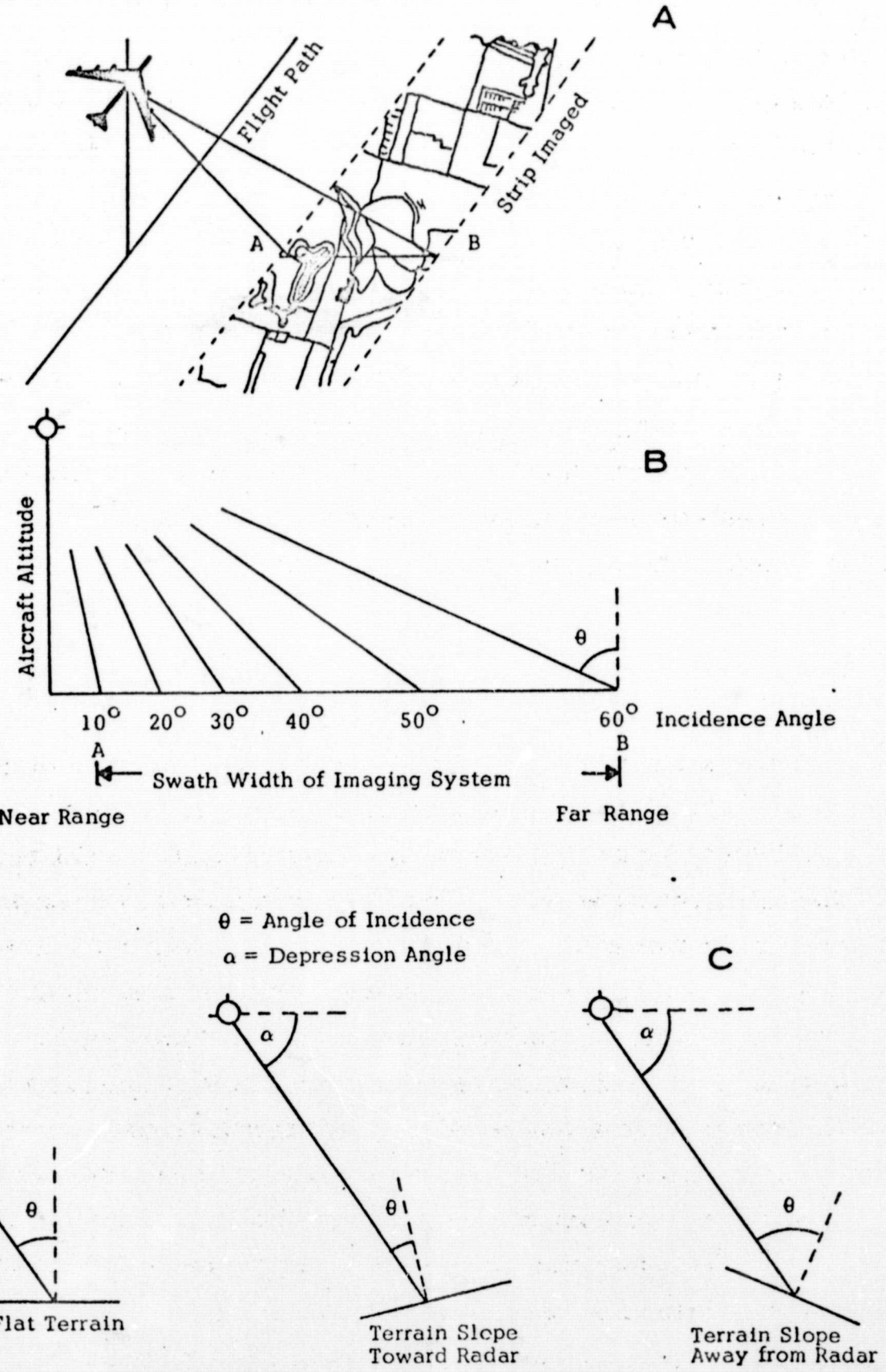

Figure 3.4 SLAR imaging system. (A) Ground coverage (after Moore and Simonett, 1967). (B) Hypothetical swath width and respective incidence angles for flat terrain from near to far range, (after McCoy, 1967), (C) Effect of terrain slopes on incidence angles.

If terrain slopes are inclined at an angle toward the imaging radar and the effective angle of incidence decreases (with increasing terrain slope angle) to a point where the angle of incidence equals the angle of slope, vertical incidence (maximum reradiation) is the result. Conversely, if terrain slopes are inclined away from the imaging radar, the angle of incidence increases (with increasing terrain slope angle) to a point where grazing (maximum shadow) is the resultant. These contrasting angles of terrain illumination are somewhat analogous to the situations encountered when gathering remote sensor data by vertical aerial photography. When the sun is essentially at the zenith, shadowing is minimized; however, as the sun approaches the horizon, shadowing of terrain features correspondingly increases. Thus it is possible to image extremely rugged topography with SLAR imaging systems, and have equivalent slopes along the swath width fully illuminated in the near range, and in partial or complete shadow in the far range.

3.2.2 Surface Roughness

Surface roughness is a geometric property of the terrain and is the most important influence upon the return signal as it dictates the extent of scattering which forms the reradiation pattern field. Surface roughness is not an absolute roughness, but the relative roughness expressed in wavelength units. Terrain surfaces may be divided into two major categories according to surface roughness, depending upon the relationship of the root mean square (rms) surface roughness to the signal wavelength, λ. For rms surface roughness much less than a wavelength ($\lambda/10$) the surface appears "smooth" to the imaging radar, while for surface roughness on the order of a wavelength or more, the surface appears "rough." For a more general example, a terrain surface can be classed according to roughness between the extremes of a perfect specular reflector (no scattering), where backscatter exists only near vertical incidence, to an isotropic scatterer, where the scattering coefficient is independent of the angle of incidence.

3.2.3 Frequency and Dielectric Constant

Varying the frequency of the wave incident upon a surface of any roughness produces an effect similar to variations in surface roughness. In addition, however, variations in frequency affect the scattering coefficient due to the frequency dependence of the complex dielectric constant of the terrain. For two comparably rough surfaces, the difference in their scattering coefficients is indicative of the difference in their dielectric properties. The complex dielectric constant is proportional to moisture content and porosity of the surface material (Taylor, 1959; Lundien, 1965).

3.2.4 Polarization

In the traditional SLAR configuration the electric vector is radiated and received horizontally, and thus receives the designation "like-polarized." Independent of the transmitted polarization, the return signal will be depolarized as a function of certain terrain parameters. The cross-polarized return can be displayed simultaneously with the like-polarized signal, if the system is capable of receiving both polarizations.

Comparison of SLAR imagery where like and cross-polarized return signals are simulatneously collected has revealed significant differences which may be used for terrain identification (Dellwig and Moore, 1966; Ellermeier and Simonett, 1965); however, only the like-polarized return was available for the Panama imagery. Variations between like and cross-polarized terrain returns must be considered as two entities: first the radar return as a function of polarity of the transmitted signal alone, and second the radar return as a function of both polarity of the transmitted signal and the depolarizing properties of the terrain.

3.3 Resolution and Detectability[4]

Before concluding this chapter on radar operation it is necessary to define both radar resolution and radar detectability. Depending on the

[4]The discussion concerning detection and resolution is summarized from Moore (1966).

resolution of a particular radar system, it may not be possible to resolve (i.e., separate on the imagery) two objects only a hundred feet apart. Yet, one of the objects may be detectable even though it has dimensions several feet across. For example, a metel fence post may be clearly detectable on the radar imagery although it is impossible to distinguish between fence posts spaced closely enough to be below (or within) the resolution distance of the radar system.

Radar resolution with conventional SLAR systems varies in dimension in both range (normal to ground track) and azimuth (parallel to the ground track) directions. The range resolution of SLAR systems is determined by the pulse duration (pulse length) of the transmitted energy (Figure 3.5A), i.e. $c\tau/2$ (where $c = 3 \times 10^8$m and τ = pulse length). When the radar energy is incident at depression angle β as shown in Figure 3.5B, the range resolution dimension on the ground equals $c\tau/2\cos\beta$. Thus objects separated by a distance equal to or less than $c\tau/2\cos\beta$ will not be resolved as individual targets and will appear on the radar as signal return from a single resolution cell. If the separation distance between two objects exceeds $c\tau/2\cos\beta$ then the two targets will be resolved.

In the azimuth direction the dimension of the resolution cell is limited by the product of the slant range and the dimension of the half-power beamwidth[5] (measured from the sides of the antenna pattern where the gain is three decibels down from maximum) of the directional antenna (Figure 3.5C). The azimuthal resolution is then expressed as $R_s B_\Theta$, where R_s is the slant range and B_Θ the half-power beamwidth.

$$R_s B_\Theta = \frac{HB_\Theta}{\sin\beta} \; ;$$

H = alt. above terrain, β = depression angle. The area of the resolution

[5] The width of the main lobe of an antenna pattern at the half-power points is called the beamwidth of the antenna, and when beam pattern is plotted in decibels against angular direction, the half-power points are the 3db points on the decibel plot (Wheeler, 1967).

cell or area of the pulse packet (cross-hatched area Figure 3.5) can be expressed as:

$$A_p = R_s B_\Theta \left(\frac{c\tau}{2\cos\beta}\right) = \frac{HB_\Theta c\tau}{2\sin\beta\cos\beta} = \frac{HB_\Theta c\tau}{\sin 2\beta}$$

Since the azimuth beam is angular in shape, the azimuthal resolution is not a constant value in the range direction (Figure 3.5A), and the width across the beam is a function of slant range. The beam width (B_Θ) of the directional antenna is directly proportional to the operational wavelength (λ) and inversely proportional to antenna length. Thus, azimuth resolution can be improved by reducing the wavelength, increasing antenna length, or both. The operational wavelength is usually selected because of desirable terrain reradiation characteristics, and consequently proper azimuthal resolution is generally achieved by antenna design. Significant resolution improvement has been achieved by employing signal processing called synthetic aperture. A narrow beam width can be achieved by storing the signals returned from a large number of pulses in some sort of a memory, retaining both phase and amplitude relationships, then processing the signals the same way that a large antenna processes them. Thus, although the real antenna may only be a meter long, the signals stored and processed over a flight of 400 meters long results in a synthetic antenna 400 meters long.

As previously discussed, the range resolution of a SLAR system is dependent on the pulse length (τ). As range resolution is improved by decreasing the pulse length of the transmitted pulse however, the average power also decreases (power is defined as energy emitted per unit time). A method of overcoming this limitation is achieved by frequency modulating the transmitted pulse (pulse compression techniques). The reader is referred to Beatty, et al., (1965), Klauder, et al., (1960), Wheeler, (1967), and Nims, (1968) for a discussion of power constraints when utilizing pulsed radar systems.

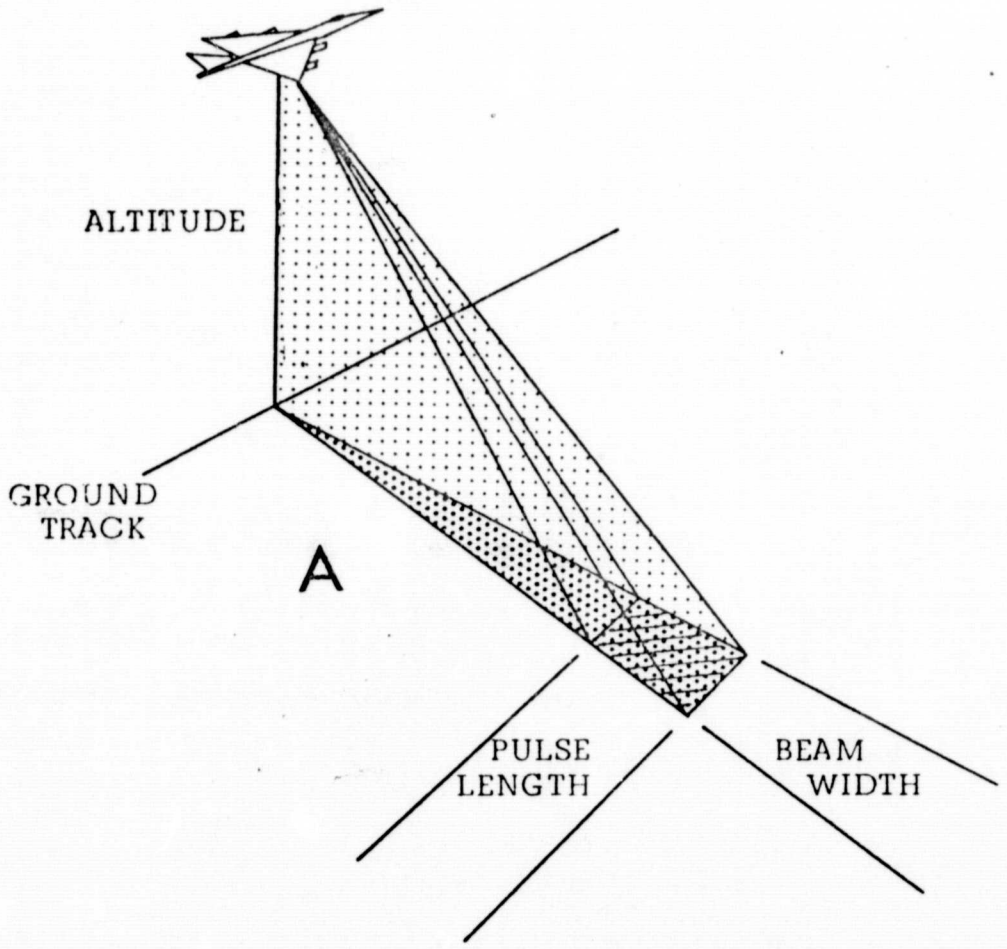

PULSE LENGTH

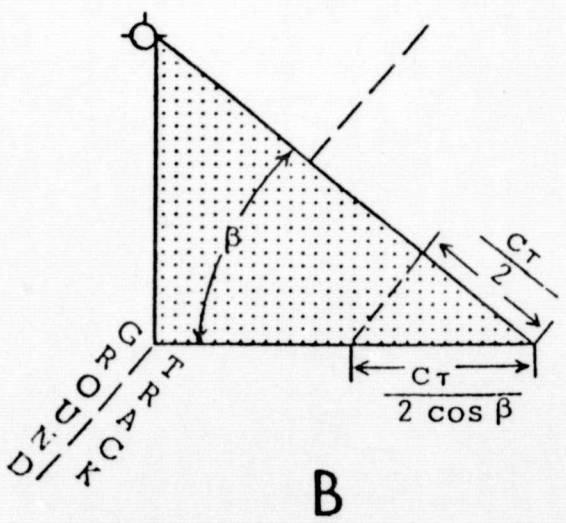

Range resolution at depression angle β, $c = 3 \times 10^8$ m/sec., and τ = pulse length.

BEAM WIDTH

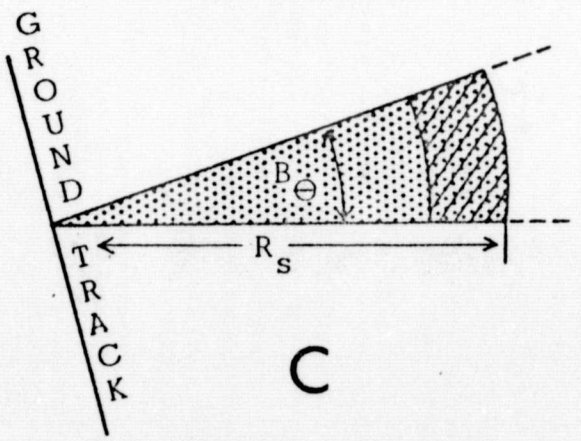

Azimuth resolution = $R_s B_\Theta$, where R_s is slant range and B_Θ is half-power beam width.

Figure 3.5 SLAR imaging system resolution. (A) Pulse length and beam width in relation to ground track (after Beatty et al., 1965). (B) Range resolution. (C) Azimuth resolution.

3.4 Radar Geometry[6]

SLAR systems use either a slant range or ground range presentation on their image recording CRT indicators. Slant range sweeps are linear, so the spacing between return signals on the image is directly proportional to the time interval between the terrain features being recorded. For ground-range sweeps, the spacing is modified (hyperbolic waveform applied to CRT sweep circuitry) to equate the image scale to that which the terrain features would actually have on the ground. The distinction between ground range and slant range is illustrated in Figure 3.6. The time required for the return signal to reach the receiver from points a, b, and c is exactly the same as the time interval from a', b', and c. On slant range imagery the return signals are recorded with a spatial separation directly proportional to the time interval between them. Thus, on the slant range presentation the distance from the radar to feature a' represents the slant range of SR_1 and the distance to b' is SR_2, etc. With a ground range presentation the radar and terrain features at a, b, and c are represented by the ground range distance of GR_1, GR_2, and GR_3 respectively. By knowing the radar altitude of the aircraft and measuring the slant range to a terrain feature, the ground range can be calculated. For example in Figure 3.6, $GR_3 = \sqrt{SR_3^2 - h^2}$.

3.4.1 Imagery Scale

Two different flight parameters affect both the range and azimuth scales of a slant range imagery display. The range scale can vary with aircraft altitude, and the azimuth scale is dependent on the synchronization between aircraft and film speed (previously illustrated in Figure 3.2). Naturally, SLAR systems are designed to produce imagery with minimal scale distortions; however, aside from any inherent errors, changes in either aircraft altitude or incorrect film synchronization generally necessitates scale determination for each flight or separate strip of imagery. Aside from the

---

[6]Discussion in part summarized from LaPrade and Leonardo, (1968).

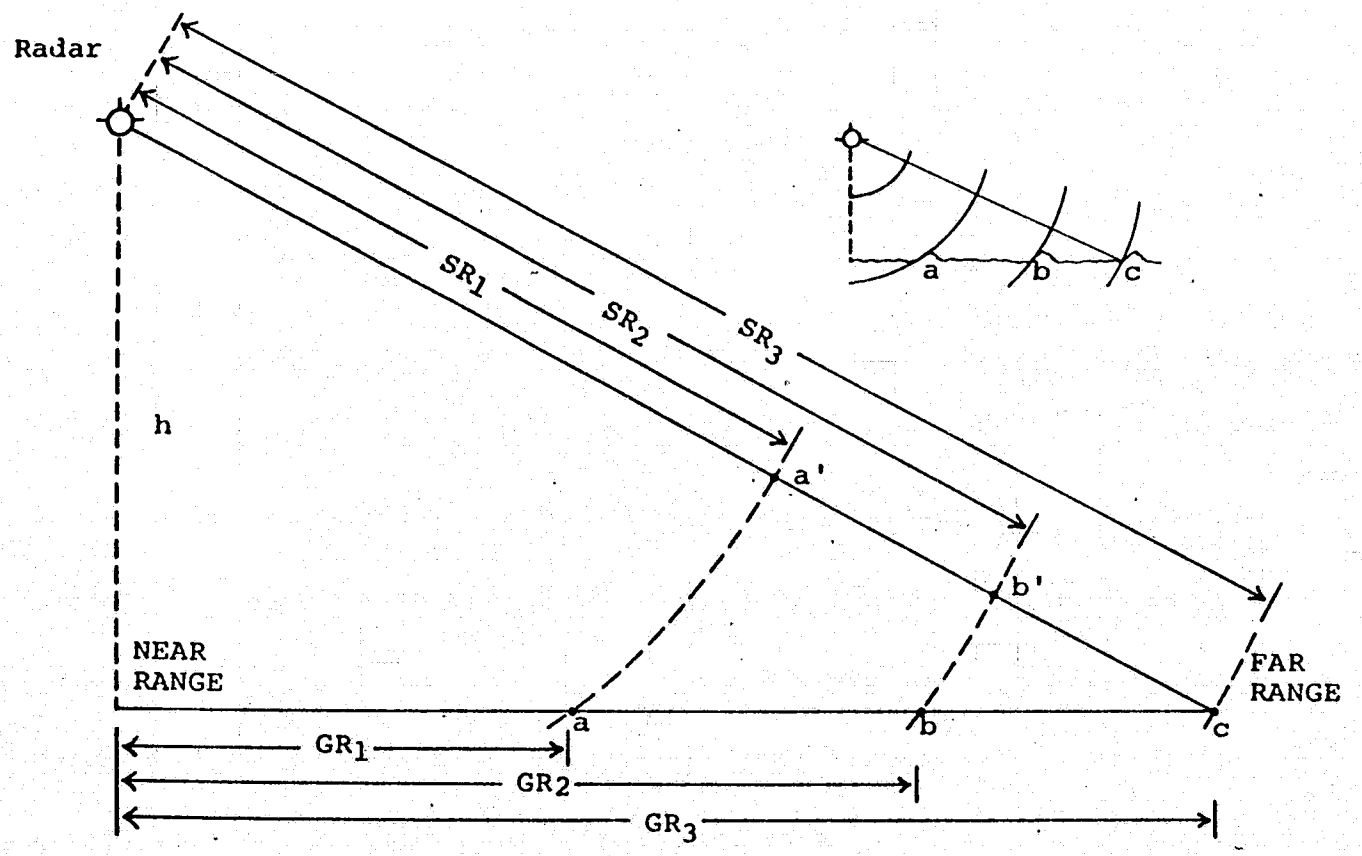

Figure 3.6 Measurement of slant range and ground range.

flight parameters which influence image distortion, one of the most obvious scale distortions on slant range imagery is the continuous scale change in the range direction (orthogonal to ground track). Figure 3.7A illustrates the geometry of a square grid system that is crossed by two diagonal features; in one case showing the ground range geometry and in another example the slant range geometry. In the far range on the slant range display, the distance between adjacent points varies only slightly, whereas in the near range, large changes in scale occur. This discrepancy between slant range and ground range distances can also be illustrated graphically as shown in Figure 3.7B, where the ratio of slant range to ground range distances show a wide variation in the near range. The distortion of near-range, scale compression as shown by slant range imagery formats does, in fact, influence both the accurate determination of distances and the interpretation of geologic terrain parameters such as shape and geometric orientation. McCoy (1967) was especially cognizant of this distortion when measuring stream basin parameters, and he made an effort to avoid drainage basins lying in the near range portion of slant range radar images. The near range compression and its resultant effect on the portrayal of geometric shape is illustrated in Figure 3.8, where the outlines of several islands north of the La Palma Peninsula (8°24'N, 78°09'W) were sketched directly from the radar imagery. Using imagery obtained from six different flights, the outline of the islands show great distortion in the extreme near range (flights A,F), moderate distortion in the near range (flight E), and somewhat uniform outline in the mid-range (flights B, C, D). The elongation of these islands parallel to ground track (flights A and F) is of particular significance for the geologist concerned with delineating linear landforms which might have structural significance.

Obviously, the scale distortions inherent to slant range imagery precludes its use for accurate planimetric measurements; however, both range and azimuthal scales can be computed that are satisfactory for geological reconnaissance studies. This computation can be accomplished most easily where a known distance between two points on the ground can be compared with the same two points on the radar imagery, or if the ground distance is not known, the relationship between radar image geometry, air-

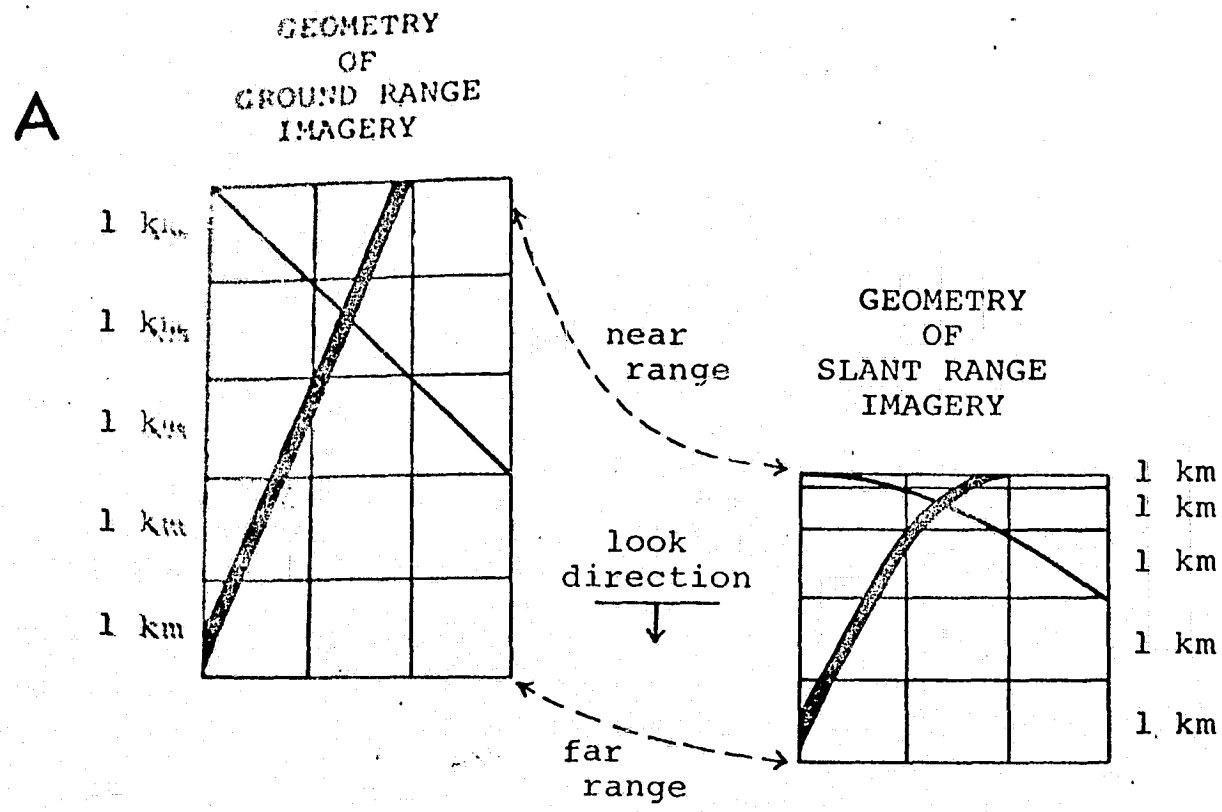

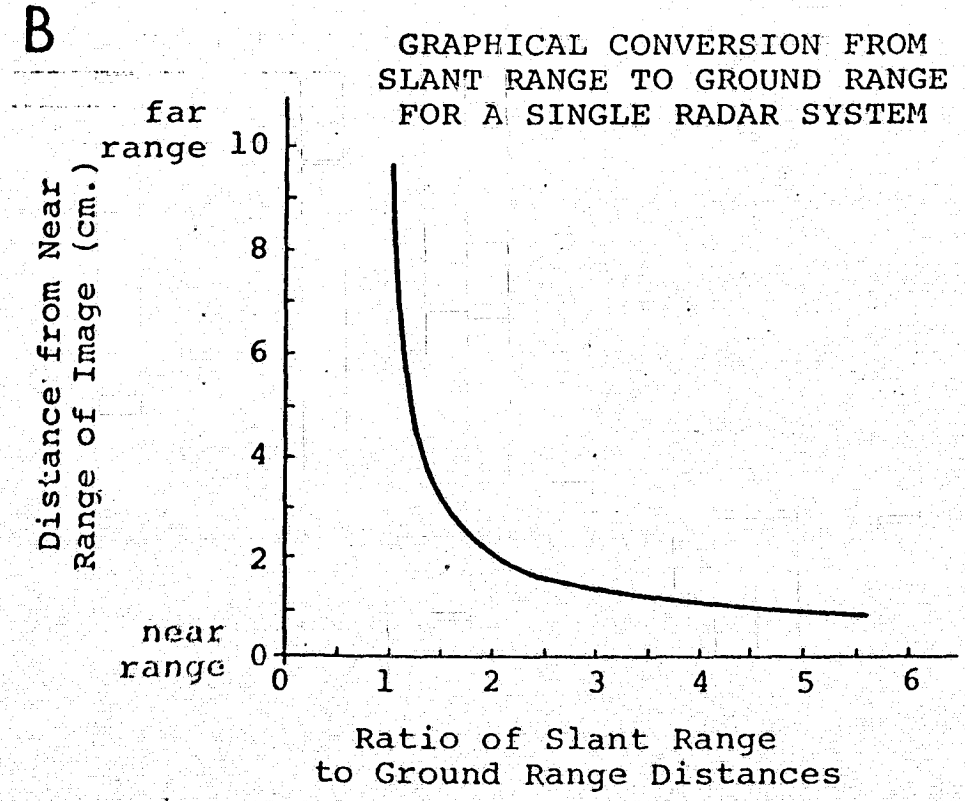

Figure 3.7 Comparison of slant range and ground range. (A) Geometry of slant range and ground range presentation, (after Innes, 1968). (B) Graphical conversion from slant range to ground range for a single radar system, (after McCoy, 1967).

Figure 3.8 Effect of near-range compression on geometric shape, La Palma Peninsula, Darien Province, Panama (prepared by A. J. Lewis).

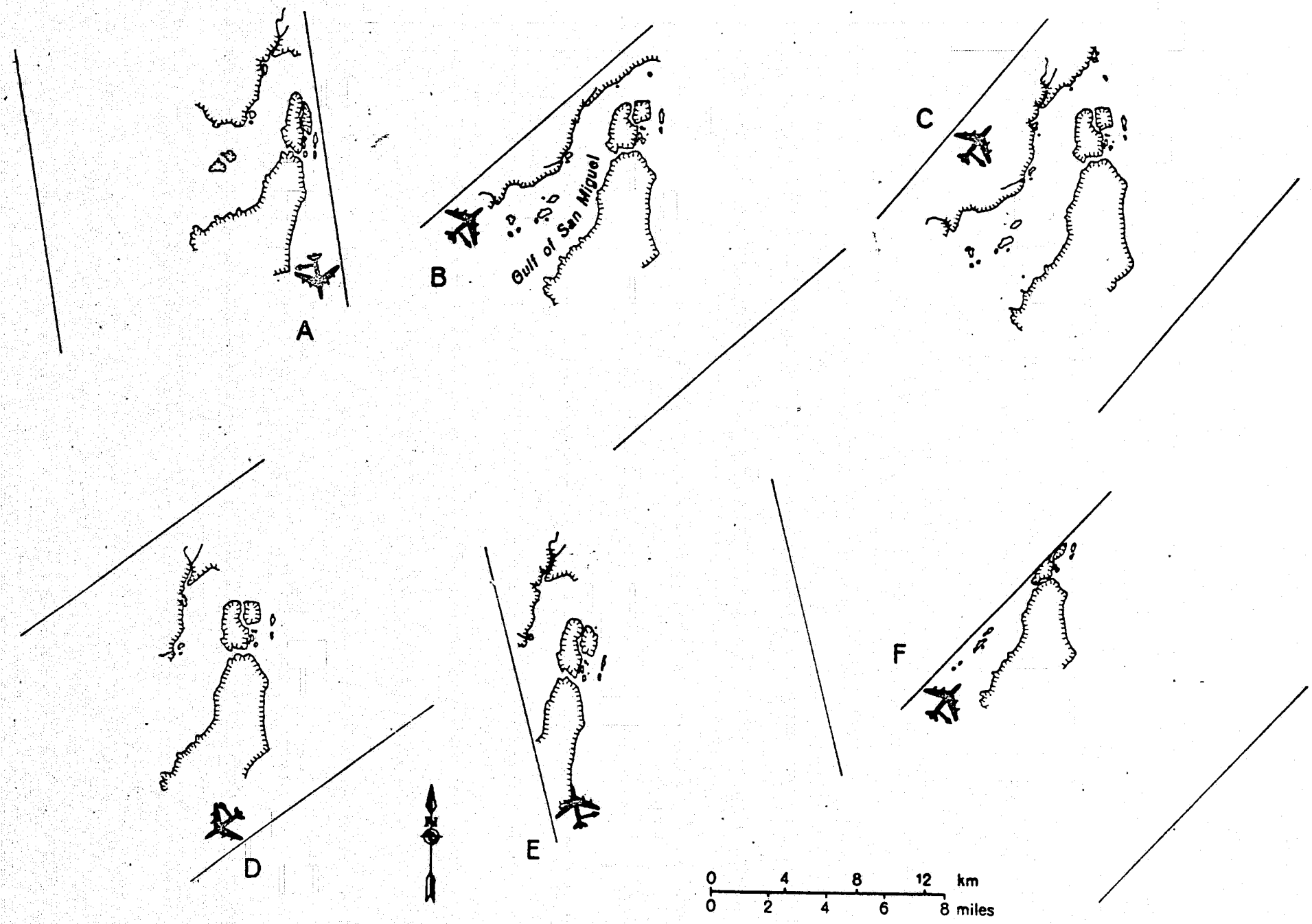

craft velocity and image distances will yield a slant range scale (Barr, 1968). A more sophisticated method of slant-range image restitution, capable of correcting many of the slant-range imagery distortions has been described by Scheps (1960).

It is important to note, that although direct cartographic applications of SLAR imagery may be somewhat limited, topographic information for contour mapping can be obtained simultaneously with SLAR imagery. The utilization of interferometric techniques for obtaining elevation data will be discussed in Section 3.6, entitled "Topographic Mapping."

3.4.2 Radar Foreshortening[7]

Radar foreshortening, a distortion inherent to all radars imaging irregular terrain surfaces, is the variation in the length of equal terrain slopes when the slope measurements are taken at different incidence angles. The slant range length measurements (L) of terrain slopes on radar imagery are a function of the depression angle(α) and the terrain slope β, i.e., $L = f(\alpha, \beta)$.

Figure 3.9(A) illustrates the time intervals between equally spaced radar energy pulses which intercept the terrain at certain "ranges" from the transmitter. On radar imagery the distances between terrain features are recorded as a function of the time interval required for RF energy to traverse the corresponding separation distance. The actual lengths of terrain slopes ab and bc are equal; however, on the radar imagery, the length of slope ab would appear considerably shorter than bc. As a time discriminant, the slope ab is much less than one (time) "range unit" ($T_2 - T_3$) whereas slope bc is greater than two (time) "range units" ($T_3 - T_5$). It is obvious from Figure 3.9A, that terrain surfaces sloping toward the radar will appear shortened, in contrast to those surfaces sloping away from the radar.

This foreshortening phenomenon is shown in a somewhat more analytical illustration in Figure 3.9C where the length of the terrain slopes

---

[7] Summarized in part from a discussion on radar foreshortening by Kirk, et al., (1968).

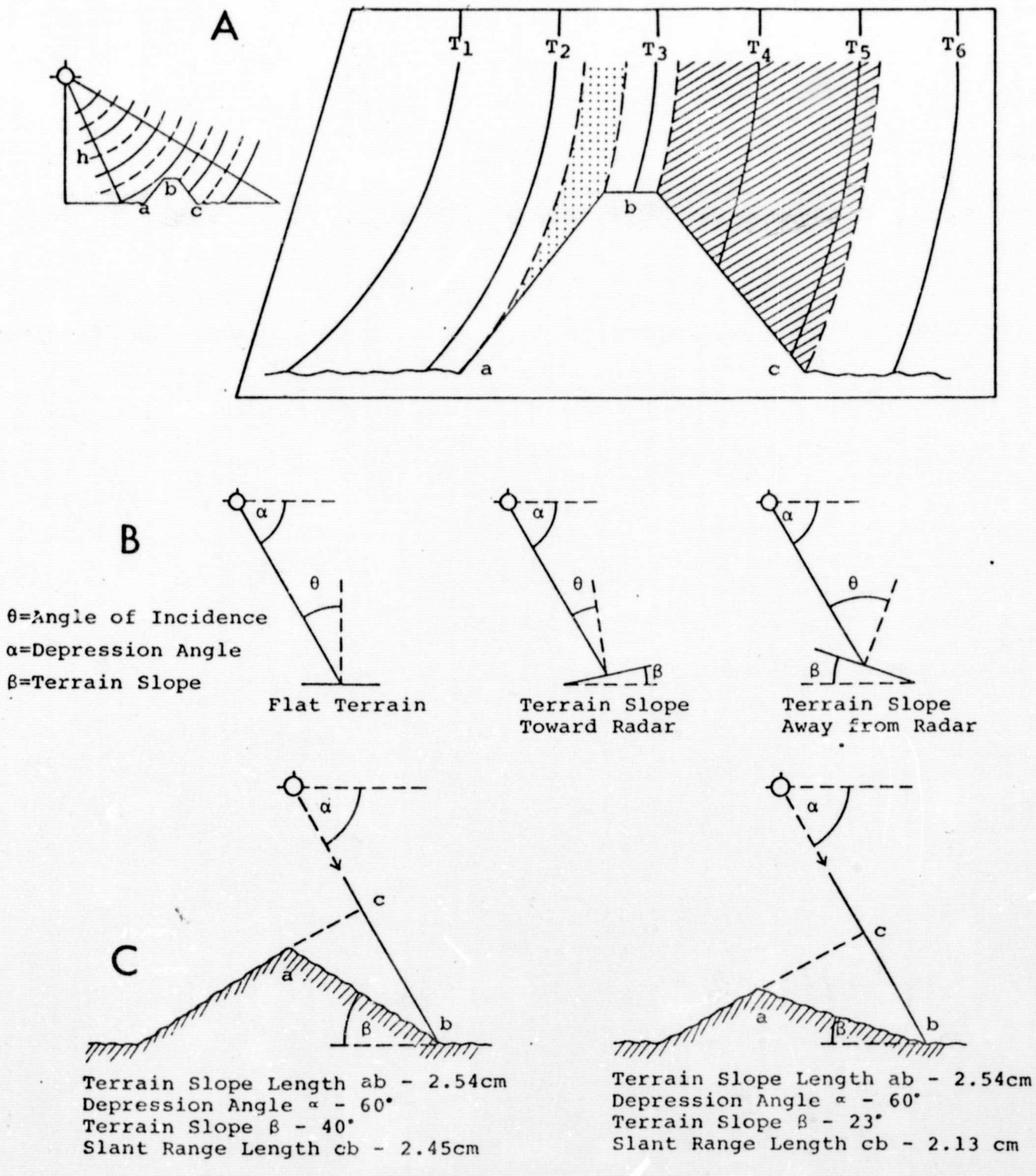

Figure 3.9 Radar foreshortening. (A) Time measurements from transmitter, (after Kirk, et al., 1968). (B) Relationship between angle of incidence and terrain slope. (C) Variations in slant range measurements, (after McCoy, 1967).

ab are equal, the depression angles α are equal, but the change in terrain slope β can result in differences in the slant range length (cb) of the two slopes. The relationship between terrain slope, depression angle and the resultant incidence angle can be seen clearly in Figure 3.9B. Where the incidence angle approaches grazing (90°) the amount of radar foreshortening will be minimal, but where the incidence angle approaches the normal, the effect of foreshortening is maximized.

3.4.3 Radar Layover[8]

As previously discussed, a radar imaging system is time dependent, i.e., the return signals are directly proportional to the time interval (range) between the transmitter and the terrain feature being imaged. Because of this radar characteristic, one geometric distortion most often evident on radar imagery (especially in mountainous areas) is that terrain features of appreciable height appear to "lean" toward the nadir of the aircraft. Radar layover is caused by the radar signal intercepting the top of an object before it intercepts the bottom. Illustrated in Figure 3.10, the top terrain feature 1 is recorded on the imagery prior to the base because the slant range distance from transmitter to the top of the feature (SR_t) is less than the slant range distance to the base SR_b. With terrain feature 3, the top and base are imaged as a single point; whereas terrain feature 4 is imaged normally, i.e., with base portrayed closer to the nadir of the aircraft. The slant range distance to the base of feature 4 (SR_b) is less than the slant range distance to the top SR_t. Radar layover is much more prevalent in the near range than in the far range.

3.5 Radar Shadow

Shadows which are usually present in aerial photography are a function of both the position of camera and sun. Radar provides its own "illumination" and radar shadows are always 'created' on that side of a

---

[8] Discussion in part summarized from Barr, (1968)

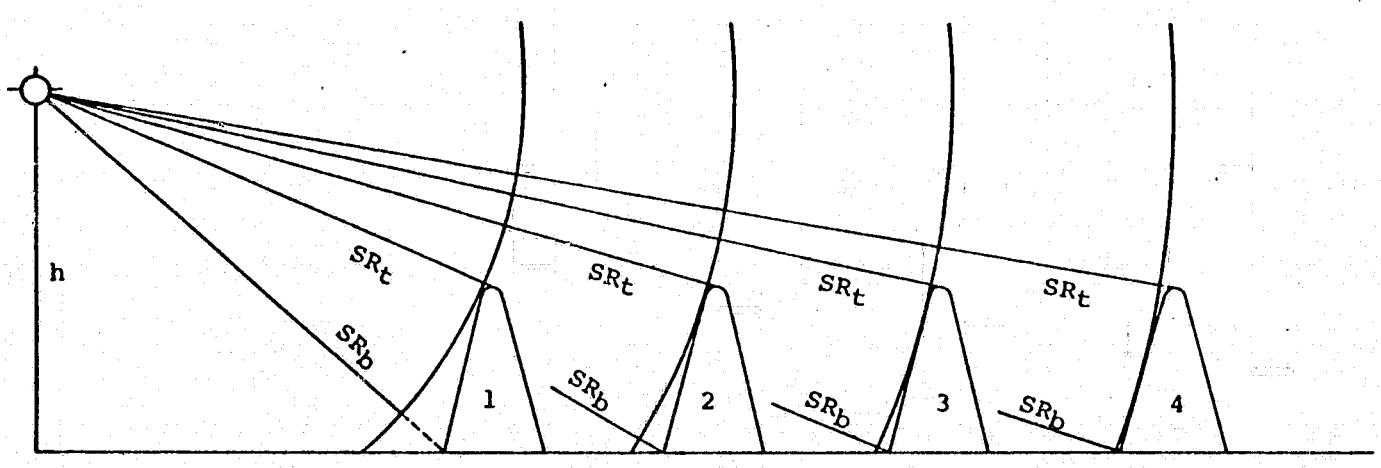

Figure 3.10 Radar layover, a function of the slant range to the transmitter.

terrain feature most distant from the transmitter. The radiated energy does not pass through objects, and consequently a shadow or "no show" area is produced on the far side of terrain features of even moderate relief. Radar images the terrain at comparatively low incident angles and the shadows formed on the imagery are analogous to those shadows formed on aerial photographs taken at low sun angle. Figure 3.11 illustrates the shadowing characteristics associated with SLAR systems. The shadow of terrain features (of equal height) being viewed from the near to far range will increase as the angle of incidence increases (depression angle decreases). Thus, a terrain feature which causes extensive shadowing in the far range may be completely "illuminated" in the near range.

Although some of radar's inherent distortions can, in some instances, be considered minor disadvantages for geological interpretations, these same distortions have been used advantageously for radargrammetric purposes. For example:

(1) Radar Shadowing -- Useful in determining the relative elevations of features producing the shadows (Levine, 1960; McAnerney, 1966; McCoy 1967; and Barr, 1968).

(2) Radar Foreshortening -- This distortion has been ingeneously exploited for the accurate determination of terrain slope (McCoy, 1967). This utilization of one of radar's "disadvantages" will be discussed in detail later in this study (Section 4.7).

(3) Radar Layover -- This type of distortion is useful for the determination of radar parallax, necessary in the use of stereoscopic imagery (Beatty, et al., 1965, and Barr, 1968).

3.6 Radar Topographic Mapping

While aerial photography can provide data for the production of highly accurate topographic maps, the collection of these data is severely limited by light and weather conditions. Consequently, there are many regions in the world which are poorly mapped or partially unmapped be-

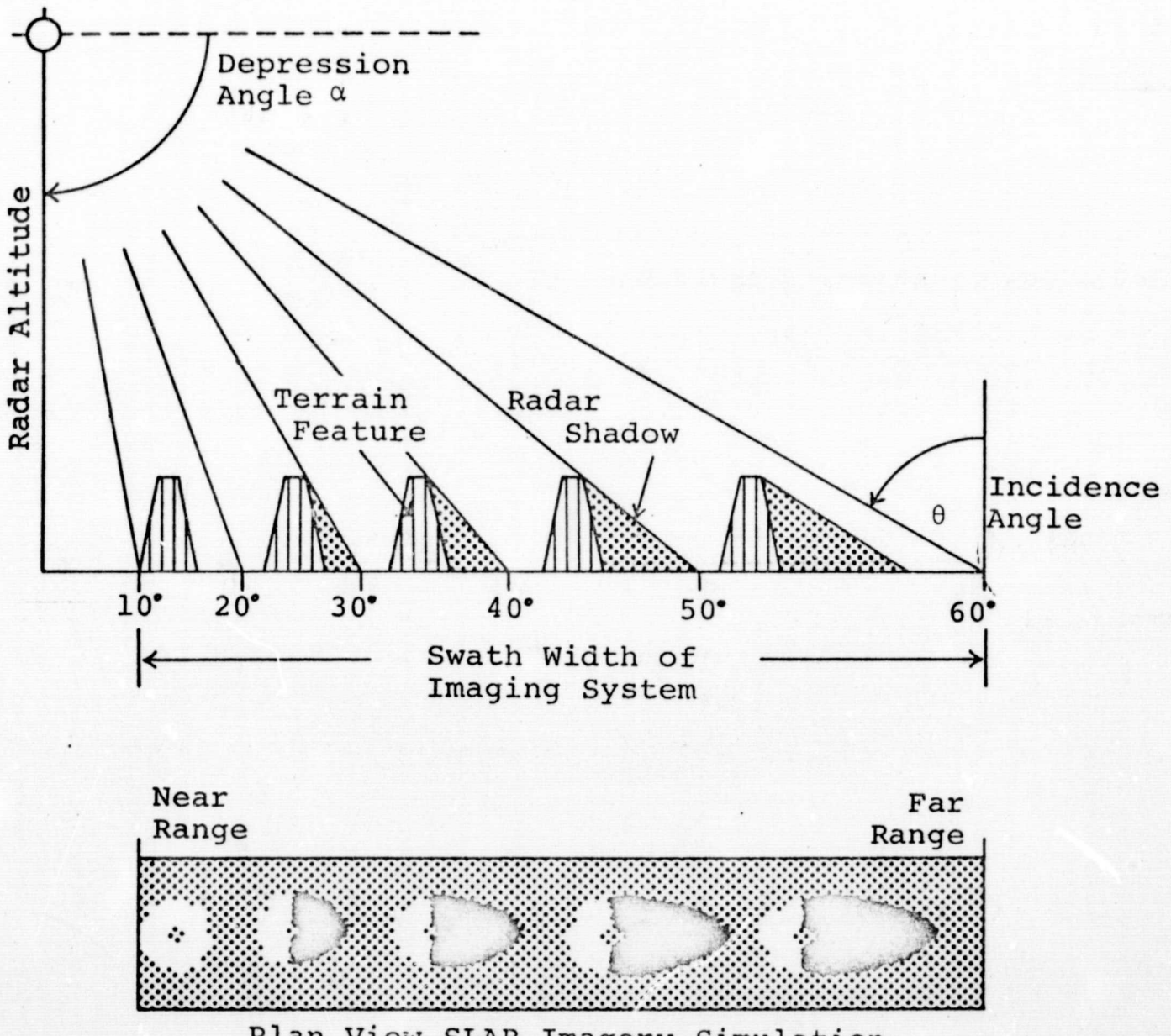

Figure 3.11 Shadowing characteristics associated with SLAR imaging systems.

cause of the inability to obtain aerial photographs. During the past decade, various all-weather mapping techniques have been evaluated by the U. S. Army Engineer Topographic Laboratories (USAETL), and SLAR systems have been selected as having the best overall qualities for topographic mapping. It was this selection which initiated an operational suitability testing of radar mapping in Panama.

One of the distinct benefits of this radar mapping program has been the compilation of original topographic map coverage (contour interval 100 meters) at a scale of 1:250,000. Although the evaluation of this topographic map was not an objective of this author's study, it is felt that a discussion of the data gathering system is intimately associated with the acquisition of the Panama imagery. Similarly, a suitable topographic map is a fundamental requisite for most geological reconnaissance studies.

3.6.1 Radar Interferometer[9]

Topographic information suitable for contour mapping can be obtained simultaneously with SLAR imagery by using interferometric techniques. Two parallel antennas are displaced vertically from each other, at a preset distance. The signal (or wave) arriving at one antenna from a specific terrain point will have a certain phase relationship relative to the signal received at the other antenna. Thus, if the crest of a wave reradiated by a terrain feature is received at one antenna, while a trough is received at the other antenna, then the addition of the electrical signals will result in zero signal return. This null point (maximum out of phase) will occur at a fixed depression angle below the antenna boresight (perpendicular bisector of the line connecting the two antennas) as shown in Figure 3.12. All other terrain features at the same depression angle are also in the null and furnish maximum out of phase signals to the antennas.

---

[9]Discussion summarized from Levine, et al., (1966)

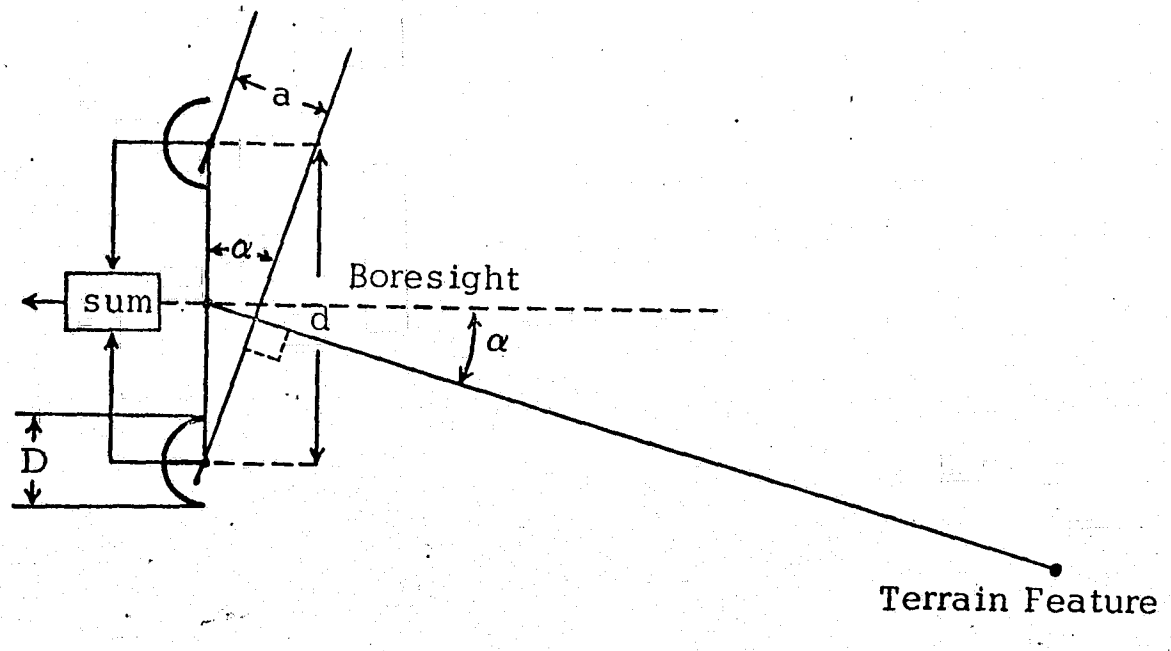

Figure 3.12 Radar Topographic Mapping. Interferometric Model (Modified from Levine, et al., 1966).

The derivation of single or multiple null angles is shown in Figure 3.12. A wave front (surface of equal field strength at any instant) reaches the lower antenna before the upper one, and the distance is a function of the time taken to traverse the distance a, where

$$a = d\sin\alpha$$

or in wavelengths

$$\frac{a}{\lambda} = \frac{d}{\lambda}\sin\alpha$$

Therefore, whenever a is $\lambda/2$, or an integral number of wavelengths greater than $\lambda/2$, the return signals cancel and a null occurs for

$$\frac{d}{\lambda}\sin\alpha = n + \frac{1}{2},\ n = 0,\ 1,\ 2,\ 3,\ 4....$$

The angular spacing between nulls $\Delta\alpha$ is approximately

$$\Delta\alpha \doteq \frac{\lambda}{d}$$

The entire range of angles from which waves can be accepted for a given antenna is λ/D, where D is the antenna (aperture) height, and the number of obtainable nulls is

$$N = \frac{d}{D}$$

3.7 Radar Mosaic

A cursory examination of the uncontrolled radar mosaic (Figure 2.3) can lead to the erroneous conclusion that the mosaic represents accurate presentation of the terrain configuration. The mosaic at first appears to provide the geologist with an accurate portrayal of the landscape similar to a shaded-relief map, revealing detail far greater than presented on a physiographic map of comparable scale; however, upon scrutiny numerous errors of varying magnitude become evident. Because the radar mosaic was originally the only suitable base map for the Darien area, a considerable amount of time was spent in an attempt to correct or at least document the errors. The majority of the errors appear to be inherent in mosaic construction utilizing unrectified slant range imagery. When overlapping strips of radar imagery (obtained from opposing look-directions, i.e., 180 degrees apart) were mosaicked, topographic inversion added to the difficulty of a point by point comparison and the detection of errors.

Presenting an accurate picture of surface drainage (an integral part of base map construction) on the uncontrolled radar mosaic was an insurmountable task. The inherent difficulties of mosaicking a slant range presentation (closely analogous to trying to mosaic oblique aerial photographs) has introduced areas of redundancy and omissions as well as offset along both X and Y axes. Drainage basins and segments of streams were duplicated, deleted, or aligned improperly in relation to other basins when the splice was around the basin, or in relation to the streams within the basin when the splice was down the thalweg. Differences of geometry between the single flight coverage used on the radar mosaic and multiple flight coverage on the original radar imagery also added to the overall problem of transferring information from the original imagery to a suitable base map.

Final documentation of the errors in the mosaic is presented in Figure 3.13. Areas of duplication have been outlined and indicated by diagonal lines running roughly north to south. X's have been used to indicate that a segment of the landscape has been omitted. Further indication is given by the symbols DB, PDB, and MM which respectively mean omission of a complete drainage basin, part of a drainage basin, or river meanders. Offset has been corrected, as best possible, by the use of double pointed lines, and the region at each end of the line should be juxtaposed. Two areas indicated by diagonal lines extending from east to west are believed to be incorrect, but whether the error is duplication or omission or a combination of the two cannot be determined.

Fortunately, the availability of a radar-derived topographic map (prepared from rectified radar imagery) eliminated using the uncontrolled radar mosaic as a base map; however, it is felt that a presentation of some of the errors inherent in slant range image mosaicking should be illustrated in this particular study.

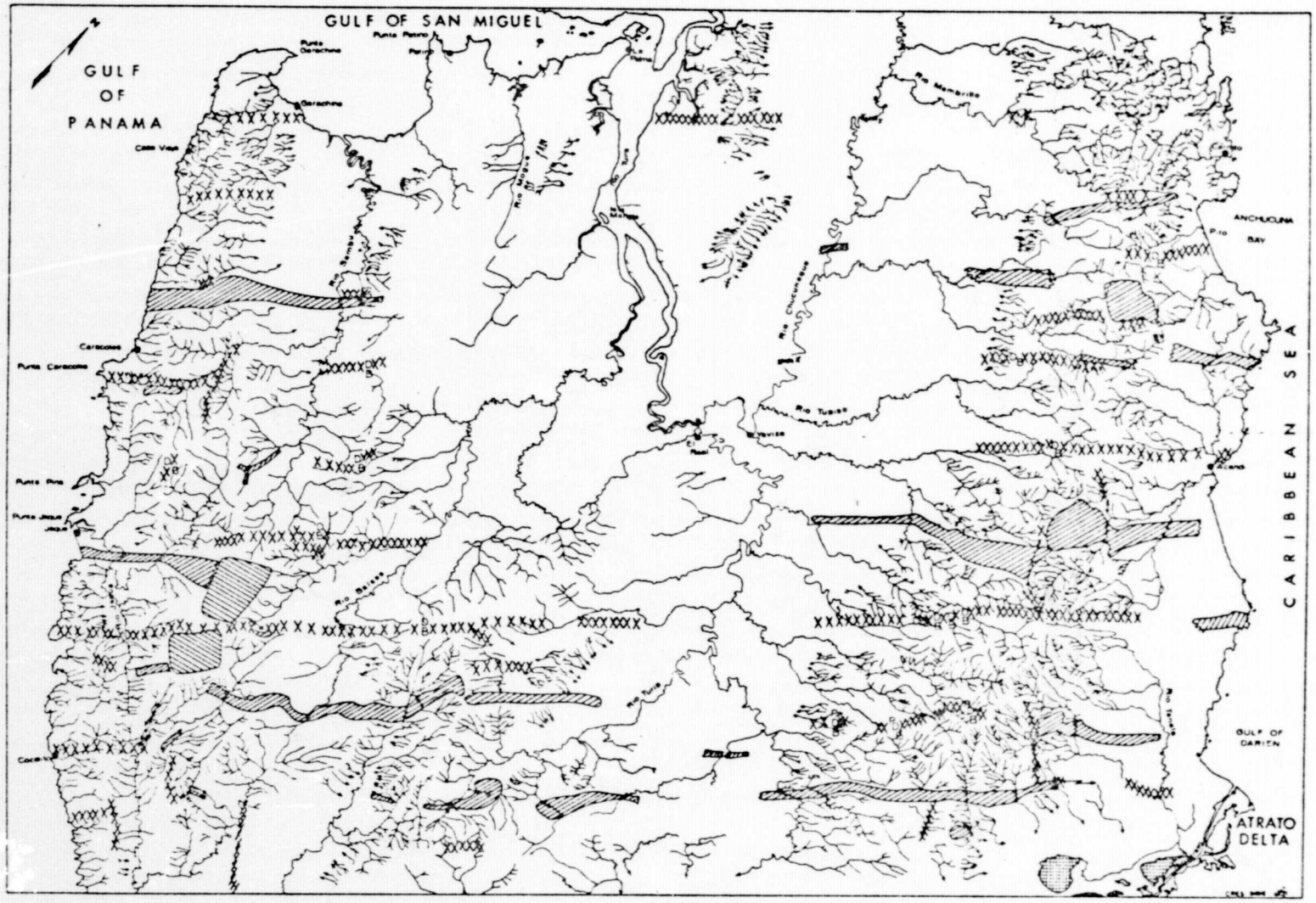

Figure 3.13 Documentation of errors incorporated in the radar mosaic (Figure 2.3).

CHAPTER 4

RADAR IMAGERY INTERPRETATION

When using most remote sensors which are concerned with any part of the electromagnetic spectrum other than visible light, the geologist is initially handicapped because he cannot normally utilize the interpretive techniques which were developed through experience. Instead, the geologist must discover new "signatures" which may yield clues to identifying a particular terrain feature as it appears on the output array of any sensing system. With the output array of SLAR systems (radar imagery) however, (aside from the inconvenience of limited stereoscopic vision) basic interpretive techniques developed for photogeologic interpretation are quite applicable. Most competent photogeologists will find the transition from interpreting aerial photographs to interpreting radar imagery very similar to the transition required for changes from photography to infrared imagery.

To those unfamiliar with techniques in photogeologic interpretation it sometimes comes as a surprise to find that effective interpretation can be accomplished even when a canopy of vegetation masks the terrain. Especially for photogeologic studies using large scale photography (1:20,000), foliage may inhibit interpretation, but by no means prevents it. As photographic scale diminishes, the interpretive disadvantage of vegetal cover commonly lessens because gross features become more obvious. The radar system used to gather the imagery of Darien does not possess significant vegetation penetration capability, and consequently the interpretation was performed upon imagery which basically portrayed the top of a continuous canopy of jungle vegetation. However, it is a natural assumption that in the moist tropics, and especially the tropical rain forest such as that found in the Darien area, that certain edaphic factors which are directly attributable to parent material should be reflected in the floristic composition, and thus enable inferences to be made as to rock type.

The geologist who utilizes reconnaissance data for geologic syntheses usually has four ultimate objectives: (1) correlation of out-crops from one location to another, (2) determination of the stratigraphic sequence, (3) delimitation of rock types or lithologic units, and (4) determination of geologic structure. Radar imagery provides the geologist with a terrain format approximating a three-dimensional strip map which can reveal varying amounts of geologic information depending on the terrain environment and stage of erosional development.

The process of interpreting and mapping geologic features from radar imagery is both complex, and almost totally qualitative in nature. The experience, judgement, and ability of the interpreter to evaluate the significance of many different types of terrain data are directly reflected in final interpretive product. Therefore, as with photogeology,[10] radargeology must be approached with the full realization that geologic interpretation can only be accomplished if adequate scrutiny is given to all of the following elements: (1) the pattern and distribution of outcrops, (2) drainage, (3) vegetation, and (4) landforms and structural configuration. Similarly, the analysis of tone, texture, shape, and pattern become recognition elements on the radar imagery which contribute to the interpretation of geologic data. It is important to emphasize that the resultant product is an interpretation, and as such, the information inferred is of a tentative nature until proven in the field.

4.1 Tone

Tone can be defined as the intensity of signal backscatter, converted to a video signal and recorded on photographic film as shades of gray from black to white. The tone on radar imagery in vegetated areas is dependent on such variables as spacing of individual trees, spacing of branches, size and density of leaves, and orientation and slope configuration of the plant

[10] For detailed discussions of photogeologic interpretation the reader is referred to Miller, 1961; Ray, 1960; Lueder, 1959; and Colwell, 1952.

community. Where vegetation is sparse (such as in arid and semi-arid environments), the radar imagery tone is influenced by the scattering characteristics of the terrain, i.e. surface roughness, geometric orientation, and effective incidence angle. Tonal variations can be seen on all radar imagery, and depending on the terrain environment, analysis of these tonal contrasts can contribute much information for geologic interpretation. For example, tonal contrasts can be correlated with rock type in the Virgin Mountains area of Arizona (Figure 4.1A); differences in tonal variations between aerial photography and radar imagery are also illustrated in Figure 4.1B,C.

Black - Radar shadow (example, southeast of Area D).
Dark Gray - Areas of Tertiary lava (G,J,O) and areas of fine-grained sediments (N,P).
Medium Gray - Alluvial sediments (A,R) and both flat lying and dipping Paleozoic strata (E,H,I).
Light Gray to White - Area of Conglomerates (west of M).

Tonal variations on the radar imagery of the Darien area yielded minimal interpretive information because of the transitional character of the jungle vegetation (i.e., no distinctive boundaries). However, in the mangrove swamp areas, and along the flood plains of major rivers, the signal scattering from certain plant communities resulted in varying tonal contrasts which did contribute indirectly to the geological interpretation.

4.2 Texture

Texture can be defined as the degree of erosional dissection which results in an aggregate of unit features reflected in the terrain configuration. Examples of various "terrain textures" which are indicative of certain rock

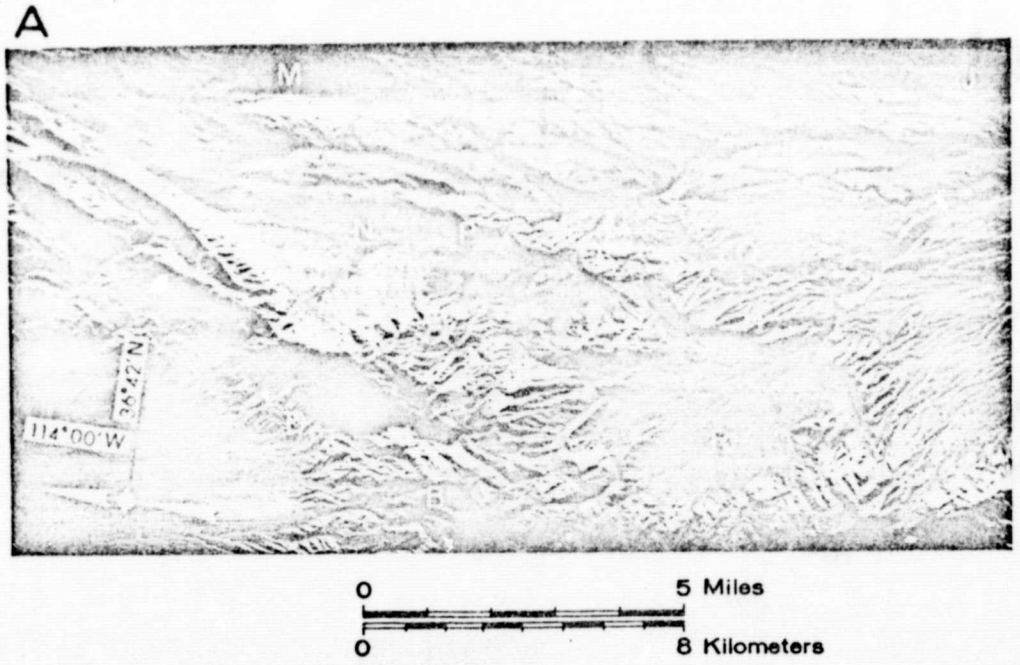

VIRGIN MOUNTAINS AREA, ARIZONA

Figure 4.1 Virgin Mountains area, Arizona. (A) Radar imagery. (B) Aerial photograph. (C) Radar imagery enlargement 2x.

types of the Darien area are illustrated in Figures 4.2 and 4.3.[11] Fine-textured drainage which is indicative of non-resistant fine-grained sedimentary rocks is illustrated in Figure 4.2 i,k,l; and Figure 4.3 a,g,h,l; whereas the coarser-grained sediments generally display a coarse-textured drainage as illustrated in Figure 4.2 h, left half; j, right half; Figure 4.3 a,c. In contrast to the texture of sedimentary rocks, igneous rocks generally have a massive appearance on radar imagery distinguished by rugged and peaked divides as shown in Figure 4.2 a,b,d,e; Figure 4.3 k, right half; or where erosion has nearly base-leveled an area, they may be reflected in a hummocky, rounded topography as in Figure 4.2c.

The differentiation of rock type on radar imagery using texture as a discriminant is especially well illustrated in Figure 4.1A (Virgin Mountains). Areas J, G, and O which represent different locations on the same lithologic unit (flat-lying Tertiary basalts) have a topographic texture that contrast sharply with the exposed, underlying Paleozoic sedimentary strata. Similarly, in area M, the feather-like texture of sedimentary strata also appears as an anomolous texture among the flat lying lavas. The hackly texture of the igneous rocks at location D contrast with the folded sediments of area C.

4.3 Shape

Shape can be defined as a spatial form with respect to a relatively constant contour or periphery (Ray, 1960). Numerous geologic features can be interpreted primarily by their shape alone, i.e. alluvial fans which can

---

[11] The geographic center of each "Topographic texture" can be referenced to Plate I as follows: Figure 4.2 (a) 8°13'N, 77°13'W; (b) 8°24'N, 77°23'W; (c) 8°12'N, 78°12'W; (d) 7°19'N, 77°51'W; (e) 7°52'N, 78°04'W; (f) 8°00'N, 78°08'W; (g) 7°47'N, 77°31'W; (h) 8°33'N, 77°34'W; (i) 8°04'N, 77°39'W; (j) 7°59'N, 77°35'W; (k) 7°53'N, 77°28'W; (l) 8°16'N, 78°11'W.

Figure 4.3 (a) 8°19'N, 77°40'W; (b) 8°11'N, 77°35'W; (c) 8°10'N, 77°30'W; (d) 8°20'N, 77°52'W; (e) 8°11'N, 77°47'W; (f) 8°00'N, 78°08'W; (g) 7°56'N, 77°53'W; (h) 7°56'N, 78°14'W; (i) 8°09'N, 78°03'W; (j) 7°37'N, 77°48'W; (k) 7°33'N, 77°41'W; (l) 8°21'N, 77°13'W.

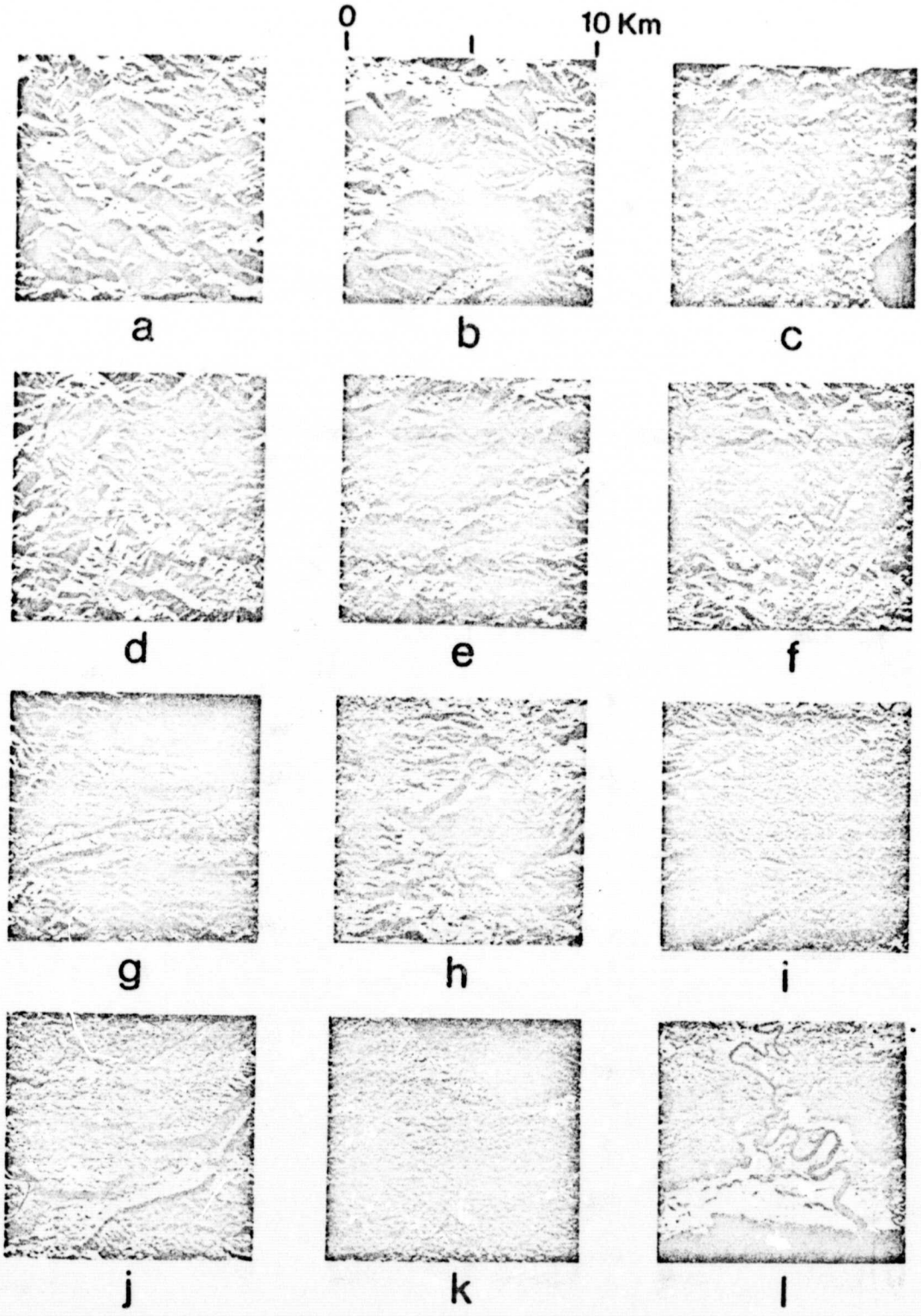

"TOPOGRAPHIC TEXTURE" FROM RADAR IMAGERY

DARIEN PROVINCE, PANAMA

Figure 4.2

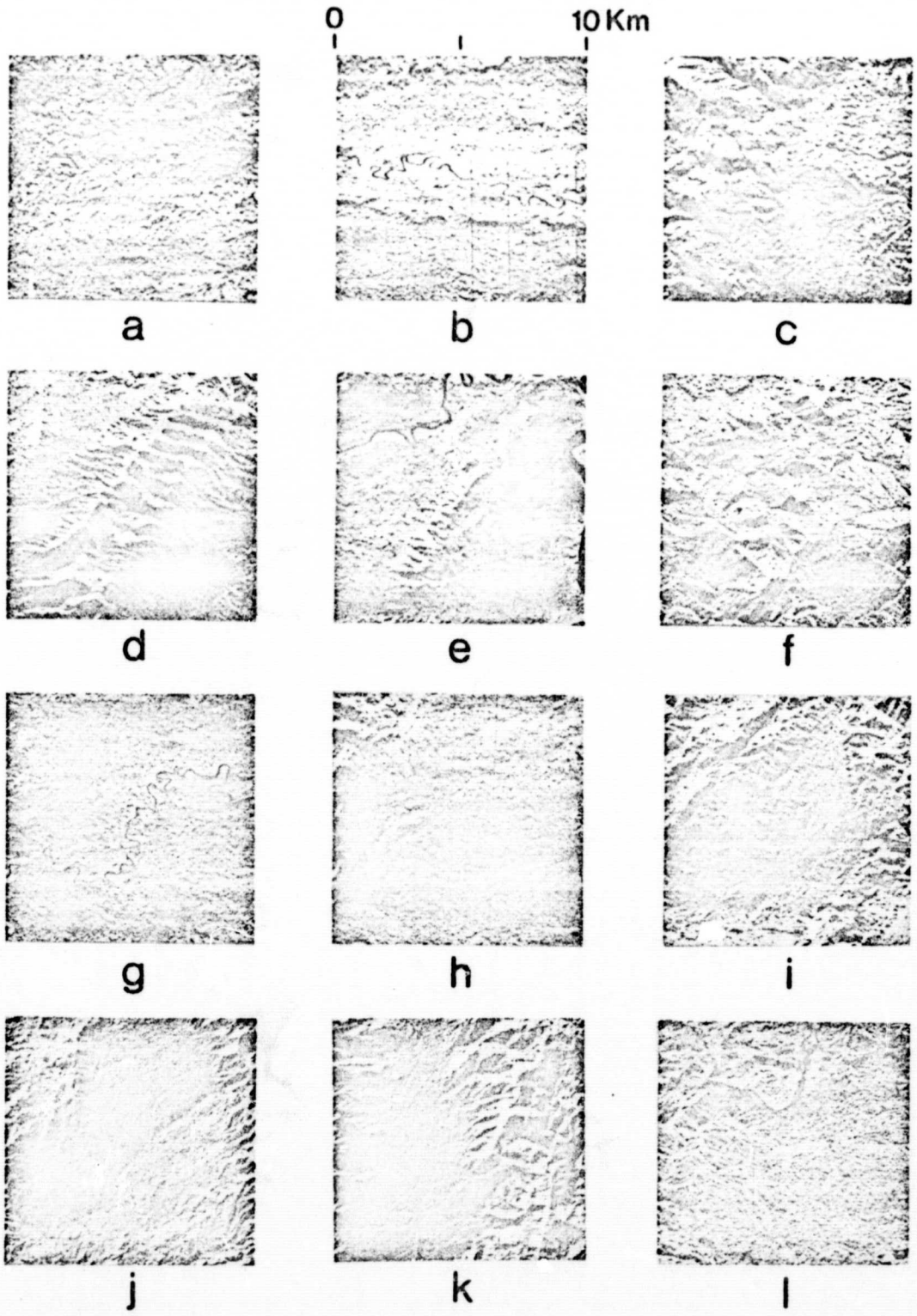

"TOPOGRAPHIC TEXTURE" FROM RADAR IMAGERY
DARIEN PROVINCE, PANAMA

Figure 4.3

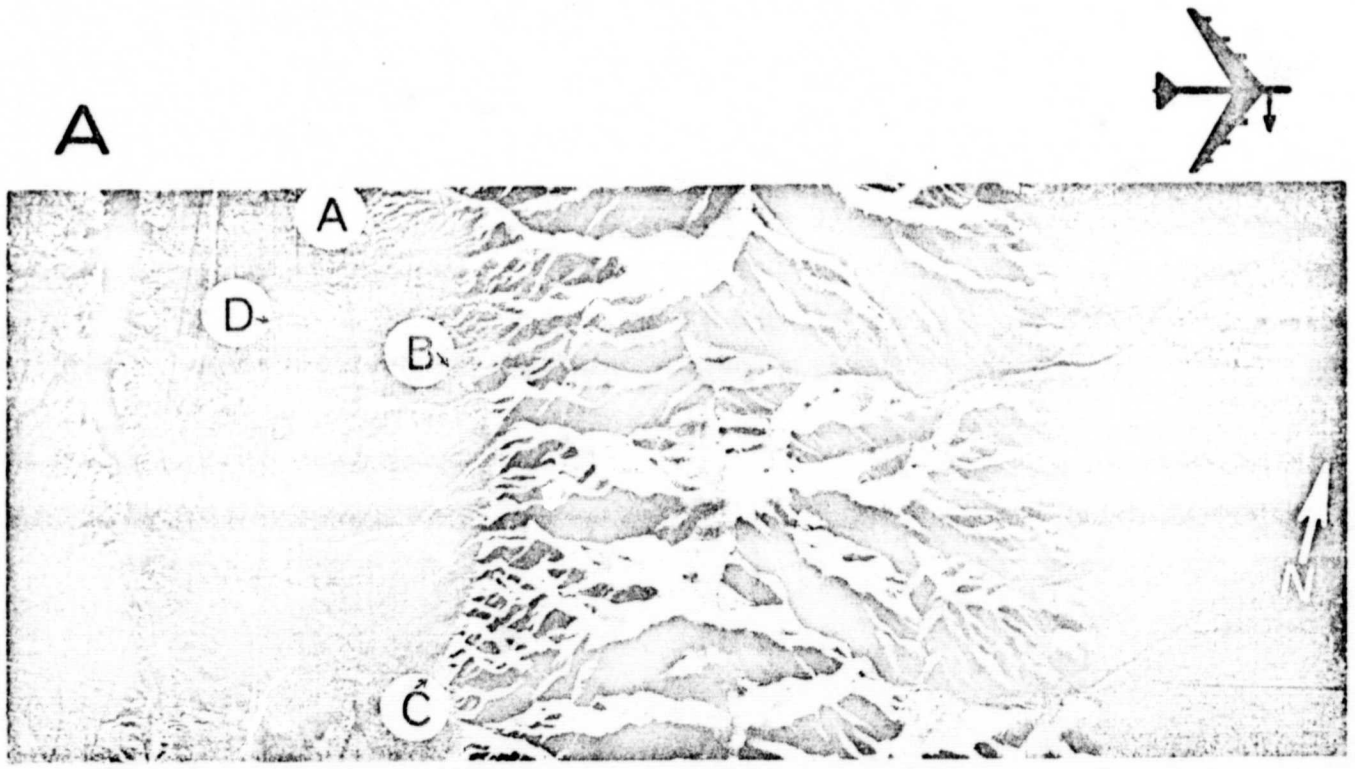

CENTRAL HUMBOLDT RANGE, NEVADA

Figure 4.4 Central Humboldt Range, Nevada
(A) Look-direction, south. (B) Look-direction, north.

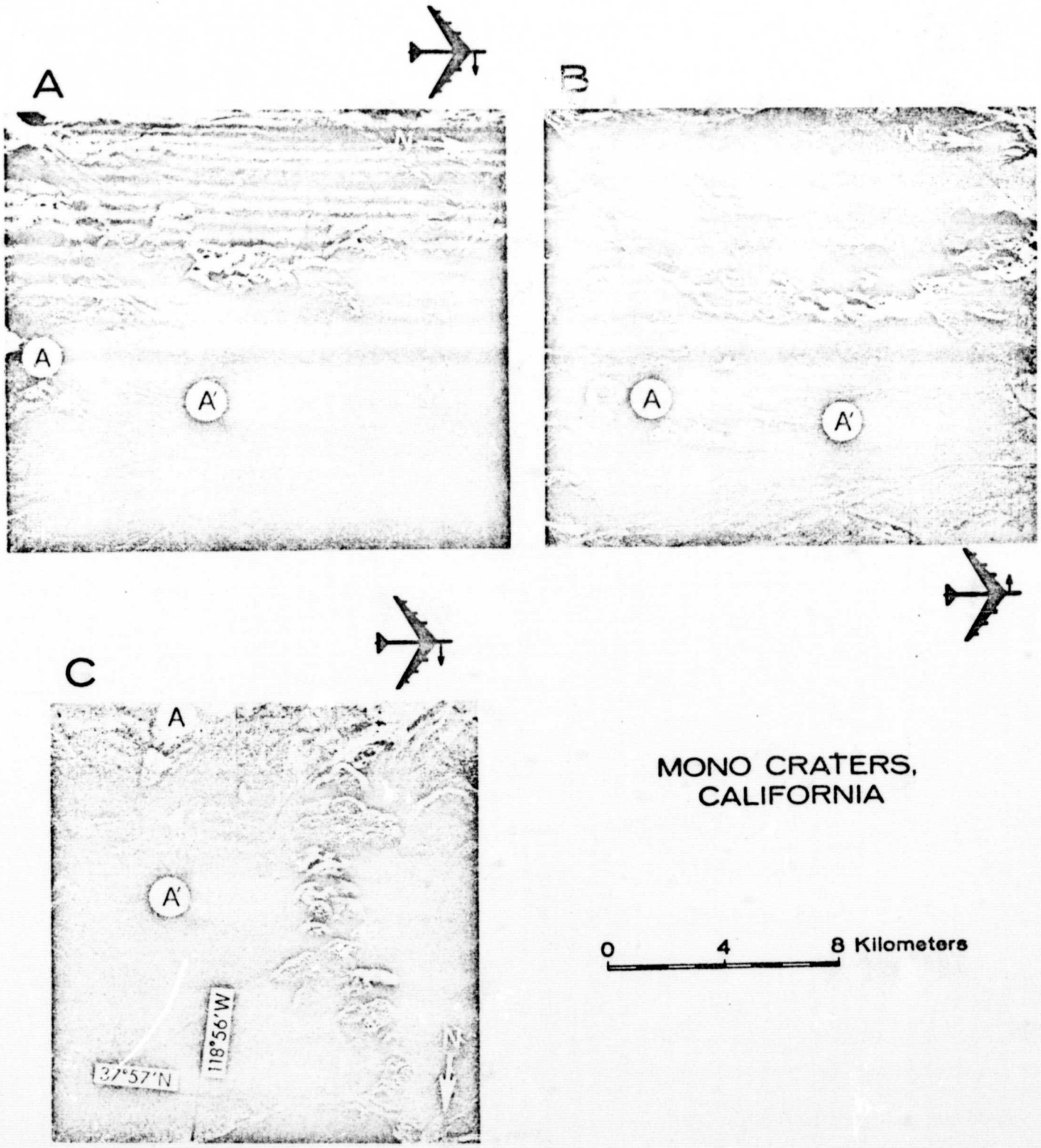

Figure 4.5 Mono Craters, California
(A) Look-direction, east. (B) Look-direction, west. (C) Look-direction, north.

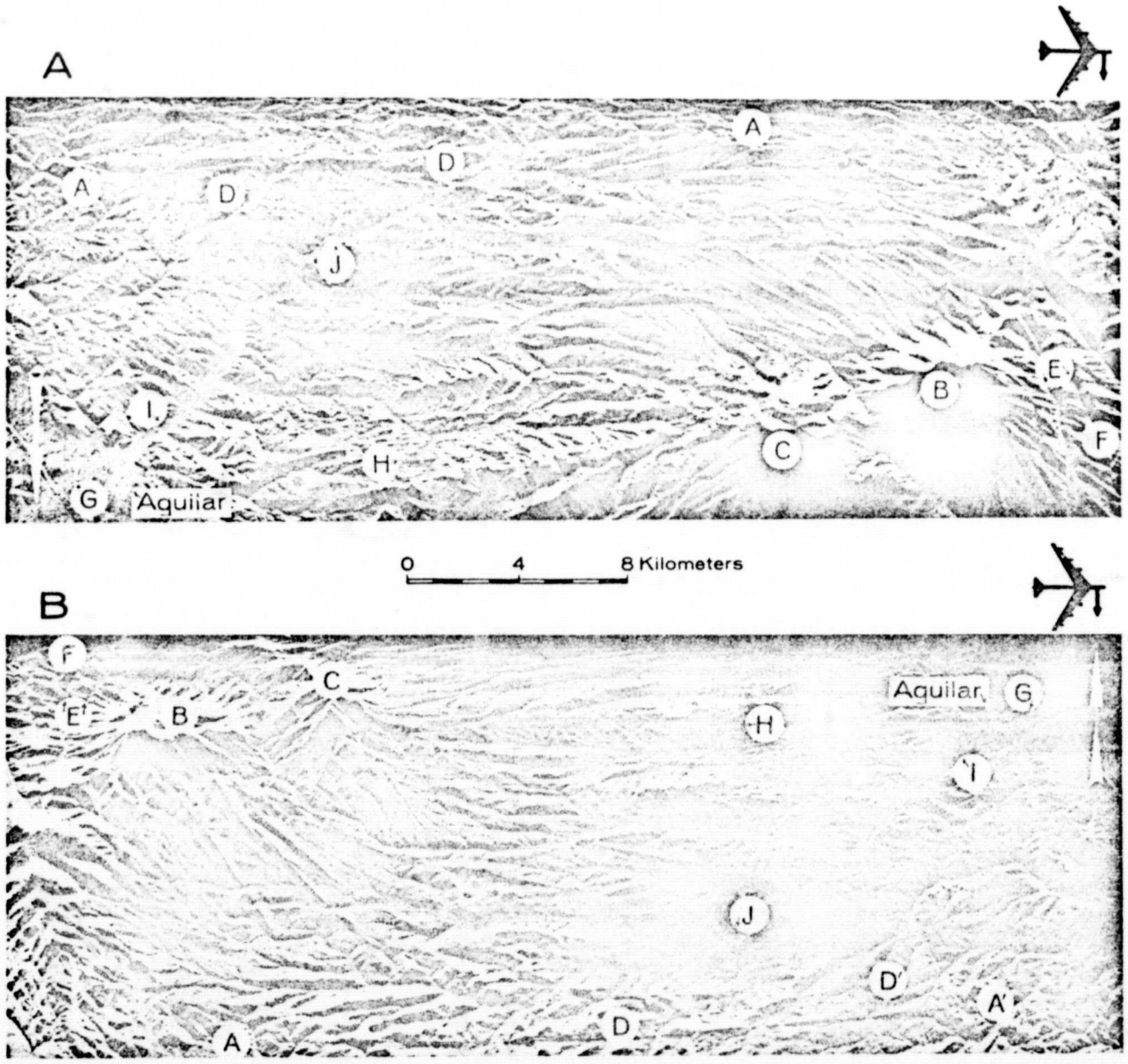

SPANISH PEAKS, COLORADO

Figure 4.6 Spanish Peaks, Colorado
(A) Look-direction, north. (B) Look-direction, south.

exposed to erosion (which is the case in Darien for the rock sequence underlying Eocene strata), the flows are indistinguishable from resistant sedimentary rocks. This is not a disadvantage unique to radar imagery, however, since the same interpretive problem faces the photogeologist (Ray, 1960; Smith 1943).

4.5.1 Igneous Intrusive

Intrusive igenous rocks commonly have a wide variety of structural relations with the surrounding country rock that can usually aid in their interpretation from radar imagery. The massive appearance, rugged terrain, domal areas reflecting radial drainage, dike systems, and intricate criss-cross pattern of linear features all contribute to the recognition of this rock type.

4.6 Lithologic Interpretation - Sedimentary

The two main problems in studying sedimentary rocks on radar imagery, as in the field, are those of determining the stratigraphic sequence and of making correlations from place to place. The criteria employed are borrowed from field practice and certain of these are more effectively applied on imagery than in the field, owing to the better perspective afforded. The relative age of beds is simply ascertained by the law of superposition, and subdivision of a provisional empirical character may be made purely on the basis of surface expression.

The physical expression of folding or alternation of bedding in most sedimentary rocks is fundamental to their interpretation on radar imagery. Differential erosion of sedimentary rocks usually provides the unique topographic expression which can be interpreted on the imagery. Generally, fine-grained sediments are reflected in fine textured drainage (Figure 4.2 k, i; Figure 4.3 a, g, h, l), and similarly, coarse-textured drainage suggests resistant coarse-grained sedimentary rocks (Figure 4.2 h, left half; Figure 4.3 c), although the drainage in some cases can be more indicative of structure than of lithology (Figure 4.3 d, e). Drainage characteristics may

suggest broad rock groupings, but no one drainage pattern is diagnostic of sedimentary rocks, although annular and trellis drainage generally suggest sedimentary rocks or close metamorphic equivalents (Ray, 1960).

Where exposures are adequate and structure is not too complicated, a continuous sequence may be worked out, with subdivisions distinguished on the basis of tone, apparent thickness, and texture. Later, field work will translate these units into terms of actual lithology or established stratigraphic divisions. Lithologic identification cannot be conclusively determined from the interpretation of radar imagery alone. When using radar imagery for reconnaissance mapping, the stratigraphic terminology used will be dependent upon the amount and detail of the collateral data available.

4.6.1 Unconsolidated Sediments

The identification of most surficial deposits on radar imagery is highly dependent on landform analysis association, i.e., wide river valleys, meandering stream channels, etc. Although alluvial deposits of sand and gravel were evident in the field along some of the mountain streams and along the major tributaries of the Darien, these sediments cannot be defined on the radar imagery except at the mouth of the Rio Tuira, Rio Mogue, Rio Sambu, and Rio Jaque which have been mapped through inference, i.e., broad river basins. The alluvial deposits mapped along the beaches of the Caribbean coast have been identified because of the associated beach ridges. Some of the depositional sites of alluvial-sea muds, which develop contemporaneously with mangrove swamp evolution, can be inferred through interpretation of radar imagery. The foliage of the tidal mangrove swamps produces a high degree of radar signal scattering which results in a distinctive texture and tone on the radar imagery (Figure 4.2 1).

4.7 Strike and Dip

Through the analysis of radar imagery, topographically expressed

folded strata can be readily identified (Figure 4.3 d,e). Particularly in areas where slightly deformed rocks are well exposed, dipping strata may be clearly defined in landform configurations such as erosional hogbacks (Figure 4.1A, area E; Figure 4.2 h; and Figure 4.3 c).

Slope measurements are an integral part of any detailed geomorphic or hydrologic analysis, and where the dip of strata approximates the terrain slope, dip slope measurements can be equally important in geological studies. When the terrain configuration is indicative of a situation where terrain slope and bedding dip are approximately equal, the strike and relative dip can be estimated. Under certain conditions, however, precise dip measurements can be obtained directly from monoscopic radar imagery. Methods for terrain slope measurements from monoscopic radar imagery, utilizing two different radar "looks" of the same terrain slope, were revealed in a study by McCoy (1967) conducted at the University of Kansas.

McCoy's methods were used for all of the numerical dip measurements indicated on the geological reconnaissance map (Plate I), and have been calculated as follows:

If the same slope is viewed from two opposite directions along parallel flight paths (Figure 4.7), then the angle of slope may be determined as a function of two depression angles (Θ_i measured in degrees) and two slant range measurements (L_i), i.e., $\alpha = f(\Theta_1, \Theta_2, L_1, L_2)$, (Dalke and McCoy 1966).

In order to express the relationship of L_1 and L_2, it is convenient to make a ratio $R_L = L_2/L_1$, and thus reduce the length parameter to one value. The following steps lead to a solution of the slope angle α.

$$\frac{L_2}{L_1} = R_L = \frac{\cos(\alpha + \Theta_2)}{\cos(\alpha - \Theta_1)}$$

$$R_L \cos(\alpha - \Theta_1) = \cos(\alpha + \Theta_2)$$

$$R_L (\cos\alpha \cos\Theta_1 + \sin\alpha \sin\Theta_1) = \cos\alpha\cos\Theta_2 - \sin\alpha\sin\Theta_2$$

$\alpha = 20^{\circ}$

$\theta_1 = 50^{\circ}$

$\theta_2 = 50^{\circ}$

$L_1 = 2.3$

$L_2 = 0.9$

$R_L = .39$

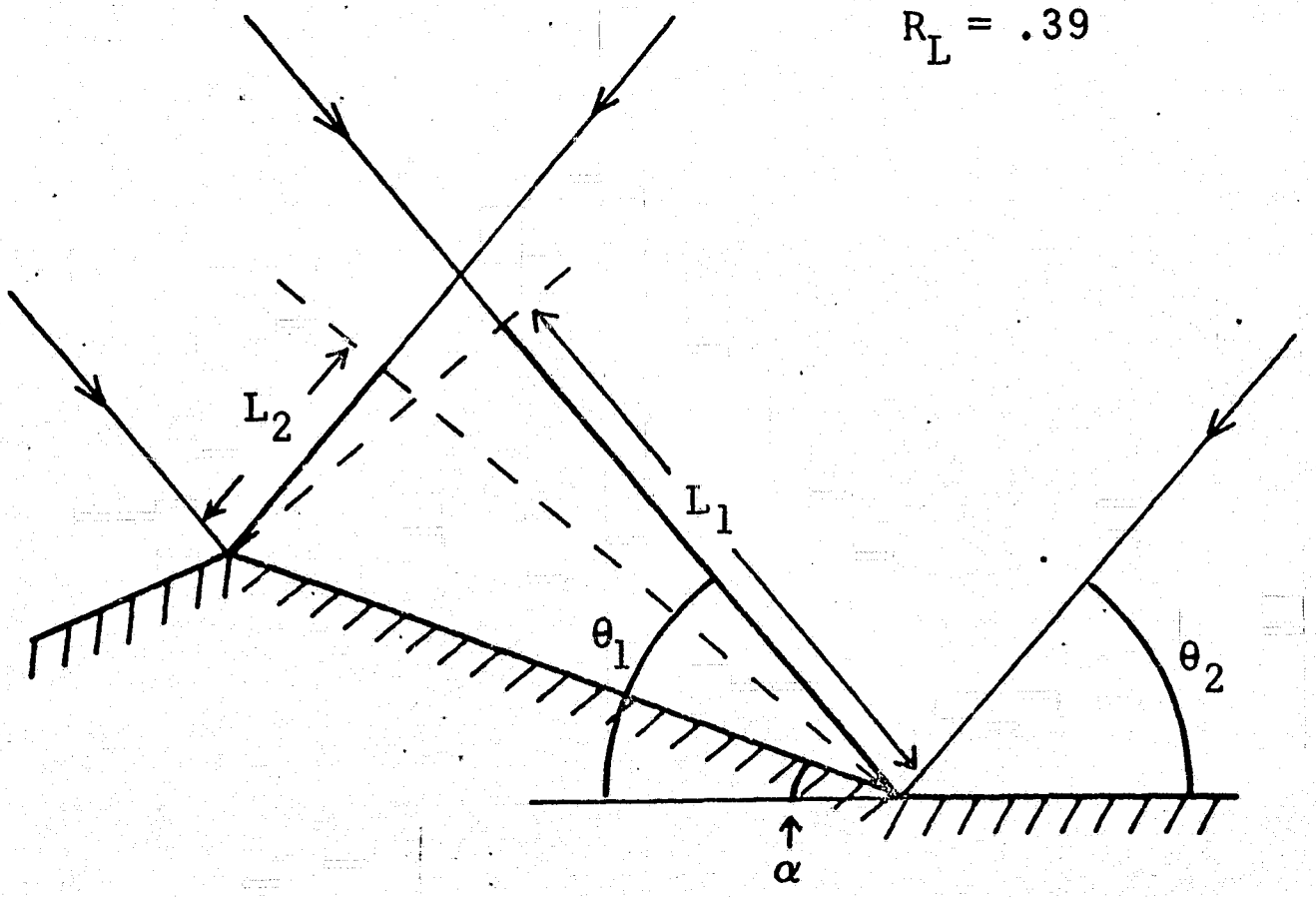

Figure 4.7 Viewing the terrain slope, α, from two different look-directions, resulting in two depression angles, θ, and two slant range lengths, L (from McCoy, 1967).

$$R_L(\cos\Theta_1 + \tan\alpha\sin\Theta_1) = \cos\Theta_2 - \tan\alpha\sin\Theta_2$$

$$\tan\alpha = \frac{\cos\Theta_2 - R_L\cos\Theta_1}{R_L\sin\Theta_1 + \sin\Theta_2} \qquad (1)$$

Equation (1) expresses the relationship among the parameters marked in Figure 4.7. A nomogram for equation (1) provides easy entry of known variables for solution of terrain slope, (Figure 4.8). The measurements in Figure 4.7 are entered into the nomogram (Figure 4.8) as shown by the dashed line. Application of this nomogram requires the following procedure:

1. The longer slant length measurement is labeled L_1 in order to maintain $R_L < 1$.
2. The depression angle corresponding to L_1 is called Θ_1.
3. The R_L value is entered along the appropriate curved scale of the nomogram.
4. The Θ_1 value is entered along the correct radial line.
5. The intersection of the R_L line and the Θ_1 line creates point #1.
6. Θ_2 plotted on the appropriate curved scale gives point #2.
7. Place a straight edge on point #1 and #2 and read along the linear scale at the bottom of the nomogram.

Two basic assumptions are made relative to L_i and Θ_i: first, both images are the same scale, and second, the depression angles at all points along the terrain slope are equal. In cases where these criteria are not met, conversion factors may be employed. The reader is referred to McCoy's (1967) study for further discussion.

4.7.1 Limitations

The conformity of dip slope measurements obtained from the radar imagery of Darien and the actual dip slope on the ground could not be

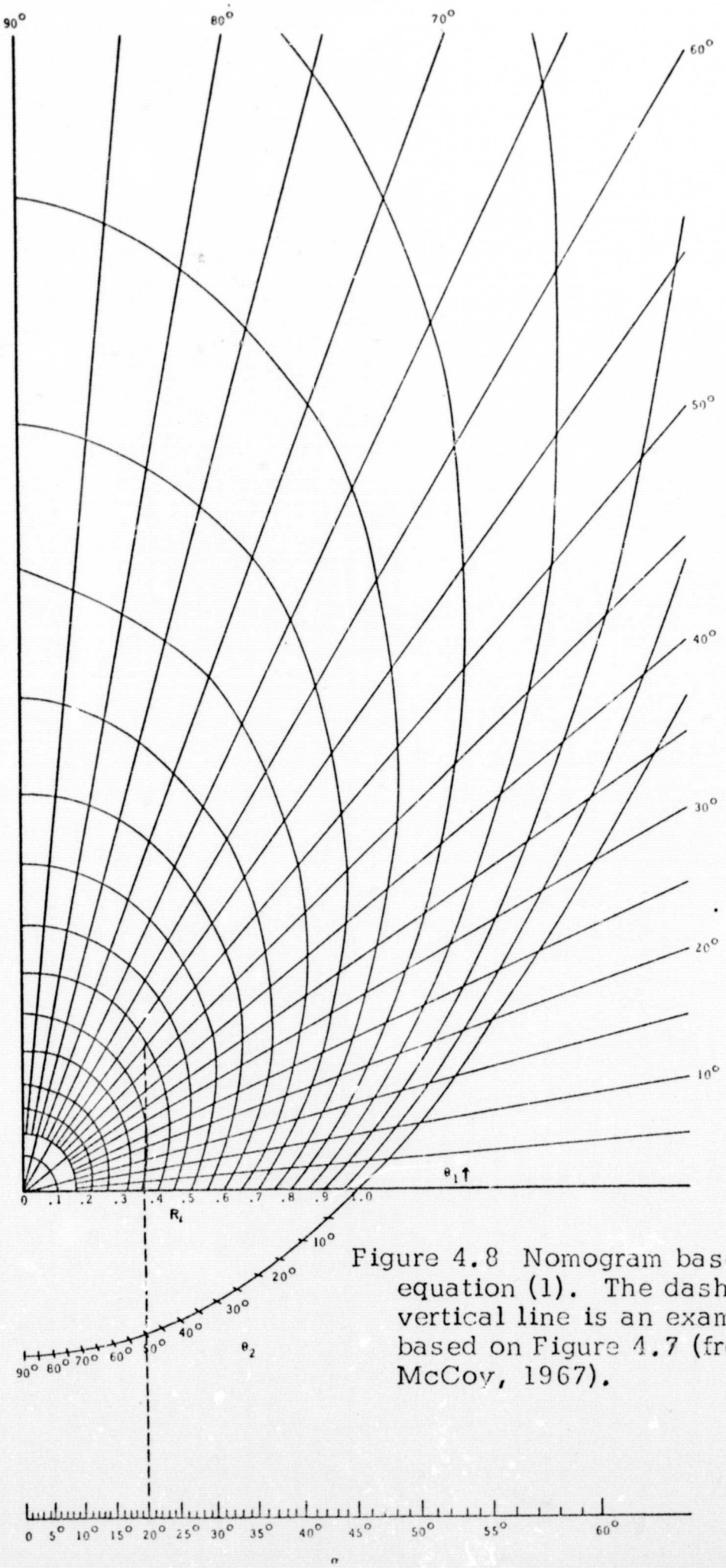

Figure 4.8 Nomogram based on equation (1). The dashed vertical line is an example based on Figure 4.7 (from McCoy, 1967).

determined because of the limited field data available; however, in McCoy's study, radar-derived terrain slopes were within one degree of the map-derived measurements. The accuracy of radar-derived dip slopes is highly dependent on precisely locating the same two terrain points on two different images between which the slant range slope lengths are measured. Inherent imagery distortions previously discussed makes this phase of dip slope determination exceedingly difficult, a fact also noted by McCoy. The fact that the accuracy of slope measurements is dependent on lengths measured perpendicular or approximately perpendicular to ground track also limits the flexibility of gathering dip slope data.

4.8 Faults and Joints

The distinction between faulting and jointing on radar imagery, as with airphoto interpretation, is often very difficult. As pointed out by Lueder (1959) when discussing photogeologic interpretive methods in areas in which conclusive fault evidence is absent, it is common to consider the longer, stronger linears as faults, whereas the shorter criss-crossing linears are interpreted as joints or joint systems. In recent studies concerned with radar geologic interpretation (Dellwig, et al., 1966; Kirk and Walters, 1968) it has been a common practice to conform to the terminology of "undefined" linear used by Lattman (1958) for photogeologic interpretation, i.e., the term fracture trace being used to differentiate those natural linear features expressed (on aerial photographs) continuously for less than one mile, and the term lineament for those linear features expressed continuously for greater than one mile. Even though corroborative field data are extremely limited within the Darien area, the terms fault and joint have been retained in this study in order to conform with the terminology prevalent in most photogeological reconnaissance studies.

Generally, where flat-lying or gently folded sedimentary rocks are examined in the field, most joints are steeply dipping or vertical, evenly or regularly spaced, and commonly consist of two prominent sets. On aerial photographs these joints appear as intersecting lines, which may give a

blocky appearance to the topography (Ray, 1960). When considering radar imaging systems however, it is important to stress that joint systems (a group of joints with a characteristic pattern) rather than individual joints, are recorded on the radar imagery. Basically, this is a function of the resolution of the particular sensor involved, and not at all dissimilar to the reduced resolution encountered when utilizing high altitude or orbital photography for geologic interpretation. Analogous to joint patterns observed in the field, joint systems on radar imagery tend to "fingerprint" certain mappable units (Lueder, 1959) so they can be traced more readily on the imagery, or recognized in a new area under similar structural or terrain conditions. For example, in fine-grained clastic rocks, the joint systems are more closely spaced than in coarse clastic rocks. Similarly, joint systems expressed in sedimentary rocks are usually regularly spaced as contrasted with those joint systems in igneous rocks (Ray, 1960).

Side-look radars, because of their extensive areal coverage and synoptic presentation, enable the interpreter to integrate subtle topographic differences over long distances, thus providing a distinct advantage for delineating linear features which are usually indicative of faulting. Fault interpretation from radar imagery is usually based on two main recognition categories: (1) persistent linears, and (2) offsetting linear patterns or major changes in lithology, structure, vegetation, and erosional dissection.

CHAPTER 5

LOOK-DIRECTION ANALYSIS

SLAR imaging systems, because of their large areal coverage, enable the eye to integrate subtle topographic differences over long distances. This synoptic presentation in combination with an oblique angle of the incident "illumination" provides enhancement of topographic features which may not be evident on conventional aerial photography even when viewed stereoscopically. Thus, the geologist is able to see the terrain portrayed in a configuration that is normally not available to him. Many examples have been cited in the literature where radar has actually defined structural features such as lineaments and faults which had not been previously detected using normal geological reconnaissance methods (Dellwig, et al., 1968; Kirk and Walters, 1968; Hackman, 1966; MacDonald, et al., 1967; Snavely and Wagner, 1966; Fisher, in Levine, et al,, 1966; Dellwig, et al., 1966; and Cameron, 1965). Unfortunately, multiple imagery passes were not available for most of these studies, and consequently the influence of a preferred look-direction (direction orthogonal to ground track of aircraft) could not be evaluated. Similarly, because most areas were covered by only a single strip of imagery the aspect of repeatedly recognizing anomalous terrain features with multiple flight coverage has not been documented.

The radar imagery of eastern Panama and northwestern Colombia has provided multiple imagery passes (in most cases four orthogonal look-directions and in all cases, at least two) over the entire region. The imagery was also collected during a three week time period which eliminates any speculation about seasonal changes which might influence the rain forest canopy, and thus affect the radar imagery.

The Panama imagery data have been analyzed in a semi-quantitative fashion, but before discussing these data, it is necessary to illustrate specific examples where the look-direction appears to influence geologic interpretation. The various sites illustrated have been selected

both to provide case examples familiar to most geologists of specific geologic terrain environments, and because more than one strip of imagery was available for study in each area.

5.1 Spanish Peaks, Colorado

The Spanish Peaks region comprising approximately 5200 square km is located mainly in Las Animas and Huerfano Counties in south-central Colorado (Figure 5.1). This region is well known to geologists for its diverse igneous rocks and structures, and topography is dominated by intrusive and extrusive igneous rocks: stocks, plugs, dikes, and sills which have invaded the sedimentary rocks over the entire region (Johnson, 1968). Although large igneous masses are characteristic of the areas of maximum local relief (2,375 meters), dike protuberances ranging up to 30 meters in both width and height dominate the terrain of flat lying sedimentary rocks. Most dikes are members of an extensive radial dike system associated with the main igneous mass of the Spanish Peaks.

Radar imagery of this region is ideally suited for evaluating look-direction, first because of the numerous rectilinear features which are topographically expressed, and second because of the availability of two separate strips of imagery, flown from opposing look directions. When comparing the two radar images of the Spanish Peaks (Figure 4.6), the differences in shadowing by the dominant terrain features when imaged from opposite directions is especially striking. West Spanish Peak and East Spanish Peak ((B) and (C) respectively of Figure 4.6) are "illuminated" in both the near and far ranges. On image A the two peaks (B) (C) cast a large distinctive shadow in the far-range, whereas the same two features have minimal shadowing in the near-range (image B). Similarly, dikes (A)-(A') (D)-(D'), and (J) which are features #138, #149, and #196 respectively on Figure 5.1, are accentuated by shadowing in the far-range of image B, whereas these same features are less pronounced in the near range. On image A, dike (D)-(D') is subdued to such an extent that it is almost undetectable. This same distinction between the appearance of terrain

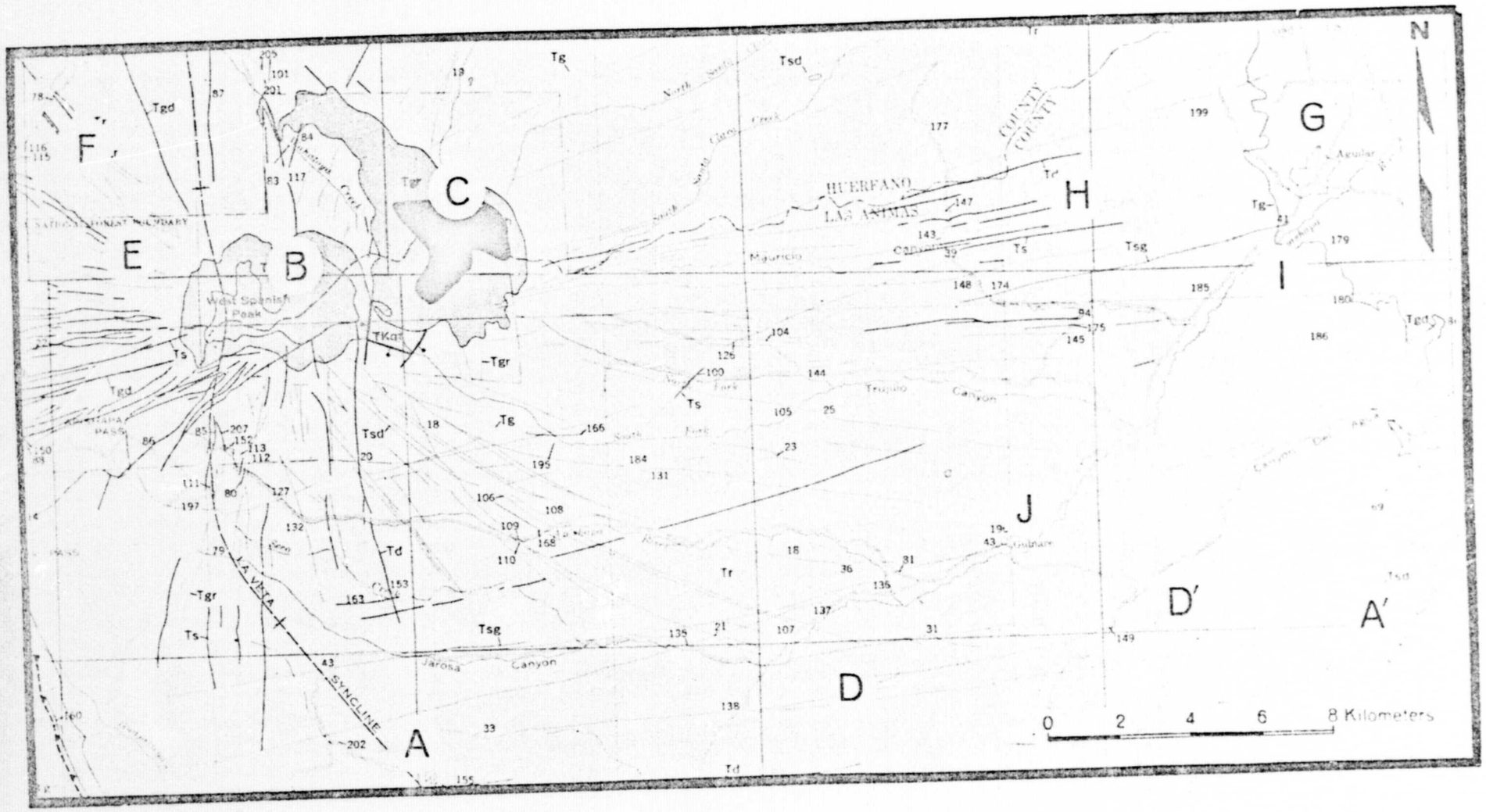

SPANISH PEAKS, COLORADO

Figure 5.1 Portion of the geologic map of the Spanish Peaks area, Colorado (after Johnson, 1968)

features in the near and far ranges is illustrated east of area (H) where a subparallel dike system is much better defined in the far-range of image A than in the near range of image B.

The imagery of Spanish Peaks also reveals the influence of look-direction on the delineation of stream drainage patterns. In the far-range of image A the channel of the Apishapa River (G) can be easily traced; however, the same stream channel in the near-range of image B is poorly defined. The perimeter of the drainage basin west of location (I) can be easily outlined on image A, but this operation is much more difficult on image B(near range).

Near range compression, a characteristic of all slant range systems (and previously illustrated in Figure 3.7A) is disadvantageous when attempting to delineate topographic features which are oblique to the flight path. The presentation of the linear valleys of Figure 4.6 in area (E) on image A(far-range) can be contrasted with area (E) of image B (near range).

5.2 Central Humboldt Range, Nevada

The Humboldt Range of western Nevada characterizes Basin and Range fault-block mountains, i.e., subparallel block-faulted mountain ranges separated by alluvial valleys of approximately equal size. The core of the central range illustrated in Figure 4.4 is composed predominantly of Triassic volcanics, whereas limestones comprise the younger strata flanking the Mountain Range on the west. The limestone-alluvium front-fault along the western front of the range is particularly pronounced on image A between (b) and (c). The northward-trending, westward dipping, high angle normal fault is conspicuous because of the triangular faceted, truncated spur ends, and steep, V-shaped canyons. On image B, taken from the opposite look-direction the fault scarp is not as conspicuous nor as well defined.

Analysis of both images reveals that the accentuation of the fault scarp on image A is caused by the northwesterly orientation of the triangular slope facets bounding the fault scarp. These slope facets, oriented toward the look-direction, result in an extremely high return as compared with the lower return observed on image B. This preferred orientation highlights the

alluvial-fault contact when imaged from one direction, but is not as well defined from an opposite look-direction.

The effect of shadowing in the delineation of minor streams is illustrated at location (D). In the far-range of image B the delicate dissection of topography resulting in numerous distributaries in the alluvial apron is well defined, but the same pattern cannot be detected in the near range of image A. The delineation of distributaries in the far range is totally attributable to alternate highlighting and shadowing which is totally absent in the near range.

A somewhat analogous situation is illustrated on images from Mono Craters, California (Figure 4.5). Minor tributaries ((A)-(A')) carved in a topography of pumice ash and lapilli are well defined on the two images A and B in which the look-direction is orthogonal to the drainage. The same terrain features can only be delineated in part on image C, where the look-direction is parallel to the tributaries.

5.3 Trinity Range, Nevada, and Seaview Area, Washington

Most SLAR system designs attempt to provide the interpreter with imagery of acceptable resolution and uniform scale. In practice, however, distortions may require scale determination for each imagery pass. The SLAR imagery of Panama, used for this study, has known and correctable scale changes, i.e., the scale in the azimuth direction is constant (assuming synchronization between aircraft velocity and film-speed velocity), whereas the scale in the range direction is variable. Thus, when terrain features are imaged from two orthogonal look-directions, a significant difference in scale between these features is apparent. For example, in Figure 5.2 the distances between (A)-(A') and (A')-(B) are variable on images A and B. The same situation exists on images C and D where distances (B)-(C) and (D)-(C) do not coincide.

Even though the scale differences are correctable, these distortions in combination with topographic accentuation caused by preferential look-direction will obviously influence the interpreter's ability for geologic

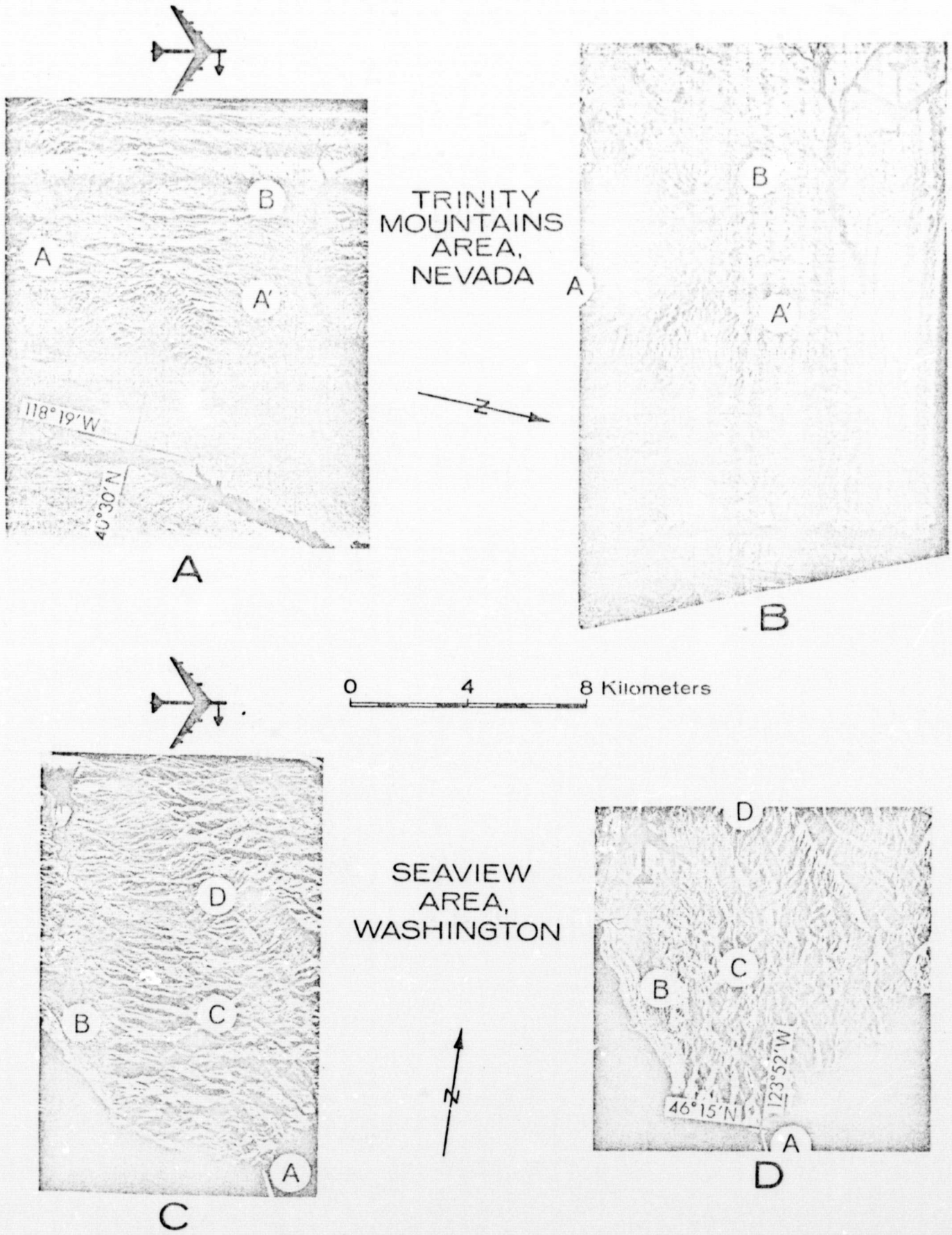

Figure 5.2 Trinity Mountains area, Nevada. (A) Look-direction, east. (B) Look-direction, south. Seaview area, Washington, (C) Look-direction, south. (D) Look-direction, east.

evaluation. This combination of distortions is particularly obvious in Figure 5.2A and B, in the Trinity Mountains area of Nevada. An intense north-trending joint system (resulting in a serrated topography of igneous rocks) is obvious on image A between locations (A) and (A'); however, the same linear alignments is conspicuously absent on image B. The look-direction for image A is perpendicular to the linear trends, whereas the look-direction for image B is parallel to the linears. The distance between (A')-(B) on image B is also greater than the distance between the same two features on image A. An analogous situation is apparent in the Seaview area of Washington where westerly-trending, linear valleys have been developed coincident with the outcrop belts of volcanic rocks which trend northwesterly across images C and D, being limited on east and west by points (B) (C). The distance between (B) and (C) is greater on image C than on image D.

In both of these examples, an "elongation" in the azimuth direction is obvious. The combination of preferential look-direction and "elongation" has enhanced the linearity of the terrain features, whereas supression of these same features is obtained with an orthogonal look-direction. If only images B and D were available for geologic interpretation, the linearity of the topography of these two separate geographic areas would not be detectable.

5.4 Boston Mountains, Arkansas

Multiple flight coverage over the southern portion of the Boston Mountains, Arkansas, has provided radar imagery over a geographic area that has received considerable attention by geologists involved in remote sensor studies (Dellwig, et al., 1966; Kirk and Walters, 1968; Dellwig, et al., 1968; and Kirk, et al., 1968). The detection on radar imagery, of a pronounced system of north-south trending lineaments was the primary reason for concentration of effort in this particular area (Dellwig, et al., 1966). Field studies and light aircraft flights over the area show that the lineaments, originally delineated on low-resolution radar imagery are, in fact, structurally controlled stream valleys which appear to have the same general trend as one of the dominant joint-sets which are recorded in outcrops.

A portion of this area is shown, and the north-south linearity of several stream valleys is well illustrated, in Figure 5.3. Three different directions have been provided, 1) look-direction perpendicular to the linear stream valleys (image A), 2) look-direction oblique to the stream valleys (image C) and 3) look-direction parallel to the trend of the stream valleys (image B). On the imagery of the flight perpendicular to these linear trends (image A) the enhancement of valleys (A)-(A'), (D)-(D') is particularly striking. These same valleys however, do not express the distinctive linear parallelism on image B. Similarly, the linearity of (F)-(F') is well defined on image B(look-direction orthogonal to stream valley), whereas on image A no such distinction can be made. Numerous other examples can be isolated when comparing images A and B, especially when the minor tributaries are examined (see for example, Area (C)).

Image C provides us with an intermediate look-direction, i.e., between the look-directions of A and B. The imagery produced at this intermediate look-direction appears to have compromising qualities for the detection of linear topographic features. This is to say that image C displays most of the linear features discussed above at an intermediate stage of definition between suppression and accentuation.

The question naturally arises, does look-direction influence the detection of lineaments in the terrain environment of the Boston Mountains (i.e., heavily wooded) even though most of the lineaments are expressed as stream valleys having a local relief up to 270 meters? Obviously, if the linearity of the stream valleys in this area had not been previously recognized on other imagery passes, and if only image B were available for analysis, the north-south linearity and parallelism of (A)-(A') and (D)-(D') could not have been interpreted. Thus, it is concluded that even in this region, for complete geological analysis, multiple flight coverage will be required.

5.5 Panama Imagery

The geological interpretation of radar imagery is based on the analysis of tone, texture, pattern and shape. Shape and pattern are pro-

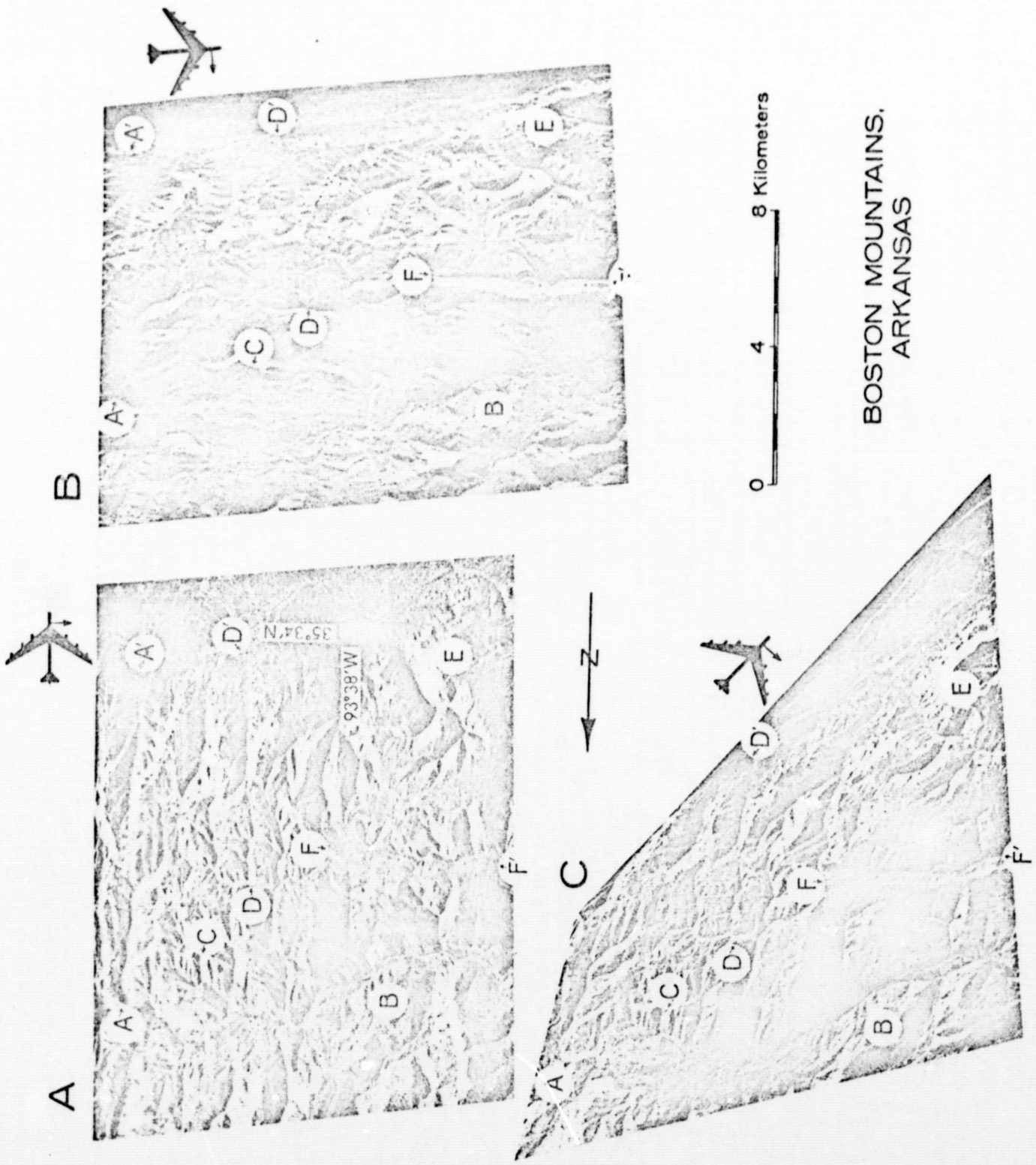

Figure 5.3 Multiple flight coverage, Boston Mountains, Arkansas. (A) Look-direction, west. (B) Look-direction, north. (C) Look-direction, northwest.

bably the two most important recognition elements because most interpretations begin with the detection and identification of the most conspicuous terrain features which might have geological significance. Structural features such as faults, joint-systems, and folds, which are usually expressed in the terrain configuration, can range in discreteness from very subtle to very conspicuous, depending on the topographic expression. The detectability of such features on radar imagery depends on the terrain configuration and the ability of the interpreter to identify them; however, this detection should be the result of a logical scientific approach where convergence of evidence is a requisite.

Evaluation of radar-derived terrain parameters presents a multivariable problem. Ignoring the inherent distortions of radar imagery, the quantification of radar-derived, geological parameters becomes a complex procedure because of 1) the divergent terrain environments in which these parameters are expressed, 2) the intricate relationship between terrain parameters and the radar return signal recorded on the imagery, and 3) the highly subjective approach necessary for the initial selection and identification of any geologic parameter interpreted from radar imagery. Making note of these qualifications, an attempt has been made to systematically analyze the data provided by the multiple flight coverage in the Darien area.

The detectability of faults, joint-fracture systems, and dip slopes was selected for look-direction analysis because 1) they are significant to geologic reconnaissance studies, 2) in the tropical terrain environment these features are usually reflected in the topographic configuration which is recorded on the radar imagery, and 3) regardless of the rock type involved these are ubiquitous features. In previous radar geology studies (Dellwig et al., 1968; Kirk, et al., 1968; and MacDonald, et al., 1967) it has been observed that relative relief is one of the determining factors for the radar enhancement of certain geological features. For the present study it was determined that two subcategories (based on local relief) would be applicable for the look-direction analysis; one subcategory less than 50 meters relief, and the other subcategory greater than 50 meters relief. These two topographic subdivisions are extremely subjective, at least in the Darien area,

because of the limited topographic field data available. It is important to emphasize that the boundary (i.e., 50 meters) between subdivisions of local relief is not a critical factor other than distinguishing between "high" and "low" relief areas. When sufficient multiple flight coverage becomes available in the United States, or any other country where adequate topographic data are available (contour interval 6 meters or less), a more definitive subdivision between "high" and "low" relief can be ascertained. Before examining the data from Table 5.1, which is a summary of the data from Appendix A, it is necessary to define some of the terms used in this look-direction analysis:

Azimuth: Azimuth is the angular relationship between radar look-direction (orthogonal to ground track of the aircraft) and the geologic feature imaged. For example, a geologic feature such as a fault, oriented perpendicular to look-direction would have an azimuth of 90 degrees, whereas a fault, reflected in a terrain configuration parallel to the look-direction would have an azimuth of 0 degrees.

Detectability: A particular terrain configuration is sufficiently distinctive on at least one imaging pass to be interpreted as a specific geologic feature.

Non-detectability: The interpretive evidence on any single imaging flight will not support identification of a specific geologic feature, even though the precise geographic position of this feature has been established on a previous imaging pass.

Matrix: The term total matrix as used in this study refers to the number of imaging passes over a defined geologic category. For example, for any specific geologic feature, a maximum of four different look-directions were included in the matrix; however, in those cases where four different passes were not available, at least two passes were always included in the matrix. Thus, the matrix for faults comprise the total number of different imaging passes over a certain number of faults, where the maximum number of different look-directions for any one specific fault is four, and where the minimum number of look-directions is two. Detailed data concerning this phase of the present study are included in Appendix A.

ANALYSIS OF LOOK-DIRECTION

PANAMA IMAGERY

Geologic Feature	Total Matrix*	Topographic Relief (meters)	Matrix Sub-Categories	Percent Matrix Detected	Percent Matrix Not Detected	Dominant Azimuth† Direction
Faults	96	<50m	54	70%		55% ≧ 60°
					30%	75% ≦ 30°
		>50m	42	83%		46% ≧ 60°
					17%	71% ≦ 30°
Joint Systems	78	<50m	47	60%		36% ≦ 30°, 32% ≧ 60°
					40%	58% ≦ 30°
		>50m	31	90%		40% ≧ 60°, 35% ≦ 30°
					10%	65% ≦ 30°
Dip Slopes	65	<50m	28	71%		50% ≦ 30°
					29%	63% - dip slope toward radar
		>50m	37	87%		47% ≧ 60°
					13%	100% - dip slope toward radar

* The term total matrix as used in this study refers to the number of imaging passes over a defined geologic feature.

† Azimuth direction refers to the angle between the look-direction (orthogonal to ground track) and the geologic feature imaged.

As previously discussed, the detectability of certain geologic features is influenced by radar shadowing, and this shadowing increases from the near to far range as a function of increasing incidence angle. In order to be cognizant of the primary factors which might significantly influence a look-direction analysis, the following units have been arbitrarily selected which subdivide the imagery format into three range segments:

Near Range - incidence angles less than 55 degrees
Mid Range - incidence angles between 55 and 69 degrees
Far Range - incidence angles greater than 69 degrees

5.5.1 Significance of Data (Table 5.1)

Faults -- Faults are normally recognized on radar imagery as persistent linears which cut across lithologic or structural trends as well as the other interpretive criteria such as erosional scarps, and off-setting linears or stream patterns, etc. Regardless of the topographic relief (i.e. less or greater than 50 meters) it is obvious that as the azimuthal orientation of a fault approaches parallelism to look-direction, the detectability of this particular geologic feature decreases (75 per cent of the non-detectable matrix have an azimuthal direction of 30° or less). Where the local relief exceeds 50 meters, shadowing in the far-range is also a significant contributor to the non-detectability of faults (Appendix A). When the azimuthal direction of any fault approaches orthogonality to look-direction (greater than 60° azimuth), the detectability of such a geologic feature increases.

5.5.2 Joint Systems

The distinction between jointing and faulting on radar imagery is often very difficult, and in the absence of conclusive fault evidence, it is common to consider the longer, well defined linears as faults, and the shorter crisscrossing linears as joints or fractures. A significantly higher percentage of the joint system matrix was detectable where the terrain relief exceeded 50 meters. Obviously, because such geologic features are usually expressed as short terrain linears, their detectability on radar imagery would be signi-

ficantly increased if the terrain configuration were sufficient to produce topographic enhancement. The non-detectability of joint-systems was influenced by both topographic relief and look-direction; however, look-direction plays a dominant role in non-detectability where 58 per cent of the non-detectable joint-fracture systems were recorded in the azimuthal range of 30° or less.

5.5.3 Dip Slopes

Analysis of the data in Appendix A and Table 5.1 reveal that the detection of dip slopes is obviously influenced by both the look-direction of the imaging systems and the topographic relief of the terrain involved. When the strike of the strata is perpendicular to look-direction (and the dip slope parallel to look-direction) the strata can either dip toward or away from the radar. Where the topographic relief exceeded 50 meters, all of the non-detectable category of dip slopes had a slope toward the radar, and 63 per cent of the non-detectable dip slope category (terrain relief less than 50 meters) had a slope toward the radar. It is apparent that the influence of radar foreshortening, as dictated by look-direction, is inherently related to the non-detectability of dip slopes.

To summarize, it is apparent that look-direction does indeed influence the detectability of geologic features expressed in the terrain configuration. Depending on the relative topographic relief, effective incident angle of radar energy, and look-direction, geologic features may be advantageously enhanced or completely suppressed. Thus, to obtain the maximum benefit from radar geological reconnaissance studies in poorly mapped areas, it will be necessary to image the specific region from four orthogonal look-directions. For more detailed studies where a known terrain configuration is to be imaged, a minimum of two opposing look-directions will be required for optimum geologic interpretation.

5.6 Look-Direction vs. Low Sun-Angle

When geologic features such as joint systems, faults, or folded

strata are enhanced on radar imagery, the enhancement can usually be attributable to radar shadowing. Analogous examples of shadow enhanced geologic features have also been observed on many of the Gemini series photographs which were taken at times of very low sun-angle. From orbital altitudes, particularly with analysis of oblique images, low angles of solar illumination have proven useful for accentuating otherwise subtle relief which might have been undetected (Wobber, 1968). The question then arises would aerial photography afford the geologist an improved interpretive tool if the photography were obtained at low-oblique sun illumination, and if so, would radar imagery still provide the geologist with unique terrain information for geological analysis?

The standard procedure for the acquisition of reconnaissance photographic coverage in most geographic areas is to obtain the photography between 1000 hours and 1400 hours. These particular times normally provide optimum lighting to minimize the effect of shadowing which, in the past, has been a hindrance for measurement of strike and dip or tracing formation contacts. What effect, however, would a lower sun angle have on the resultant photography if the aerial photographs were gathered either earlier or later in the day, and would certain terrain features be enhanced to such a degree that new information might be provided for geologic interpretation? To illustrate the effect of sun angle in the photographic interpretation of aerial photographs, Hackman (1967) conducted an experiment in which a three-dimensional, plaster terrain model was photographed while controlling the incidence angle of illumination. Using photographs obtained at 10 degree increments of illumination, ranging from incidence angles of 90 degrees (illumination angle of 0 degrees) to 20 degrees (illumination angle of 70 degrees), Hackman concluded that as the angle of incidence (complement of the angle of illumination) increased, tone differences became less apparent; but the enhancement of terrain features by shadowing became more apparent (Figure 5.4). Hackman suggested that photographs taken at both high and low sun-angle would provide the interpreter with the greatest amount of terrain data, and if only one sun-angle was available, 60 degrees

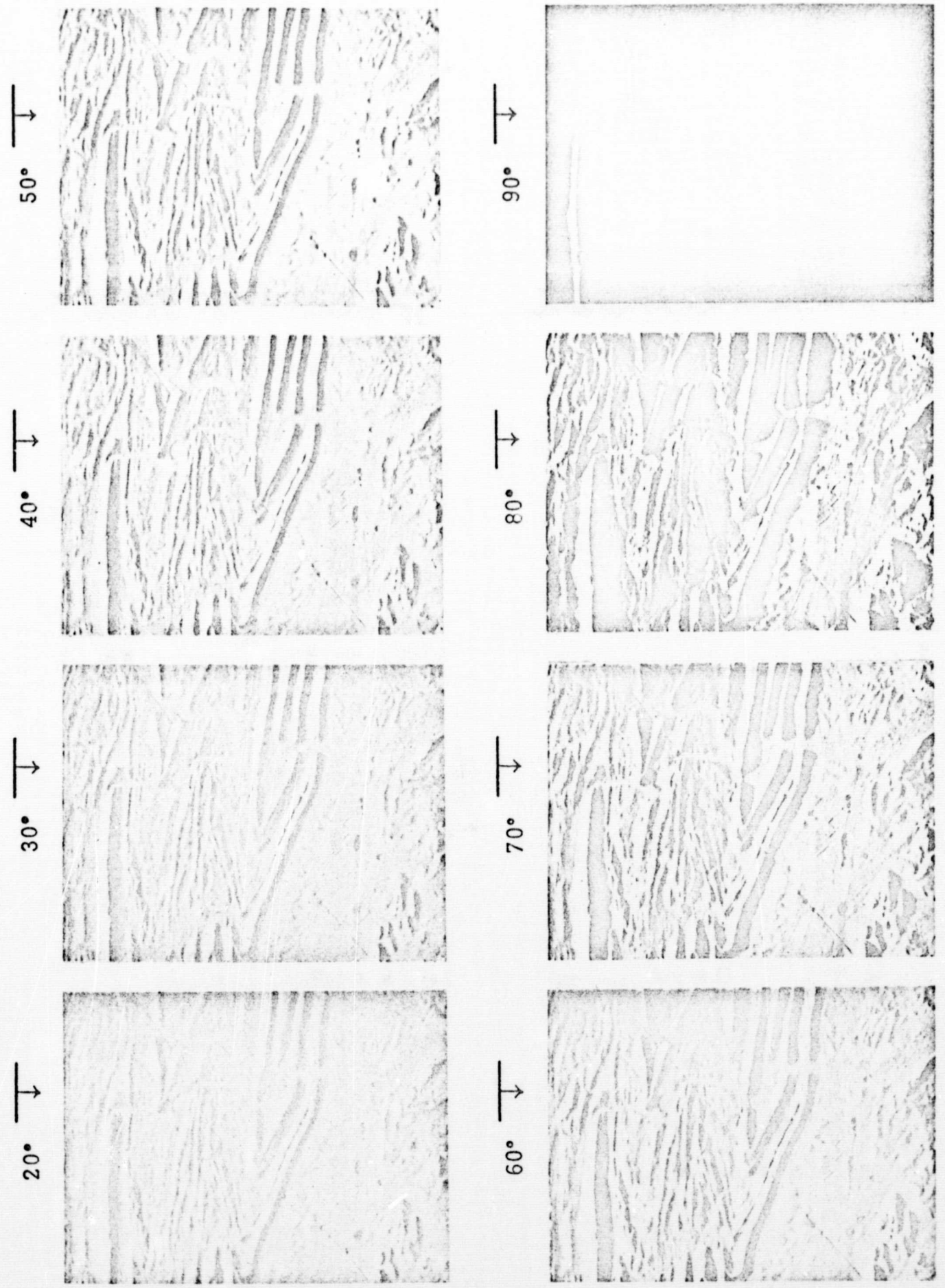

Figure 5.4 (Modified from R. J. Hackman)

incidence (30 degree angle of illumination) would be most satisfactory. It is especially important to note that in areas of low relief, photographs taken with the light source at an incidence angle of 80 degrees or more (illumination angle of 10 degrees or less) provided enhancement of subtle differences in relief and textural pattern that would otherwise be unrecognizable.

Thus, on initial examination of the data presented in Hackman's experiment, one might conclude that the so-called "advantage" of oblique imaging radars (which results in shadow-enhanced terrain features) might also be available at certain sun angles during the acquisition of conventional aerial photography, even though this quality may have been previously overlooked when adhering to the requisites for collecting conventional stereo coverage. Unfortunately, such a conclusion would be somewhat premature and only partially correct, because the exploitation of any prescribed earth-sun relationship necessitates a preset flight schedule embracing a limited time period. For example, if low sun-angle photographic coverage is desired for a known terrain configuration which is dominated by north-south linear trends, maximum terrain enhancement on the photography could only be achieved during early morning or late afternoon flights. However, during this same time of flight coverage any east-west trending linear features would be suppressed because of the absence of shadowing. Thus, low sun-angle photographic coverage would only provide maximum enhancement for those terrain features which were in proper alignment to produce shadowing. This limitation would be especially critical if the desired incidence sun-angle was in excess of 80 degrees.

With SLAR imagery systems, terrain features can be imaged from multiple look-directions, and at preselected incidence angles. This capability would be particularly advantageous in an area where only limited reconnaissance data are available. Here the selection of preferred look-directions would result in the enhancement of certain structural trends. Similarly, if geological reconnaissance data are desired in an area of relatively unmapped terrain, sufficient overlap at varying incidence angles can be obtained in order to provide shadow enhancement for 1) the high relief areas (incidence angles less than 30 degrees), 2) moderate relief areas

(incidence angles between 30-60 degrees) and 3) low relief areas (incidence angles of 60 degrees or more).

CHAPTER 6

PANAMA STRATIGRAPHY

The inaccessibility and high cost of exploration have essentially limited the extent of our knowledge of Panamanian geology. Aside from a geologic strip map (approximately 9 kilometers wide) extending from San Miguel Bay 8°25'N, 78°10'W (Plate I) on the Pacific side, to Punta Sasardi (beyond northern limit of Plate I) on the Caribbean side at 8°55'N, 77°15'W (IOCS, 1968), the only detailed geologic maps that are available were compiled for engineering geologic studies within the Canal Zone.

Although geological reconnaissance mapping (scale 1:500,000) of the entire Isthmus was attempted by Terry (1956), much of eastern Panama was left unmapped because of insufficient data. A generalized geologic map of Central America (scale 1:1,000,000) published by Roberts and Irving (1957) was later modified (Woodring, 1958) to include all current published data for Panama, and although the scale is approximately 1:2,000,000 this map synthesizes the most recent geologic map data of Panama.

6.1 Basement Rock Complex

The basement complex is defined as a series of rocks, usually igneous and metamorphic, generally with complex structure, beneath dominantly sedimentary rocks (AGI Glossary, 1957). In this present study, the basement complex refers to undifferentiated pyroclastic, intrusive and extrusive igneous rocks, and minor sedimentary rocks which unconformably underlie the Tertiary sedimentary sequence. Although the age of the basement rock complex is unknown, it is probably of Cretaceous age, similar to the widespread volcanic and associated rocks throughout the Caribbean region (Woodring, 1957).

Most of the mountain ranges of central and eastern Panama consist principally of altered basaltic and andesitic lavas, tuff and agglomerate

intruded by dioritic and dacitic rocks (Woodring, 1958). The most recent field data (IOCS, 1968) from the Darien indicate that the core of the Serannia del Darien of northwestern Darien Province is dominated by basalt, basalt porphyry, and amygdaloidal basalt intercalated with tuff and agglomerate. Basalt, diabase, and dacite comprise the basement rock complex in the San Miguel Bay area, with rocks of andesitic and basaltic composition dominating the Pacific coast ranges, and the mountains along the Colombian border.

6.2 Sedimentary Strata

The gross regional geology of central and eastern Panama reflects the dominance (over half) of igneous rocks that form the high rugged uplands and coastal ranges. Between the coastal ranges are the central lowlands of the Isthmus which are underlain by a sequence of Tertiary deposits, for the most part marine, ranging in age from Eocene to Pliocene. The Tertiary deposits of eastern Panama and northwestern South America are reported (Olsson, 1942a) to have a remarkable similarity both in faunal and stratigraphic development, even though today these deposits are separated by high uplifted mountains.

In this study, because of the sparse stratigraphic data available within the Darien area, it has been necessary to obtain, and rely heavily upon, those data from adjacent areas. The stratigraphic information presented in Table 6.1 represents a summary of those data which are most pertinent to the present study. For a more detailed discussion of the stratigraphy of Panama, the reader is referred to Woodring (1957,1958); Terry (1956); Olsson (1942a); Sapper (1937); and Schuchert (1935).

AGE		SHELTON (1952) Central Darien Province	TERRY (1956) Eastern Panama		IOCS STUDY (1968) Northwestern Pacific Side	Darien Atlantic Side	WOODRING (1957) Gatun Lake Caribbean Coast Canal Zone	MacDONALD (1969) Darien Province and Northwestern Colombia	AGE	
PLIOCENE	Late	Chucunaque Fm.	Chucunaque Fm.		Sabana Beds			Pliocene to Upper Miocene	Late	PLIOCENE
	Middle								Middle	
	Early						Chagres Sandstone		Early	
MIOCENE	Late	Pucro Fm.						?,	Late	MIOCENE
	Middle	Lower Gatun Fm.	Gatun	Pucro Member			Gatun Fm.	Upper	Middle	
				Lower Gatun				Lower		
	Early	Aquaqua Fm.	Aquaqua Fm.		Pacific Tufts	Clarita Limestone	PACIFIC SIDE Panama Fm. Cucaracha Fm. Culebra Fm.	Lower Miocene	Early	
OLIGOCENE	Late		Arusa Fm.		? ?		Late: Calmito Fm. (Late)	Upper Oligocene	Late	OLIGOCENE
	Middle	Arusa Shale			?		? Bohio Fm. (Late)	Middle Oligocene	Middle	
	Early	Clarita Limestone					Early: marine mbr.? (Early) Bas Obispo Fm.	? ?	Early	
EOCENE	Late	Corcona Fm.	Eocene		?	Morti Tuffs	Gatuncillo Fm.	Eocene	Late	EOCENE
	Middle	?							Middle	
	Early	?	?		?			? ?	Early	
Paleocene		Agglomerate	Chert		?		?	?	Paleocene	
Pre-Tertiary		Basement Complex					Basement Complex	Basement Complex	Pre-Tertiary	

Table 6.1 Correlation Data, Eastern Panama and Canal Zone.

CHAPTER 7

GEOLOGICAL RECONNAISSANCE MAP INTERPRETATION

Prior to the 1920's, geological reconnaissance surveys in the Darien area were stimulated both by the search for gold, and for site locations for a possible sea level canal. One of the earliest reconnaissance surveys (geographic) was conducted in extreme southeastern Darien and the Atratro Delta area of Colombia. This survey conducted in 1875-77 was in connection with a French scheme to construct an interoceanic canal (Wyse, 1877). In southernmost Darien Province, near the abandoned village of Cana (Approximately 7°40'N, 77°39'W), exploration was carried out in the late 1800's in connection with the legendary Espiritu Santo gold mine. This mine, later called the Darien Gold mine, is known to have been in periods of sporadic operation from at least the early 1700's to 1911 (Woakes, 1923). Although other geological exploration by mining companies has been conducted in the Darien since 1900, the data have not generally been released.

Geological exploration for oil was initiated by Sinclair Panama in 1925 when three shallow test holes were drilled to 332, 1100, and 1200 meters. The deepest of these three tests was drilled on Yape anticline, 8°07'N, 77°35'W. Between 1925 and 1927 three shallow wells were drilled by the Gulf Oil Company in the Garichine basin area of San Miguel Bay. Two of these tests were located in the vicinity of 8°04'N, 78°15'W, and the third well at approximately 8°03'N, 78°18'W.

Shelton (1952), in conjunction with field work associated with petroleum exploration, provided geologic data for the central part of the Tuira-Chucunaque basin, while Terry (1956) reported on the regional geology of eastern Panama. Subsequent to the work of Shelton and Terry, the most recent and deepest drilling test was completed (dry hole) by the Delhi-Taylor Corporation in 1961 at a total depth of 3498 meters. This test hole was located on the Rancho Ahogado anticline centered at 8°35'N, 77°53'W.

Schmidt, et al., (1947) reported on the reconnaissance geology along the Calidonia Bay "Route 10" in extreme northwestern Darien Province, extending from San Miguel Bay (8°25'N, 78°10'W) to the Comarca de San Blas on the Atlantic side (8°55'N, 77°15'W). Detailed geological exploration has recently been completed by the Interoceanic Canal Study Commission (IOCS, 1968) along approximately the same route examined by Schmidt, et al., (1947). The IOCS study represents the most recent geologic data available for the Darien, and will be referred to frequently in the present study.

7.1 Reconnaissance Mapping

The term reconnaissance is applied to incomplete or generalized mapping which usually precedes more detailed or localized studies. Similarly, reconnaissance mapping can also enlarge the scope of local studies providing a general geologic picture of the surrounding region. From a practical stand-point, reconnaissance mapping may be the only feasible method for geological exploration because of the limitations of time, funds, adequate base maps, and accessibility.

Probably the most important interpretive phase of geological reconnaissance mapping with radar imagery is selecting rock units that have sufficient areal extent to be significant and are still distinctive enough on the imagery to be easily mapped. One is generally restricted by the scale of the imagery, but the primary limitation for the differentiation of rock units (either on aerial photographs or radar imagery) is topographic relief. Depending on the rock type involved, climatic conditions, thickness of the regolith and vegetal canopy, radar imagery may reveal abundant interpretive data, or it may show almost none. The geologic data interpreted from radar imagery for this study were derived from surrogates rather than through direct identification. Similarly, the time-stratigraphic assignments used for the map units (Plate I) have been inferred from corroborative data, and are obviously not interpretable from radar imagery.

7.2 Igneous Rock Interpretation - Plate I

The basement complex exposed in over half of Darien Province is

the least known because these rocks generally occupy the rugged inaccessible mountain ranges along both coasts and along the Panama-Colombia border. Using the interpretive techniques previously discussed, analysis of the radar imagery reveals that the axes of the principal mountain ranges of Darien have a rugged, massive texture indicative of igneous rocks. The absence of shape and texture of stratification is also conspicuous. The gross regional aspects of the distribution of these igneous rocks can be seen by comparing the radar mosaic (Figure 2.3) with the geological reconnaissance map (Plate I).

The extent of topographic expression of this igneous complex is dependent upon the erosional maturity and the extent to which the rock is deformed or fractured. For example, in some of the high-relief areas, major joint systems have developed resulting in angular, choppy, erosional remnants whose jutting edges dominate the topography (Figure 4.2 a,b; Figure 4.3 k, right half). Similarly, rectangular drainage patterns dominate both the high and low relief areas, and this topographic texture is especially well developed in the Cordillera de Jurado south of latitude 7°45'N (Figure 4.2 d,e).

In the interior mountain ranges where the relief is more subdued, fractures are mainly represented by joint systems and angularities in the drainage texture, such as those developed between 8°00'N and 8°15'N in the Serrania de Bagre (Figure 4.2 f). Where joint systems are weakly expressed, widely spaced or absent, a more rounded, hummocky texture dominates the topography, such as that displayed north of the Serrania de Bagre between latitudes 8°09'N and 8°15'N (Figure 4.2c).

Unless the boundary between the igneous rock complex and sedimentary strata is conspicuously defined by topographic texture or faulting, the precise separation of these two rock types on the imagery is exceedingly difficult. Where problem areas exist, boundaries between the rock types have been indicated with question marks on Plate I.

7.3 Sedimentary Rocks - Plate I

The recognition criteria used for radar imagery interpretation have

been presented and it is now appropriate to relate why the rock units appearing on the geological reconnaissance map (Plate I) have been interpreted in their respective locations. For simplification of this discussion, these rock units will be examined relative to their location in the following physiographic subdivisions:

Tuira-Chucunaque Basin -- trending southeasterly from 8°31'N, 77°56'W to the Colombian border at 7°42'N, 77°36'W.

Sanson Hills -- trending southeasterly from 8°30'N, 78°03'W to 8°11'N, 77°47'W.

Rio Balsas Embayment -- centered at 8°00'N, 77°50'W.

Sambu Basin -- centered at 7°51'N, 78°11'W.

Pirre-Jurado Intermontane Basin -- located between the Serrania de Pirre and Cordillera de Jurado, with the largest basin centered at 7°38'N, 77°48'W.

Caribbean Coastal Area -- trending southeasterly along the Caribbean Coast from 8°10'N, 77°30'W, to the Atrato Delta in Colombia at 8°05'N, 77°05'W.

Mogue Embayment and Lowlands -- centered at 8°03'N, 78°05'W and extending northwestward to San Miguel Bay.

7.3.1 Tuira-Chucunaque Basin

On the east side of the Tuira-Chucunaque basin, strata of Eocene age have been mapped bordering the basement complex of Pre-Tertiary age. At the northwestern end of the basin these strata are composed of an interbedded sequence of shale, sandstone, limestone, tuff, and agglomerate,

similar to those described along the Rio Morti (IOCS, 1968) and Rios Topaliza, Chico, Tuquesa, Maraganti, and Membrillo (Shelton, 1952). From the Rio Pucuro southeast to the Colombian border the lithologic composition of this stratigraphic unit has not been described from field studies. From the interpretation of the radar imagery, however, the topographic textures appear similar to those characteristic of the Eocene strata to the northwest, and this stratigraphic unit has been inferred along the entire eastern flank of the basin.

West of the Tuira basin on the east flanks of the Serrania de Pirre, and Cerro Setetule, a stratigraphic sequence ranging in age from Eocene to Miocene has been inferred. Especially along the flanks of the Setetule anticline, the oldest strata of this sequence have extremely steep dips (58 degrees measured at one location on the imagery), and although the alternation of resistant and non-resistant strata are evident (Figure 4.2 g, upper left corner), specific stratigraphic units cannot be interpreted. Unfortunately, in this area, the stratigraphic sequence inferred (Plate I) is extremely provisional. On the northeast flank of Pirre anticline, (Figure 4.2 i) however, the Upper Oligocene sequence has a recognizable topographic texture that can be correlated with similar strata and texture on the southern end of the Tuira basin (Figure 4.2 k).

In the northern half of the map, traversing in a northwesterly direction toward the center of the Tuira-Chucunaque basin, an upper-Middle Miocene sequence of sedimentary rocks form another distinctive topographic texture interpretable from the radar imagery. This upper-Middle Miocene sequence of shales, sandstones, and sandy limestones is characterized by several ridge-forming, massive, fossiliferous sandy limestones (Figure 4.3 b). Between the two rock sequences (Middle Oligocene and upper-Middle Miocene) which are interpretable from the imagery, three other stratigraphic units have been inferred: Upper Oligocene, Lower Miocene, and lower Middle-Miocene. Because of the lithologic similarities of these strata, (dominated by shales with intercalated thin sandstones and limestones) and somewhat uniform dips, these units could not be differentiated in the northern half of the basin, and the mapping of these three units is based primarily on the work of Terry,

(1956); Shelton, (1952); and M. D. Quigley, Sinclair Research Center, Tulsa, Oklahoma (Personal Communication). In the southern half of the basin (southeast of the Rio Yapi, 8°09'N, 77°29'W) however, both the Lower Miocene and lower Middle-Miocene sequences appear to be more calcareous in composition, forming a hummocky terrain (Figure 4.2 k). In the vicinity of the headwaters of the Rio Tuira, near the Colombian border, this same sequence is not sufficiently distinctive in topographic expression (Figure 4.3 f), and interpretation is impossible. Thus, because field data are not available, the inferred distribution of these strata is somewhat speculative.

7.3.2 Sanson Hills

In the northwestern half of the Tuira-Chucunaque basin, a series of asymmetrical, en echelon anticlines have strata exposed at their cores which have been reported (Terry, 1956) to range in age from Eocene to Middle Oligocene. However, along the northern extension of this anticlinal trend (approximately 25 kilometers north of 8°30'N, 78°03'W) the oldest strata exposed in the anticlinal cores have been placed at a probable Oligocene or Early Miocene age (IOCS, 1968). The texture of the ridge-forming Middle Oligocene strata which was distinctive on the radar imagery east of the Rio Chucunaque (Plate I) is not as apparent in the area to the west, and absolute correlation is impossible. Also, the apparent lithologic similarities between the oldest strata exposed on the crests of the anticlines and the younger strata exposed on the flanks has resulted in a somewhat similar textural appearance for these formations (Figure 4.3 d,e). Differentiation of individual map units is further complicated by steep dips on the flanks of the anticlines. Without detailed field data these formations could not be correlated from opposite sides of the basin when relying solely on radar imagery as the data source. It is apparent that the interpretation of radar imagery has contributed little to unraveling the stratigraphic problems of this particular area, and as might be expected, considerable field work will be necessary before the stratigraphy of this area will be fully understood.

7.3.3 Rio Balsas Embayment

Sandy shales and sandstones of Eocene age have been reported (Terry, 1956) on the Rio Pihuila, (7°57'N, 77°50'W) a tributary of the Rio Balsas, but other corroborative data are extremely limited for this area. The distinctive massive bedded appearance on the radar imagery of the Miocene and Oligocene strata of the Tuira-Chucunaque basin is conspicuously absent, and a more delicate texture indicative of thinner bedded strata is apparent (Figure 4.3 g). Although dip slopes are not sufficiently defined on the radar imagery to enable dip measurements, sufficient texture is revealed to indicate that more than just Eocene strata occur in this area. Based on minimal interpretive evidence, four stratigraphic units have been indicated in this area, i.e., Lower Miocene to Eocene.

7.3.4 Sambu Basin

On the east flank of the Serrania del Sapo and northeast flank of the Sierra de Jungurudo, the radar imagery reveals a stratigraphic unit with a distinctive topographic texture which may be correlative to the Middle Miocene sequence in the Tuira-Chucunaque basin. This unit appears to be traceable to the headwaters of the Rio Sambu, in the vicinity of 7°28'N, 77°59'W. Other than the inferred position of the Middle Miocene sequence, the stratigraphic relations shown on Plate I for the Sambu Basin are almost totally dependent on those data presented by Terry (1956), Sapper (1937), and H. T. Donaldson, Ferris and Company, Washington, D. C. (Personal Communication).

7.3.5 Pirre-Jurado Intermontane Basins

Sediments correlative with those of Eocene age have been inferred in the intermontane basins between the Serrania de Pirre and Cordillera de Jurado. The age assignment is based on Terry's work, in which he reported exposures of infaulted or infolded sediments of Eocene age in these areas. Schuchert (1935) has similarly reported that east of the drainage of the Rio Salaqui (7°32'N, 77°41'W) orbitoidal limestones of Eocene-Oligocene age

are present. The topographic texture is not distinctive (Figure 4.3 j,k), being very similar to the texture of finer-grained sediments found in the Tuira-Chucunaque basin.

7.3.6 Caribbean Coastal Area

Similar to many parts of Darien Province lacking potential for petroleum exploration, this part of the Darien is almost totally unmapped. East of the Continental Divide, approximately 25 kilometers north of the Rio Membrillo (8° 41'N, 77° 45'W) a narrow sequence of highly weathered tuffs, tuff breccias, and agglomerates have been reported to be of Eocene age (IOCS, 1968). Examination of the radar imagery in this area has allowed definition of terrain texture correlative with the Eocene strata which are positioned between the Continental Divide and Caribbean Sea. A similar topographic texture has been recognized to the southeast along the Caribbean Coastal area where these sediments lack the massive character of the basement complex and also lack the diagnostic landforms (hogbacks) of the Oligocene or younger sediments on the west side of the Serrania del Darien (Figure 4.3-*l*). Landforms indicative of bedding are not apparent on the radar imagery in this area, but this may be in part related to the large amount of intercalated volcanics. As previously discussed, the contact between the basement complex and overlying Eocene strata can be extremely difficult to determine if the weathering characteristics of the lithologies involved are somewhat similar, thus in the Caribbean Coastal area, the boundaries inferred are highly provisional.

7.3.7 Mogue Embayment and Lowlands

In the vicinity of the mouth of the Rio Mogue bordering San Miguel Bay, Terry (1956) has mapped undifferentiated Oligocene volcanic clastics interbedded with marine shales. To the southeast, however, only the basement complex has been mapped. Examination of radar imagery from this particular geologic environment reveals one of the major problems confronting the interpreter, i.e., separation of stratigraphic units where the topo-

graphic expression of contrasting rock types are very similar.

A narrow band of linear ridges indicative of steeply dipping beds have been located between 8°17'N, 78°05'W and 8°08'N, 78°02'W (Figure 19i center). However, the main portion of this mapped unit (centered at 8°03'N, 78°05'W) generally lacks erosional features indicative of bedding, and also lacks the hummocky texture characteristic of deeply eroded igneous rocks. Similarly, although joint systems are observed, they are not as abundant as in the surrounding igneous complex. As previously mentioned, to the northwest in the vicinity of San Miguel Bay bordering the Rio Sambu, Terry (1956) has mapped interbedded sediments and volcanics of Oligocene age; however, on the opposite side of the bay what appears to be a comparable stratigraphic sequence has been mapped as interbedded sediments and volcanics of Early Miocene age (IOCS, 1968). To avoid confusion, and because of the inadequacy of field data the stratigraphic unit in question has been assigned a Miocene-Oligocene(?) age (Plate I).

7.3.8 Evaluation - Sedimentary Rock Interpretation

In summary, the terrain configuration of major rock types determines whether these units can be distinguished from one another. Only in areas where lithologic contrasts are expressed topographically can boundaries, relative stratigraphic sequence, and correlation from one area to another be accomplished using radar imagery. The surface expression of individual lithologic units within a major rock type varies with both local terrain conditions and the geologic environment, thus presenting a different interpretive problem in each new area. If some corroborative information concerning the local stratigraphy is available, the problem is simplified, and correlation between lithology and a distinctive appearance on the imagery can be accomplished. For geologic reconnaissance mapping, and from a practical standpoint, the recognition of the individuality of a specific map unit is generally more important than the identification of lithologic type, and where the former can sometimes be accomplished, the latter is impossible. Lacking collateral data, lithologic interpretation from radar imagery is considered exptremely provisional.

7.4 History of Sedimentation

In eastern Panama, a zone of Tertiary sedimentary rocks extends east up the Rio Bayano (Figure 7.1) and into the Rio Tuira-Chucunaque basin of Darien Province, then southeasterly toward the Rio Atrato Valley of northwestern Colombia. Nygren (1950), with access to subsurface geologic data, has concluded that the present Atrato Valley of Colombia is superimposed on the former axis of maximum Tertiary deposition. The main axis of this sedimentary trend (named the Bolivar geosyncline by Schuchert, 1935) extends for nearly 1700 kilometers; from Central Panama to the Rio Atrato Valley, then southwestward to the Gulf of Guayaquil in southern Ecuador. Thus, the distribution of Tertiary marine deposits indicates a main seaway separating the continents of North and South America, although the precise geologic history may be somewhat in doubt.

The geologic history of the Bolivar geosyncline was presented by Nygren (1950) and the following represents a summary of his data: Marine transgression began in the Bolivar geosynclinal area during Middle Eocene and progressively encroached from the north and south until the seaway was completely open in Early Oligocene. Deposition was continuous until Late Oligocene when tectonic activity tended to shallow the seaway. Sediments more characteristic of a mixed marine and continental environment continued until Middle Miocene. Although marine sedimentation persisted in the deep gulf areas of both ends of the geosyncline, non-marine deposits generally prevail in the sedimentary rocks of Late Miocene and Pliocene age.

Several geologists (Schuchert, 1935; Terry, 1956; Lloyd, 1963) have regarded the arc of eastern Panama from the Colombian border to the Canal Zone in Central Panama (Panama Spur of Lloyd, 1963) to be quite distinct, geologically, from western Panama and Costa Rica, but geologically similar to the Choco basin of Colombia, located on the northwestern corner of the South American continent. Recent studies based on the distribution of Miocene mammals (Whitmore and Stewart, 1965) provide evidence that the San Blas area (including all of the Serannia del Darien) previously called the Panama Spur, was probably not connected to the South American continent

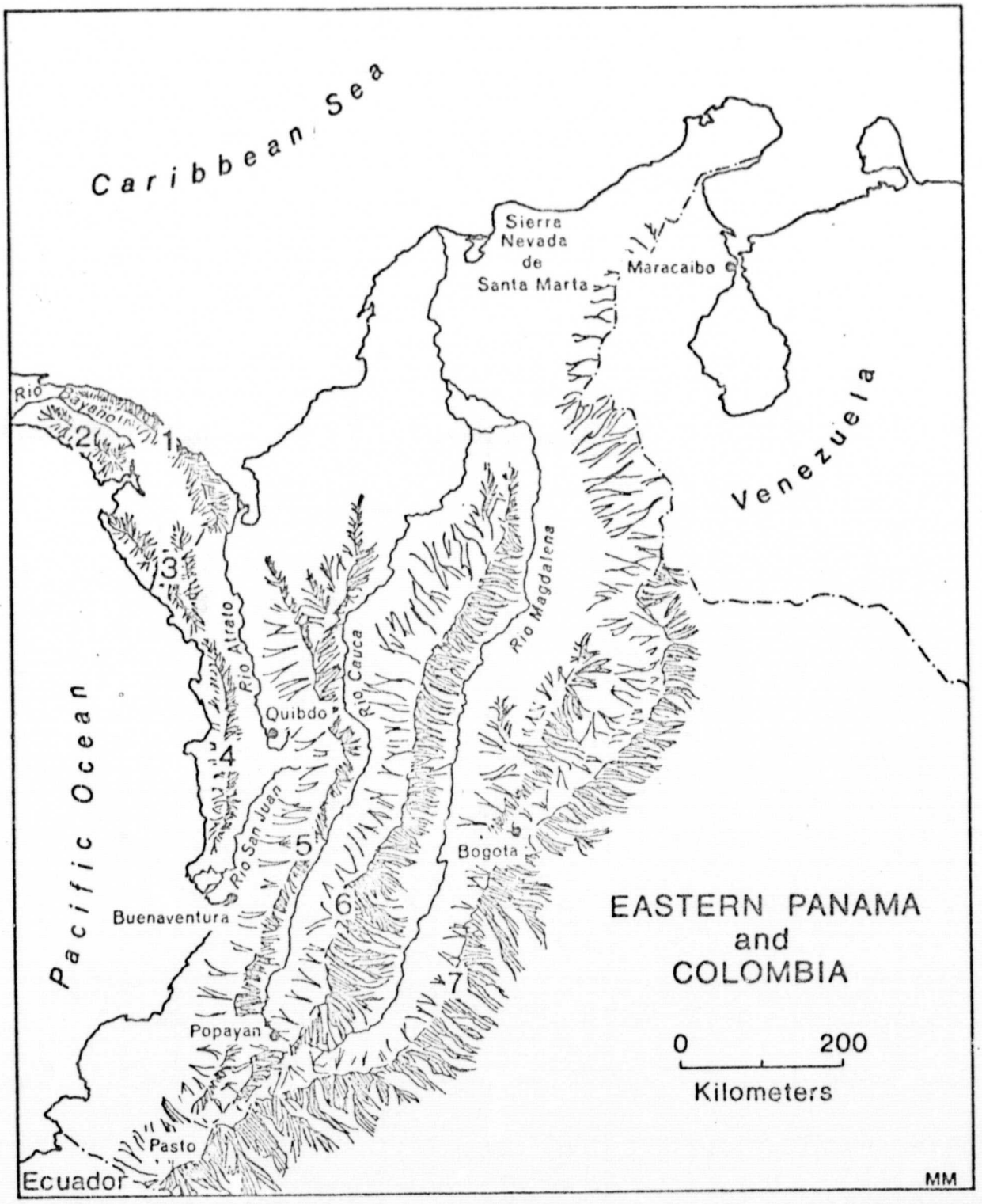

MOUNTAIN RANGES:

1. Serrania del Darien
2. Serrania de Maje
3. Serrania del Sapo
4. Serrania de Baudo
5. Cordillera Occidental
6. Cordillera Central
7. Cordillera Oriental

Figure 7.1

until late Tertiary time across the Bolivar geosyncline, and existed as a large stable island, intermittently connected to western Panama. Thus, Whitmore and Stewart contend that the presence of Miocene mammal fossils of North American affinity in central and western Panama indicate that western Panama and Central America were attached to North America throughout much of the Tertiary, but portions of the isthmus were broken up into an archipelago.

7.5 Structure - Background

The structure of eastern Panama has been described as being more similar to that of northwestern Colombia than western Panama and Costa Rica; thus, it is necessary to briefly summarize the structural framework of that portion of the South American continent which is linked to Central America through Panama.

Colombia lies along the northwestern flank of the Guiana Shield, the structural grain of which is reflected in the simple folding of the eastern part of the country; however, western Colombia is independent of the shield structure, and is influenced primarily by the tectonics of the complexly folded Andean system (Olsson, 1956). Thus, the western half of Colombia has been strongly folded and faulted along with the rest of the west coastal area of South America, resulting in a series of high cordilleras known as the Colombian Andes. The backbone of the Colombian Andes emerges from Ecuador as three distinct mountain ranges (1) the Cordillera Occidental, (2) the Cordillera Central, and (3) the Cordillera Oriental (Figure 7.1). Standing as outliers of the main ranges are the Sierra Nevada de Santa Marta (exhibiting a structural grain and rock type similar to that of the Cordillera Central) on the northern coast east of Rio Magdalena, and the Coast Range or Serrania de Baudo on the Pacific coast paralleling the Cordillera Occidental in geographic position (Figure 7.1).

Broadly speaking these five Colombian ranges can be geologically categorized as two distinct segments; an eastern segment containing the younger Cordillera Oriental, composed primarily of marine sediments, and a

western segment including the Cordilleras Occidental and Central, plus the Coast Range and Sierra Nevada de Santa Marta, all being primarily of igneous and metamorphic composition with subordinate sedimentary rocks. The main mountain ranges (Cordilleras Occidental, Central, and Oriental) correspond to the primary tectonic provinces of Colombia, exhibiting marked structural characteristics and different ages of uplift (Oppenheim, 1952). Similarly, these ranges are separated from each other by deep longitudinal fault depressions which constitute the valleys of major northward flowing rivers, the Rio Magdalena, and the Rio Cauca (Olsson, 1942 b). The structural elements of the Colombian Andes provides both a northwest and northeast structural grain in northern Colombia, whereas in the south the influence of Andean tectonics provides a northeasterly trend.

The Cordillera Occidental or Western Range of the Colombian Andes (rising to altitudes of 2500-4000 meters) trends in a northeasterly direction after emerging from Ecuador. Near the Panamanian border this mountain range divides into two spurs; one swinging northeast through northern Colombia, and the other spur trending northwest across the Atrato Basin, becoming the Serrania del Darien of eastern Panama (Figure 7.1). Although the geology of the Cordillera Occidental and the Coast Range of Colombia is the least known (dictated primarily by exploratory economics) these two ranges link Colombia with Panama, and consequently some understanding of the available geologic information has pertinence to the present study.

Paralleling the continental trend of Colombia into southeastern Panama, and lying between the Atrato Valley and the Pacific Ocean, is the convexly arched (toward the northeast) Coast Range of the Itendencia del Choco; and although submerged in southern Colombia, the range can be traced as a tectonic line southward into Ecuador (Olsson, 1942 b). In eastern Panama the northwestward continuation of the Colombian Coast Range rises abruptly from the sea, forming a steep, rocky coast and is recognized as the Cordillera de Jurado and Serrania del Sapo which trends northwestward to Garachine Point at 8°05'N latitude, where its continuation borders the steep submarine escarpment of the Gulf of Panama. Anderson (1945) provided evidence that the Coast Range of Colombia is princi-

pally a basement complex composed of igneous and metamorphic rocks, overlapped by Tertiary sediments. Oppenheim (1952) later reported that the metamorphic rocks of the Coast Range are probably of Mesozoic age contemporaneous with those of the Cordillera Occidental.

The Cordillera Occidental in southern Colombia, is composed largely of low-grade metamorphic black slates and quartzites of possible Mesozoic age (Oppenheim, 1952). Northward, and extending along the central and western flanks, numerous large batholiths are exposed, revealing plutonic rocks of granodioritic, dioritic, and gabbroic composition, whereas andesites dominate the extrusive flows to the south. These batholiths constitute a large part of the Cordilleran massif much in the same way they do in the Cordillera Occidental of Ecuador (Oppenheim, 1950). Folded Cretaceous marine sediments occur in the northwestern part of the Cordillera indicating the principle period of uplift to be post-Cretaceous whereas in the northeastern branch of the Cordillera (Bolivar Province) the greatest extent of folding appears to involve Miocene sediments (Oppenheim, 1952).

Separating the Coast Range and Cordillera Occidental is the Atrato-San Juan structural trough, which is delimited on the east and west by normal faults which expose marine Tertiary sands and shales. This longitudinal depression is occupied by the Rio San Juan flowing southward into the Pacific and the Rio Atrato flowing northward into the Caribbean. The Cordillera Occidental is believed to be of a block faulted nature (Oppenheim, 1952) bounded on the west by the Tertiary Atrato-San Juan trough, and on the east by the narrow Cauca-Patia trough.

The predominant tectonic pattern of the Colombian Andes is that of block-faulting and not of overthrusting. The graben structure of the Magdalena and Cauca troughs and the absence of important regional zones of low-angle thrusting in the Colombian Andes has provided evidence (Oppenheim, 1952) to confirm this view.

7.6 Structure (Plate I)

The Serrania del Darien forms the continental divide in eastern Panama extending from the Gulf of San Blas (9°30'N, 79°00'W) to beyond

the Colombian border where it is terminated by the Atrato river basin. This structurally arcuate ridge of basement rocks, which is convex to the northeast, has been described by Schuchert (1935), and Terry (1956) as an asymmetrical anticline with steepest dips on the northeast flanks facing the Caribbean. The alignment of faults and joint systems interpreted from the radar imagery in the central and southern part of the continental divide would tend to support the broad anticlinal interpretation of this area. For example, the pattern of the joint systems and faults appear to reflect extensional fractures both perpendicular and parallel to the principle axis of the basement complex. Those features perpendicular to the axis represent extensional fractures resulting from an elongation parallel to the axis, and those features parallel to the axis which represent crestal tensional release perpendicular to the trend of the basement complex.

The structural situation along the continental divide in extreme northwestern Darien appears to be quite different from that present to the southeast. Just off the northwestern limits of Plate I, at the headwaters of the Rio Morti, the core area of the continental divide has been described as a horst, bounded by normal faults (IOCS, 1968). Immediately southeast of the area described in the IOCS Report, starting at 8°50'N and extending southeast to 8°35'N (headwaters of the Rio Tuquesa) a series of faults have been interpreted parallel to the continental divide area. These faults are probably genetically similar to those described in the IOCS Report, i.e., normal faults; however, no direction of displacement can be inferred using the imagery alone.

Paralleling the continental divide to the southwest, moderately dipping strata eventually flatten out to form the broad structural and topographic depression containing the Tuira-Chucunaque basin in the southeast, and the Bayano basin in the northwest. This continuous arcuate trough of sedimentary rocks has been previously stated in the present report to be the northwestern extension of the Bolivar geosyncline. The two most obvious structural features of the Tuira-Chucunaque basin are the Chucunaque and Tuira synclines which are separated from each other by a faulted ridge located between the Rios Chico and Yape. The steep dips (up to 22 degrees) of the

southern nose of the Tuira syncline are illustrated in Figure 4.2 g (north is toward upper right corner), whereas more moderate dips are interpreted on the northern end as shown in Figure 4.2 j (north towards lower left corner).

Five small anticlines were mapped by Shelton (1952) within the confines of the Tuira-Chucunaque basin; however, only two of these could be interpreted on the radar imagery as structural anomalies, and the appropriate map symbols on these five anticlines have been indicated on Plate I. A geomorphic anomaly of substantial size (embracing at least 400 square kilometers) is centered at 8°22'N, 77°41'W; which appears to be reflecting a subtle, subsurface, structural high. The outline of this anomaly is especially evident when one examines the drainage of the Rios Tuquesa and Tupisa on the radar Mosaic (Figure 2.3). These two tributaries of the Rio Chucunaque may be located precisely on Plate I, and then relocated on the imagery of Figure 2.3.

In central Darien Province, west of the basins occupied by the Rios Tuira and Chucunaque, a series of tightly folded asymmetrical anticlines have been mapped from the radar imagery. The largest structure, the Pirre anticline (Serrania de Pirre), and the sub-parallel Setetule anticline (Cerro Setetule), plunge to the north. These two anticlines separate the basin of the upper Rio Tuira from that of the Rio Balasas to the west. Major faulting is evident on the radar imagery on the west flank of Pirre, where Terry (1956) has reported vertical strata cut off by a high angle reverse fault. Terry has also noted strike-slip displacement (right lateral) along the Pirre fault, but this cannot be interpreted from the radar imagery. This major fault strikes approximately north-south in the area of maximum displacement.

North-northwesterly from the Pirre-Setetule anticlines, a large anticline appears to have fragmented into a series of en echelon folds. The north-trending en echelon pattern of these folds may be reflecting a dominant left lateral, strike slip motion at depth, although confirming evidence is not interpretable from imagery analysis. Two of these anticlines are bounded on the west by faults which have been inferred as high angle reverse, with the steepest dips on the west. The dip on the east flanks of these asymmetrical folds has been measured from the radar imagery up to 30 degrees. The anti-

cline centered at 8°20'N, 77°52'W (Figure 4.3 d, north is towards the upper right corner) exhibits extensional joint systems with a characteristic orientation normal to folding.

Even though the interpretation of radar imagery has revealed the accurate geometric pattern, and the probable structural configuration (not previously reported in the literature) of these tightly folded anticlines, the present study has contributed little concerning the detailed stratigraphic relationships in this area. As previously discussed on the radar imagery there are no stratigraphic sequences that can be precisely separated and correlated along the flanks of these anticlines, nor can the texture of strata from the opposite sides of the basin be matched. Data from the IOCS Report (1968) indicate that an apparent stratigraphic equivalent to the strata in the core of the northernmost anticline (8°30'N, 78°04'W) on Plate I, may be of Early Miocene age; even though Terry, (1956); Shelton, (1952); and Sapper (1937) have placed these strata at an Eocene-Oligocene age.

West of the trend of these asymmetric anticlines, the Rio Balsas embayment is separated from the Sambu basin by a fault block of basement rocks which, in places, may be overlain by Miocene-Oligocene strata. The fault bounding the Sambu basin on the northeast side has been mapped by Terry (1956) as being high-angle reverse in nature. Even though the type of displacement cannot be interpreted from the radar imagery, the total length of the fault has been extended 25 kilometers further to the southeast than had been previously reported. Southwest of the Sambu basin is another fault block of igneous basement which acts as a structural barrier between the Pacific Ocean and Sambu basin.

The Pacific coastal fault block has several features which are especially noticeable on the radar imagery. For example, at the northwestern end of this fault block there is an obvious change in trend of Garachine Point (8°05'N, 78°26'W) from northwest to northeast. This change in trend is probably related to a right lateral, strike slip fault which has been indicated on Plate I, but precise lateral offset cannot be determined through radar interpretation.

The most conspicuous fault recorded on the radar imagery is a feature that has not been previously noted on published maps. This fault can be traced on the radar imagery from a point on the Pacific coast (7°45'N, 78°17'W) southward to the Colombian border. The southeastern extension of this same fault appears to be present in the Intendencia de Choco of Colombia (Republic Colombia's 1962 edition, geologic map). In Colombia this fault appears to separate older Tertiary volcanics (on the east) from younger volcanics (on the west). The total length in both Panama and Colombia is approximately 300 kilometers. Although the radar imagery does not provide evidence for horizontal displacement, it is postulated that some right-lateral strike slip movement has taken place. This movement appears to be reflected in the associated faults which have a dominant north-northwesterly trend; i.e., in a possible second-order shear direction.

The basement rock trends of the Serrania de Pirre (trending southwest) and Serrania de Bagre (trending southeast) converge near the Colombian border, where the summits of each are leveled to a series of small flat areas, so flat that water stands in the undrained depressions (Terry, 1956). Schuchert (1935) also noted that near the Colombian border (Altos de Aspave) a series of narrow, flat-topped, south-trending ridges dominated the topography, with minor faulted and folded strips of sediments around the edges. Beyond the southern limits of Plate I, a major, flat-topped linear ridge can be interpreted on radar imagery (Figure 2.3) immediately south of the Altos de Quia (refer to Plate I for geographic location, 7°34'N, 77°31'W), which is evidently one of the many erosional remnants of a peneplane.

The Serrania de Baudo (Figure 7.1) of northwestern Colombia displays a complex structural pattern of en echelon folds and normal faults (West, 1957). A similar structural pattern is reflected in the longitudinal faults of the Pacific coastal ranges of Darien, where northwesterly trending faults are associated with north-northwesterly secondary trends. Thus, from Punta Garachine (8°06'N, 78°25'W) in the San Miguel area of Panama, to Cabo Corrientes on the Pacific coast of western Colombia, an area of structural unity is revealed. Even though joint systems and faults are defined on the radar imagery, lack of field data in this region of the Darien

prevent a valid structural interpretation. However, it is postulated that the secondary fault system associated with the major longitudinal fault system is a reflection of right lateral strike-slip movement. Regardless of the direction of movement, the structure of the Pacific Coast ranges of both northwestern Colombia and particularly the Darien of eastern Panama is directly related to the apparent northerly bowing of the Isthmus of Panama. Major uplift of the Serrania de Baudo is believed to have taken place in Late Tertiary (Oppenheim, 1952) coincident with the emergence of the Atrato-San Juan portion of the Bolivar geosyncline.

The Serrania del Darien appears to present a slightly different structural history than the geographically parallel Pacific coastal ranges. Considered to be a spur of the Cordillera Occidental (Lloyd, 1963) the Serrania del Darien is separated from northwestern Colombia by the Atrato depression. While a gentle anticlinal upwarping appears to be dominant along the continental divide of southeastern Darien near the Colombia-Panama border, block faulting prevails in northwestern Darien. This segmentation of the Serrania del Darien is compatible with the findings of Whitmore and Stewart (1968), who have reported that the San Blas area of the continental divide was detached from Colombia from Eocene to Pliocene time.

From a regional aspect, the Darien area can be subdivided into two major structural provinces: (1) the structure of Darien southeast of San Miguel Bay, southwest of the estuaries of the Rio Tuira, and southeast of the Rio Chico, and (2) the structure of Darien northeast of the estuaries of the Rio Tuira and north of the Rio Chico. The first structural subdivision is dominated by a series of fault blocks. The second structural province is dominated by normal faulting in the area of the basement complex, and high-angle reverse faulting in the areas of asymmetrical en echelon folding. In addition, these two structural subdivisions are separated by a line trending approximately east-west centered along the Rio Chico river valley, and extending from the Serrania de Barge to the Caribbean coast at Playeta (8°25'N, 77°11'W). Southeast of this line the structural pattern appears to reflect uplift and folding which exposes the basement complex; whereas to the northwest, folding of sedimentary strata appears to dominate. This is

particularly evident along the Serrania del Darien where a marked change in the outcrop width of basement rock occurs, i.e., narrow exposures to the northwest of the Rio Chico fault-line and wider exposures to the southeast of this same line. It is speculated that the Rio Chico fault-line may be the most obvious expression of a structural line of weakness extending across two thirds of the Darien, separating southeastern Darien (influenced primarily by the tectonics of Colombia) from east-central Darien (influenced by Isthmian tectonics).

7.7 Geologic History - Eastern Panama

The oldest formations exposed on the Isthmus of Panama are of volcanic origin and believed to be older than Middle Eocene age (Woodring, 1957); however, beneath these volcanics is an older tectonic arch which may have had its origin in Cretaceous or Late Jurassic time (Schuchert, 1935). The known geological history of Panama is all of Cenozoic time, and Olsson (1932) has suggested that sedimentation is intimately related to the formation of the Bolivar geosyncline. The initiation of uplift and folding which probably began at the close of Cretaceous time along the Andean geosyncline was compensated by down-warping toward the west resulting in the structural outline of the Bolivar geosyncline. Marine transgression over an erosional surface of predominately volcanic terrain was characteristic of Eocene time, with local uplift along the coastal mountain ranges. An increase in the marine character of the sediments within the Bolivar geosyncline is evidenced in Oligocene time, accompanied by increased volcanic material in the San Miguel area. By Oligocene time, the Serrania del Darien was an isolated island land mass. The long period of continuous deposition from Eocene through Early Miocene was disrupted in Middle Miocene time by uplift and erosion. In central and western Panama, all of the strata deposited from Eocene through Middle Miocene time were intruded by dikes, and flows of andesites, rhyolites and basal s (Schuchert, 1935). In central Panama, regional uplift was accompa.. ed by warping and medial doming, exposing pyroclastics and sediment / strata dipping toward the coasts

(Howe, 1908). Similarly, in eastern Panama the Serrania del Darien was faulted and folded into a broad anticlinal structure. To the southwest, the coastal and interior mountain ranges were deformed into a series of fault blocks and asymmetrical folds. The major structural trends are also reflected in the Sanson Hills area where a series of tightly folded en echelon anticlines were formed. Although active volcanism was evident during this period of uplift and deformation in central and western Panama, this was not true for the Darien area, (Terry, 1956). Final uplift during and subsequent to the deposition of the Middle and Upper Miocene strata is evidenced in the relatively non-marine and off-lap character of these sediments.

Thus, in eastern Panama, the northwestern extension of the Bolivar geosyncline was the site of marine deposition from Eocene until Late Miocene time, with the deeper areas probably receiving sediments during at least Early Pliocene time. Today the former axis of the Bolivar geosyncline approximates a long series of lowland basins in eastern Panama and northwestern Colombia.

CHAPTER 8

CONCLUSIONS

The interpretation of radar imagery facilitates physiographic differentiation and geological reconnaissance mapping on a regional scale. At a very minimum, a ready subdivision can generally be made between igneous and sedimentary rocks. Similarly, large scale structural units can be synoptically studied, and the single-strip imagery format used in conjunction with a radar mosaic enables the geologist to become quickly familiar with the essential features of structural provinces. Thus, on a regional scale, gross lithologic and structural subdivisions can be interpreted at levels of detail which often exceed those available on existing small scale geologic maps in many parts of the world.

On a more detailed scale, a relative stratigraphic sequence can be determined using radar imagery but only if the lithic units are expressed in the terrain configuration, and the structure is not too complicated. In the Darien area, because of the rather uniform nature of both the sedimentary rock sequence and vegetal canopy, subdivisions distinguished on the basis of tone, apparent thickness and texture have proven to be quite difficult; notably more so than, for example, studies in the Ouachita Mountains in the United States (Rouse, et al., 1966). Each geologic environment is relatively distinctive. Where collateral field data are available, and are used in conjunction with radar imagery interpretation, the problem becomes less complicated. Lacking such field data, however, lithologic interpretations from radar imagery are largely provisional.

Although single strip imagery can contribute significant information for geologic analysis, it is apparent from the analysis of multiple flight coverage from both Panama and several areas within the continental United States that look-direction does influence the detectability of geologic features expressed in the terrain configuration. Depending on the relative topographic relief, effective incident angle of the radar energy, and look-

CHAPTER 8

CONCLUSIONS

The interpretation of radar imagery facilitates physiographic differentiation and geological reconnaissance mapping on a regional scale. At a very minimum, a ready subdivision can generally be made between igneous and sedimentary rocks. Similarly, large scale structural units can be synoptically studied, and the single-strip imagery format used in conjunction with a radar mosaic enables the geologist to become quickly familiar with the essential features of structural provinces. Thus, on a regional scale, gross lithologic and structural subdivisions can be interpreted at levels of detail which often exceed those available on existing small scale geologic maps in many parts of the world.

On a more detailed scale, a relative stratigraphic sequence can be determined using radar imagery but only if the lithic units are expressed in the terrain configuration, and the structure is not too complicated. In the Darien area, because of the rather uniform nature of both the sedimentary rock sequence and vegetal canopy, subdivisions distinguished on the basis of tone, apparent thickness and texture have proven to be quite difficult; notably more so than, for example, studies in the Ouachita Mountains in the United States (Rouse, et al., 1966). Each geologic environment is relatively distinctive. Where collateral field data are available, and are used in conjunction with radar imagery interpretation, the problem becomes less complicated. Lacking such field data, however, lithologic interpretations from radar imagery are largely provisional.

Although single strip imagery can contribute significant information for geologic analysis, it is apparent from the analysis of multiple flight coverage from both Panama and several areas within the continental United States that look-direction does influence the detectability of geologic features expressed in the terrain configuration. Depending on the relative topographic relief, effective incident angle of the radar energy, and look-

direction, geologic features such as joint systems, faults, and dip slopes may be advantageously enhanced or completely suppressed. Thus, to obtain the maximum benefit from radar geological reconnaissance studies in poorly mapped areas, it will be necessary to image the specific region from four orthogonal look-directions. For more detailed studies where the terrain configuration is already known, a minimum of two opposing look-directions will be required over any specific geologic feature.

As also true with photogeologic interpretation, geologic interpretation of radar imagery, while providing a great deal of geologic information, will by no means supply it all, and laboratory studies should be correlated with supplementary field data. Unfortunately, corroborative field data are especially lacking in a large part of the Darien area. Those provisional interpretations made during this study will undoubtedly remain as such, for at least the foreseeable future. Radar imagery interpretation developed through the surrogate approach has provided geologic information which supports the following observations:

1. Analysis of single-strip radar imagery in combination with the radar mosaic have provided a much more accurate representation of the regional geologic relationships of eastern Panama and northwestern Colombia.
2. The regional stratigraphic relationships as interpreted from radar imagery have substantiated the reconnaissance studies of earlier investigators that a continuous belt of sedimentary rocks extends through eastern Panama into northwestern Colombia.
3. There is an apparent structural subdivision northwest and southeast of the Rio Chico fault line. The tectonic evolution of this structural boundary is intrinsically related to the present structural configuration of the Isthmus.
4. The actual structural configuration of the en echelon folds in the Sanson Hills area (Plate I) had not previously been reported on geologic maps.
5. The regional fault and joint system patterns have never been revealed in such detail as those interpretable from the radar imagery.

Thus, with the exception of those data provided by field investigation, the geologic information interpretable from the radar imagery of eastern Panama far exceed those data previously available through conventional reconnaissance methods. Certainly radar remote sensing offers the only practical technique for reconnaissance mapping in the wet tropics; however, where aerial photography can be obtained, radar imagery should be visualized as a supplement providing its own unique data contribution. Realistically appraising the inherent limitations of radar geological reconnaissance, the capability of obtaining topographic mapping data simultaneously with geologic information provides the geologist with an important exploration tool. The production of radar-derived geological reconnaissance surveys in the cloud-shrouded environments of the world should be a useful and welcome form of foreign aid.

When additional field data become available for those relatively unmapped areas of Panama and Colombia, as well as oceanographic data along the Isthmian coasts, it will be possible to relate the geologic and tectonic evaluation of eastern Panama with that of adjacent parts of Central America.

8.1 Recommendations for Further Study

The scientific evaluation of a radar imaging system presents the investigator with a multi-variable problem. For example, look-direction, incidence angle, polarization, frequency and terrain environment can, independently or in combination, affect the signal recorded on radar imagery. Those components which affect the scattering coefficients are extremely difficult to separate, yet to be meaningful and significant, a test must be able to isolate the more important variables affecting the signal array. Except for the work at Ohio State University (Cosgriff, et al., 1960) and Goodyear Aerospace (Goodyear, 1959), no adequate experiments have been conducted where the experimenters have attempted to control the terrain parameters.

while varying the radar parameters. To completely document those factors which affect the scattering coefficient (and resultant signal return), it will be necessary to design a scientific test in which the terrain parameters are variable, yet precisely controlled. Field data must then be systematically compared with the return signal array.

Among the most conspicuous features interpreted on radar imagery are those linears related to faulting and jointing. A parameter that must be defined is the apparent detection restraint which is controlled by topographic relief. Is there a topographic threshold below which linear terrain features are not detectable? Multiple frequency — flight coverage would be required over an area having numerous topographically expressed terrain features (such as the Spanish Peaks, Colorado), and where detailed topographic mapping (contour interval 6 meters or less) is also available.

Longer wavelength systems flown simultaneously with shorter wavelength systems should provide some insight as to what may be anticipated in the way of both vegetal or surficial penetration. Long-wavelength radars may contribute significant data for geologic analysis, and similarly, multi-frequency radars should aid in lithologic discrimination.

Studies using simultaneously-produced like-and cross-polarized radar imagery have demonstrated that geologists can obtain some geologic data that was unobtainable with single polarized imagery. Polypolarization imagery may enhance the interpreter's ability to discriminate lithologies, but documentation must be accomplished under a variety of known terrain conditions, utilizing multiple flight coverage and four orthogonal look-directions.

When additional radar imagery and field data become available for that portion of east-central Panama and northern Colombia which is essentially unmapped, it will be possible to relate the geology and tectonics of eastern Panama with that of adjacent parts of Central America. Similarly, analysis of these data should add some insight into the genetics and mechanics of the Isthmian arch.

APPENDIX A

LOOK-DIRECTION DATA
PANAMA IMAGERY

GEOLOGIC FEATURE	LOCATION	TOPOGRAPHIC RELIEF (Meters)	MAP ORIENTATION OF FEATURE	DETECTABILITY-RANGE-AZIMUTH PASS 1 ↗ Approx N50° E	PASS 2 ↙ Approx S50° W	PASS 3 ↖ Approx N40° W	PASS 4 ↘ Approx S40° E	REMARKS
FAULT	8°11'N 77°37'W	> 50	N 50° E	Detectable Near-Range 80°	Detectable Near-Range 80°	Detectable Near-Mid-Far 5°	Detectable Near-Mid 20°	
FAULT	8°26'N 77°14'W	<50	N 70° E	Not Detectable Mid-Far 50°	Detectable Mid-Range 60°	Not Available	Detectable Mid-Range 45°	Detectability due to vegetal contrast along fault
FAULT	8°05'N 77°57'W to 7°54'N 77°42'W	8.5 Km >50M 26.5 Km <50	N 55° W	Where relief >50 m Detectable Mid-Range 20°	Where relief <50 m Not Detectable Near-Range 30°	Not Available	Total Length Detectable Mid-Far 75°	
FAULT	8°26'N 77°18'W	>50	N 15° W	Detectable Mid-Range 20°	Detectable Far-Range 20°	Not Available	Detectable Mid-Range 30°	
FAULT (NW End)	7°45'N 78°15'W to 7°37'N 78°10'W	<50	N 45° W	Not Detectable Mid-Far 2°	Not Detectable Far-Range 5°	Not Detectable Near-Range 80°	Detectable Mid-Range 80°	Detectable only where terrain slope is away from radar. Repeatable on other southwest passes.
FAULT	8°29'N 78°03'W	>50	N 55° W	Not Detectable Mid-Range 35°	Detectable Near-Mid 15°	Detectable Near-Range 85°	Detectable Mid-Range 60°	
FAULT	8°23'N 77°53'W	<50	N 50° W	Not Detectable Near-Range 30°	Not Detectable Near-Range 25°	Detectable Near-Range 85°	Detectable Near-Range 85°	
FAULT	7°37'N 77°42'W	>50	N 60° E	Detectable Near-Range 75°	Detectable Near-Range 80°	Detectable Mid-Range 30°	Not Detectable Far-Range 25°	Not detectable on Pass 4 due to radar shadowing
FAULT	8°28'N 77°55'W	<50	N 03° W	Detectable Near-Range 50°	Detectable Mid-Range 35°	Detectable Far-Range 45°	Detectable Far-Range 45°	Fault expressed by river offset
FAULT	8°31'N 77°55'W	<50	N 65° W	Not Available	Detectable Mid-Range 35°	Not Detectable Mid-Range 30°	Detectable Far-Range 60°	
FAULT	8°22'N 77°42'W	<50	N 70° E	Detectable Near-Range 65°	Not Available	Detectable Far-Range 25°	Detectable Mid-Range 40°	Fault expressed by vegetation boundary

GEOLOGIC FEATURE	LOCATION	TOPOGRAPHIC RELIEF (Meters)	MAP ORIENTATION OF FEATURE	DETECTABILITY-RANGE-AZIMUTH				REMARKS
				PASS 1 ↗ Approx N50°E	PASS 2 ↙ Approx S50°W	PASS 3 ↖ Approx N40°W	PASS 4 ↘ Approx S40°E	
FAULT	8°02'N 77°38'W	<50	N 20° E	Detectable Mid-Far 70°	Not Available	Detectable Far-Range 40°	Detectable Mid-Far 30°	
FAULT	8°08'N 78°05'W	<50	N 65° E	Detectable Mid-Range 70°	Detectable Near-Range 65°	Not Available	Not Detectable Near-Range 25°	
FAULT	8°08'N 78°04'W	>50	N 10° W	Detectable Mid-Range 50°	Detectable Near-Range 40°	Not Available	Detectable Near-Range 70°	
FAULT	7°26'N 78°06'W	<50	N 50° W	Not Available	Not Detectable Mid-Range 15°	Detectable Near-Range 90°	Detectable Near-Range 60°	
FAULT	7°54'N 78°19'W	>50	N 10° W	Detectable Mid-Range 35°	Not Available	Detectable Near-Mid 35°	Not Available	
FAULT	7°42'N 77°46'W	>50	N 60° E	Not Available	Detectable Mid-Far 80°	Detectable Mid-Range 25°	Not Available	
FAULT	8°15'N 78°07'W	>50	N 20° W	Not Available	Detectable Mid-Range 20°	Not Available	Detectable Near-Range 75°	
FAULT	8°13'N 77°02'W	<50	N 20° W	Not Detectable Near-Mid 25°	Not Available	Not Available	Detectable Mid-Range 75°	
FAULT	8°26'N 77°14'W	<50	N 05° W	Detectable Far-Range 30°	Detectable Mid-Range 15°	Not Available	Detectable Mid-Range 50°	Fault defined in part by vegetation contrast
FAULT	8°14'N 77°02'W	>50	N 30° W	Detectable Mid-Range 25°	Not Available	Not Available	Detectable Mid-Far 75°	
FAULT	8°05'N 77°42'W	<50	N 40° E	Detectable Near-Range 90°	Not Available	Not Detectable Mid-Range 40°	Not Detectable Mid-Range 25°	

GEOLOGIC FEATURE	LOCATION	TOPOGRAPHIC RELIEF (Meters)	MAP ORIENTATION OF FEATURE	DETECTABILITY-RANGE-AZIMUTH PASS 1 ↗ Approx N50°E	PASS 2 ↙ Approx S50°W	PASS 3 ↖ Approx N40°W	PASS 4 ↘ Approx S40°E	REMARKS
FAULT	8°42' N 77°37' W	>50	N 25°W	Not Detectable Near-Range 15°	Not Detectable Mid-Far 15°	Not Available	Detectable Mid-Range 80°	
FAULT	7°41' N 77°37' W	>50	N 60°E	Detectable Near-Range 90°	Not Detectable Far-Range 70°	Not Available	Detectable Near-Range 20°	Non-detectability on Pass 2 caused by radar shadowing
FAULT	8°48' N 77°39' W	<50	N 80°E	Detectable Mid-Range 60°	Portion Detectable Near-Range 60°	Not Available	Detectable Near-Range 30°	Vegetation boundary and transition in topographic relief defines this fault
FAULT	8°04' N 77°38' W	<50	N 65°E	Detectable Mid-Range 70°	Detectable Far-Range 70°	Detectable Mid-Range 10°	Detectable Far-Range 20°	Detectability due to lithologic discontinuity
FAULT	8°05' N 77°34' W	<50	N 05°W	Not Detectable Far-Range 10°	Not Detectable Mid-Range 30°	Not Detectable Mid-Range 40°	Detectable Near-Range 80°	
FAULT	8°21' N 78°02' W	<50	N 17°W	Not Detectable Far-Range 20°	Detectable Mid-Far 25°	Detectable Near-Far 60°	Detectable (in part) Far-Range 60°	
FAULT	8°04' N 78°25' W	>50	N 20°E	Detectable Near-Range 70°	Detectable Far-Range 65°	Detectable Near-Range 40°	Not Available	
FAULT	8°01' N 78°22' W	>50	N 30°W	Detectable Mid-Range 25°	Detectable Far-Range 25°	Detectable Mid-Range 90°	Not Available	
FAULT	8°17' N 77°53' W	>50	N 70°E	Detectable Far-Range 80°	Poorly Defined Far-Range 80°	Detectable Far-Range 25°	Poorly Defined Far-Range 30°	Pass 2 - radar shadow Pass 3 - enhanced by ıdar shadow Pass 4 - radar shadow

GEOLOGIC FEATURE	LOCATION	TOPOGRAPHIC RELIEF (Meters)	MAP ORIENTATION OF FEATURE	DETECTABILITY-RANGE-AZIMUTH				REMARKS
				PASS 1 Approx N50°E	PASS 2 Approx S50°W	PASS 3 Approx N40°W	PASS 4 Approx S40°E	
JOINT SYSTEMS	8°24'N 77°45'W	<50	N 3° W	Not Detectable Mid-Range 20°	Detectable Far-Range 40°	Detectable Far-Range 65°	Detectable Far-Range 70°	
JOINT SYSTEMS	8°00'N 78°09'W	>50	N 30° W	Detectable Mid-Range 20°	Detectable Mid-Range 30°	Detectable Far-Range 70°	Not Available	
JOINT SYSTEMS	8°23'N 77°55'W	<50	N 75° E	Detectable Near-Range 60°	Detectable Mid-Range 90°	Not Detectable Far-Range 5°	Not Detectable Mid-Range 5°	
JOINT SYSTEMS	7°29'N 78°07'W	<50	N 80° E	Detectable Far-Range 40°	Detectable Far-Range 50°	Detectable Near-Range 50°	Detectable Mid-Range 30°	Steep dipping terrain towards southwest
JOINT SYSTEMS	7°29'N 77°59'W	<50	N 30° E	Not Detectable Mid-Far 65°	Not Detectable Near-Mid 60°	Detectable Far-Range 30°	Not Available	
JOINT SYSTEMS	7°31'N 78°00'W	<50	N 85° E	Not Detectable Far-Range 40°	Not Detectable Mid-Range 40°	Detectable Mid-Far 30°	Not Available	
JOINT SYSTEMS	7°58'N 78°25'W	<50	N 30° W	Poorly Defined Far-Range 30°	Detectable Near-Range 20°	Poorly Defined Mid-Range 90°	Not Available	Pass 1 - Terrain slope toward radar Pass 2 - Terrain slope away from radar Pass 3 - Terrain slope away/radar
JOINT SYSTEMS	7°21'N 77°58'W	<50	N 70° E	Not Detectable Mid-Range 50°	Not Detectable Near-Range 35°	Detectable Mid-Range 25°	Not Available 35°	
JOINT SYSTEMS	8°20'N 77°52'W	>50	N 70° E	Detectable Mid-Range 85°	Detectable Near-Range 90°	Poorly Defined Far-Range 25°	Detectable Mid-Far	Pass 3 - Extensive radar shadowing
JOINT SYSTEMS	8°39'N 77°55'W	<50	N 65° E	Detectable Far-Range 35°	Poorly Defined Mid-Range 25°	Poorly Defined Near-Range 35°	Not Available	
JOINT SYSTEMS	8°04'N 78°10'W	>50	N 60° W	Detectable Mid-Range 30°	Detectable Near-Range 30°	Detectable Far-Range 50°	Detectable Far-Range 65°	
JOINT SYSTEMS	8°09'N 78°12'W	<50	N 20° W	Not Detectable Mid-Range 25°	Not Detectable Far-Range 25°	Detectable Mid-Range 60°	Detectable Far-Range 70°	
JOINT SYSTEMS	8°09'N 78°12'W	>50	N 80° W	Detectable Mid-Range 60°	Detectable Far-Range 50°	Detectable Mid-Range 50°	Not Detectable Far-Range 40°	Pass 4 - Radar shadowing

GEOLOGIC FEATURE	LOCATION	TOPOGRAPHIC RELIEF (Meters)	MAP ORIENTATION OF FEATURE	DETECTABILITY-RANGE-AZIMUTH PASS 1 ↗ Approx N50°E	PASS 2 ↙ Approx S50°W	PASS 3 ↖ Approx N40°W	PASS 4 ↘ Approx S40°E	REMARKS
JOINT SYSTEMS	7°49'N 78°19'W	>50	N 45° E	Detectable Far-Range 90°	Not Available	Not Detectable Near-Range 30°	Not Available	Pass 3 - No shadowing in near range
JOINT SYSTEMS	7°51'N 79°21'W	<50	N 65° E	Detectable Mid-Range 60°	Not Available	Detectable Near-Range 20°	Not Available	Pass 4 - Terrain slope away from radar
JOINT SYSTEMS	7°51'N 79°19'W	<50	N 65° E	Detectable Mid-Range 60°	Not Available	Not Detectable Near-Range 20°	Not Available	Pass 4 - Slope toward radar
JOINT SYSTEMS	7°41'N 77°42'W	<50	N 60° W	Not Available	Detectable Mid-Range 70°	Not Detectable Near-Mid 20°	Not Available	
JOINT SYSTEMS	7°39'N 77°47'W	>50	N 50° E	Not Available	Detectable Far-Range 80°	Detectable Mid-Range 35°	Not Available	
JOINT SYSTEMS	8°07'N 78°08'W	>50	N 30° W	Detectable Mid-Range 30°	Detectable Near-Range 30°	Not Available	Detectable Mid-Range 70°	
JOINT SYSTEMS	8°27'N 77°16'W	<50	N 80° E	Not Detectable Near-Range 30°	Not Available	Not Available	Detectable Far-Range 35°	
JOINT SYSTEMS	8°26'N 77°20'W	>50	N 80° E	Detectable Near-Range 70°	Not Available	Not Available	Detectable Far-Range 30°	Pass 1 - Poorly defined Pass 4 - Enhanced by shadowing
JOINT SYSTEMS	8°40'N 77°23'W	<50	N 40° W	Detectable Mid-Range 30°	Detectable Near-Range 20°	Not Available	Detectable Mid-Range 60°	Pass 2 - Terrain slope away from radar
JOINT SYSTEMS	8°38'N 77°23'W	>50	N 40° W	Detectable Far-Range 30°	Detectable Mid-Range 30°	Not Available	Detectable Near-Range 60°	

GEOLOGIC FEATURE	LOCATION	TOPOGRAPHIC RELIEF (Meters)	MAP ORIENTATION OF FEATURE	DETECTABLIITY-RANGE-AZIMUTH PASS 1 ↗ Approx N50°E	PASS 2 ↙ Approx S50°W	PASS 3 ↖ Approx N40°W	PASS 4 ↘ Approx S40°E	REMARKS
JOINT SYSTEMS	9°41'N 77°35'W	<50	N 30° W	Not Available	Detectable Near-Mid 30°	Not Available	Not Detectable Near-Range 50°	
JOINT SYSTEMS	9°46'N 77°35'W	<50	N 70° E	Not Available	Not Detectable Mid-Range 20°	Not Available	Detectable Near-Mid 40°	
JOINT SYSTEMS	9°11'N 78°07'W	>50	N 05° W	Detectable Near-Range 50°	Detectable Mid-Range 45°	Not Available	Detectable Mid-Range 50°	
JOINT SYSTEMS	9°11'N 78°08'W	<50	N 85° W	Not Detectable Near-Range 25°	Detectable Mid-Range 40°	Not Available	Detectable Mid-Range 55°	Pass 1 - Dip slope toward radar Pass 2 - Dip slope away from radar
DIP SLOPE	8°11'N 77°39'W	>50	N 55° E	Not Detectable Near-Range 90°	Detectable Near-Range 75°	Detectable Near-Range 5°	Detectable Near-Mid 20°	
DIP SLOPE	7°35'N 78°07'W	>50	N 50° W	Detectable Mid-Range 5°	Not Available	Not Detectable Mid-Range 80°	Detectable Near-Range 80°	Pass 3 - Dip slope toward radar Pass 4 - Poorly defined in near range
DIP SLOPE	8°11'N 77°35'W	>50	N 55° E	Not Detectable Near-Range 90°	Detectable Near-Range 75°	Detectable Mid-Far 5°	Detectable Near-Range 20°	Pass 1 - Dip slope toward radar Pass 2 - Dip slope away from radar Pass 4 - Poorly defined in near range
DIP SLOPE	9°13'N 78°04'W	<50	N 20° W	Not Available	Not Detectable Near-Range 10°	Not Available	Detectable Near-Range 80°	Pass 4 - Dip slope away from radar
DIP SLOPE	9°02'N 77°39'W	<50	N 20° E	Detectable Mid-Range 70°	Not Available	Detectable Far-Range 40°	Not Detectable Mid-Range 30°	Pass 1 - Dip slope away from radar Pass 3 - Dip slope away from radar Pass 4 - Dip slope toward radar

GEOLOGIC FEATURE	LOCATION	TOPOGRAPHIC RELIEF (Meters)	MAP ORIENTATION OF FEATURE	DETECTABILITY-RANGE-AZIMUTH				REMARKS
				PASS 1 ↗ Approx N50°E	PASS 2 ↙ Approx S50°W	PASS 3 ↖ Approx N40°W	PASS 4 ↘ Approx S40°E	
DIP SLOPE	7°53'N 77°35'W	>50	N 5° W	Detectable Near-Range 40°	Detectable Near-Range 40°	Detectable Near-Range 70°	Detectable Near-Mid 60°	
DIP SLOPE	7°47'N 77°32'W	>50	N 25° E	Detectable Mid-Range 75°	Detectable Far-Range 70°	Detectable Near-Range 10°	Detectable Near-Range 25°	Pass 3 - Information is inferred from adjoining dip slopes
DIP SLOPE	8°11'N 77°28'W	>50	N 10° W	Detectable Mid-Range 35°	Detectable Far-Range 30°	Detectable Near-Range 70°	Detectable Mid-Range 60°	
DIP SLOPE	7°45'N 78°00'W	>50	N 85° W	Detectable Near-Range 80°	Detectable Near-Range 90°	Detectable Mid-Range 5°	Not Available	Pass 2 - Dip slope away from radar Pass 3 - Dip slope toward radar
DIP SLOPE	8°30'N 78°00'W	>50	N 40° W	Detectable Near-Mid 5°	Detectable Near-Mid 10°	Detectable Near-Range 90°	Detectable Mid-Range 90°	
DIP SLOPE	8°26'N 78°00'W	>50	N 15° W	Detectable Far-Range 40°	Detectable Near-Range 50°	Detectable Near-Range 70°	Not Detectable Mid-Range 60°	Pass 4 - Dip slope toward radar
DIP SLOPE	8°25'N 77°51'W	<50	N 45° W	Detectable Near-Range 10°	Detectable Mid-Range 5°	Detectable Far-Range 75°	Not Detectable Near-Range 80°	Pass 1 - Dip 90° to radar Pass 2 - Dip 90° to radar Pass 3 - Dip slope away from radar Pass 4 - Dip slope toward radar
DIP SLOPE	8°17'N 77°04'W	<50	N 35° W	Detectable Mid-Range 20°	Detectable Near-Range 15°	Not Available	Detectable Near-Range 90°	Pass 1 - Dip slope 70° to radar Pass 2 - Dip slope 75° to radar Pass 4 - Dip slope away from radar
DIP SLOPE	8°21'N 77°55'W	<50	N 5° W	Detectable Near-Range 20°	Detectable Near-Range 5°	Not Detectable Far-Range 90°	Detectable Far-Range 80°	Pass 1 - Slope away from radar Pass 2 - Slope ca. 90° to radar Pass 3 - Slope toward radar Pass 4 - Slope away from radar
DIP SLOPE	8°24'N 77°55'W	<50	N 10° W	Not Detectable Near-Range 20°	Not Detectable Near-Range 50°	Detectable Far-Range 10°	Detectable Mid-Far 40°	Pass 1 - Slope approx. 90° Pass 2 - Shadowing Pass 3 - Slope approx. 90° Pass 4 - Slope away
DIP SLOPE	8°14'N 77°47'W	<50	N 35° W	Detectable Far-Range 5°	Not Detectable Mid-Range 50°	Detectable Mid-Range 45°	Detectable Far-Range 10°	Pass 1 - Slope approx. 90° Pass 2 - Slope toward radar Pass 3 - Slope away Pass 4 - Slope approx. 90°
DIP SLOPE	8°09'N 77°46'W	<50	N 10° E	Detectable Far-Range 70°	Not Detectable Mid-Range 50°	Detectable Mid-Range 45°	Detectable Far-Range 10°	Pass 1 - Slope away Pass 2 - Slope toward radar Pass 3 - Slope away Pass 4 - Slope approx. 90°
DIP SLOPE	8°22'N 77°33'W	>50	N 40° W	Detectable Mid-Range 10°	Not Available	Not Detectable Near-Range 75°	Detectable Near-Range 75°	Pass 1 - Look direction almost 90° to slope Pass 3 - Slope toward radar Pass 4 - Slope away from radar

BIBLIOGRAPHY

Anderson, J. L., 1945, "Petroleum Geology of Colombia, South America," Amer. Assoc. Petroleum Geologists Bull., vol. 29, no. 8, pp. 1063-1142.

Barr, D. J., 1968, "Use of Side-Looking Airborne Radar Imagery for Engineering Soil Studies," Final Tech. Report, Geog. Sci. Div., U. S. Army Engineer Topo. Lab. (June 1968), Ft. Belvoir, Virginia, 193 pp.

Beatty, F. D. and others, 1965, "Geoscience Potentials of Side-Looking Radar," Raytheon Autometric Corp., Alexandria, Virginia, 90 pp.

Bienvenu, L. R. and R. Pascucci, 1962, "Engineering Geology from Side-Looking Radar Records," Raytheon/Autometric Corp., Alexandria, Virginia, 13 pp.

Bylinsky, G., 1968, "From a High-Flying Technology, a Fresh View from Earth," Fortune Magazine, June 1, 1968, pp. 101-148.

Cameron, H. L., 1965, "Radar as a Surveying Instrument in Hydrology and Geology," Proc. 3rd Symp. Remote Sensing of Environment, (October 1964), University of Michigan, Ann Arbor, pp. 441-452.

Colwell, R. N., 1952, "Photographic Interpretation for Civil Purposes," in, Manual of Photogrammetry, Am. Soc. Photogrammetry, 2nd ed., Washington, D. C., pp. 535-602.

Cosgriff, R. L., W. H. Peake, and R. C. Taylor, 1960, "Terrain Scattering Properties for Sensor System Design," Terrain Handbook, vol. II, Columbus, Ohio State University Press, 117 pp.

Dalke, G. W. and R. M. McCoy, 1966, "Automatic Measurement and Reduction of Drainage Basin Data," University of Kansas, Lawrence, CRES Tech. Memo 61-32, 7 pp.

Davis, B. R., J. R. Lundien, and A. N. Williamson, Jr., 1966, "Feasibility Study of the Use of Radar to Detect Surface and Ground Water," U. S. Army Waterway Experiment Station Tech. Report No. 3-727, 93 pp.

Dellwig, L. F. and R. K. Moore, 1966, "The Geologic Value of Simultaneously Produced Like and Cross-Polarized Radar Imagery," J. Geophys. Research, vol. 71, pp. 3597-3601.

_____, J. N. Kirk, and R. L. Walters, 1966, "The Potential of Low Resolution Radar Imagery in Regional Geologic Studies," J. Geophys. Research, vol. 71, no. 20, pp. 4995-4998.

_____, H. C. MacDonald, and J. N. Kirk, 1968, "The Potential of Radar in Geological Exploration," Proc. 5th Symp. Remote Sensing of Environment (April 1968), University of Michigan, Ann Arbor, pp. 747-763.

Ellermeier, R. D. and D. S. Simonett, 1965, "Imaging Radars on Spacecraft as a Tool for Studying the Earth," Proc. of Symp. on Electromagnetic Sensing of the Earth from Satellites (November 1965), Miami Beach, Florida, pp. L1-L20.

_____, A. K. Fung, and D. S. Simonett, 1966, "Some Empirical and Theoretical Interpretation of Multiple Polarization Radar Data," Proc. 4th Symp. Remote Sensing of Environment, University of Michigan, Ann Arbor, pp. 657-670.

Feder, A. M., 1957, "The Application of Radar in Geologic Exploration," Bell Aircraft Corp. Rept., Buffalo, New York.

_____, 1960, "Radar Geology," Unpublished Masters Thesis, University of Buffalo, Buffalo, New York.

Fischer, W., 1963, "An Application of Radar to Geological Interpretation," Proc. 1st Symp. Remote Sensing of Environment, (February 1962), University of Michigan, Ann Arbor, pp. 83-84.

Goodyear Aircraft Corp., 1959, "Measurements of Terrain Backscattering Coefficient with an Airborne X-Band Radar," Goodyear Aircraft Corp. Radar Terrain Return Study Final Report, GERA-463, 73 pp.

Hackman, R. J., 1966, "Geologic Evaluation of Radar Imagery in Southern Utah," U. S. Geological Survey Prof. Paper 527-D, pp. D135-D142.

_____, 1967, "Time, Shadows, Terrain, and Photointerpretation," U. S. Geological Survey Prof. Paper 575-B, pp. B155-B160.

Howe, E., 1908, "The Geology of the Isthmus of Panama," Am. Journal Sci. 4th Ser., vol. 26, pp. 212-237.

Innes, R. B., 1968, "An Interpreter's Perspective on Modern Airborne-Radar Imagery," Proc. 5th Symp. Remote Sensing of Environment, (April 1968), University of Michigan, Ann Arbor, pp. 107-122.

Interoceanic Canal Study Commission, 1968, "Geology," Final Report, Route 17, vol. I, Field Director, Office Interoceanic Canal Studies, Panama, 32 pp.

Johnson, R. B., 1968, "Geology of the Igneous Rocks of the Spanish Peaks Region, Colorado," U. S. Geological Survey Prof. Paper 594-G, 47 pp.

Kirk, J. N. and R. L. Walters, 1968, "Preliminary Report on Radar Lineaments in the Boston Mountains of Arkansas," Compass of Sigma Gamma Epsilon, vol. 45, no. 2, pp. 122-127.

_____, L. F. Dellwig, and L. F. Jefferis, 1968, "The Influence of Radar Look-Direction on the Recording of Geologic Lineaments -- A Study in the Boston Mountains, Arkansas," Unpublished manuscript, University of Kansas, Lawrence, 10 pp.

Klauder, J. R., A. C. Price, S. Darlington, and W. J. Albersheim, 1960, "The Theory and Design of Chirp Radars," Bell Systems Tech. J., vol. 39, pp. 745-808.

La Prade, G. L. and E. S. Leonardo, 1968, "Elevation Measurements from Radar Imagery," Papers from 34th Annual Meeting Amer. Soc. Photogrammetry (March 1968), pp. 153-164.

Lattman, L. H., 1958, "Technique of Mapping Geologic Fracture Traces and Lineaments on Aerial Photographs," Photogramm. Engr., vol. 24, no. 4, pp. 568-576.

Levine, D., 1960, Radargrammetry, McGraw-Hill Book Company, Inc., New York, 330 pp.

_____, C. Colbert, L. C. Graham, P. Crane, and B. B. Scheps, 1966, "Combinations of Photogrammetric and Radargrammetric Techniques," Manual of Photogrammetry, Published by Amer. Soc. Photogrammetry (3rd Edition) Banta Publ. Co., Menasha, Wisconsin, pp. 1003-1048.

Lloyd, J. J., 1963, "Tectonic History of the South Central-American Orogen," Amer. Assoc. Petroleum Geologists Memoir #2, pp. 88-100.

Lueder, D. R., 1959, "Gray Tones" in: Aerial Photographic Interpretation, McGraw-Hill Book Company, Inc., New York, pp. 76-101.

Lundien, J. R., 1965, "Terrain Analysis by Electromagnetic Means," U. S. Army Waterways Exp. Sta., Unpublished Report.

MacDonald, H. C., P. A. Brennan, and L. F. Dellwig, 1967, "Geologic Evaluation by Radar of NASA Sedimentary Test Site," IEEE Trans. Geoscience Electronics, vol. GE-5, no. 3, pp. 72-78.

McCoy, R. M., 1967, "An Evaluation of Radar Imagery as a Tool for Drainage Basin Analysis," University of Kansas, Lawrence, CRES report 61-31, 102 pp.

Miller, V. C., 1961, "Identification and Interpretation," in: Photogeology, McGraw-Hill Book Company, Inc., pp. 80-100.

Moore, R. K., 1966, "Radar as a Sensor," University of Kansas, Lawrence, CRES Report no. 61-7, 55 pp.

_____, and D. S. Simonett, 1967, "Radar Remote Sensing in Biology," Bioscience, vol. 17, pp. 384-390.

Nims, A. A., 1968, "All-weather Mapping by Radar," Westinghouse Engineer (May 1968), West. Elec. Corp., Baltimore, Maryland, 6 pp.

Nygren, W. E., 1950, "Bolivar Geosyncline of Northwestern South America," Amer. Assoc. Petroleum Geologists Bull., vol. 34, pp. 1998-2006.

Olsson, A. A., 1932, "Contributions to Tertiary Paleontology of Northern Peru, The Peruvian Miocene," Bull. Amer. Paleon., vol. 19, no. 68.

_____, 1942a, "Tertiary Deposits of Northwestern South America and Panama," Proc. 8th American Scientific Congress, Washington, 1940, vol. 4, Geological Sciences, pp. 231-287.

_____, 1942b, "Some Tectonic Interpretations of the Geology of Northwestern South America," Proc. 8th American Scientific Congress, Washington, 1940, vol. 4, Geological Sciences, pp. 401-416.

_____, 1956, "Handbook on South American Geology," GSA Memoir 65, pp. 295-325.

Oppenheim, V., 1950, "The Structure of Ecuador," Amer. J. Sci., vol. 248, pp. 527-539.

_____, 1952, "The Structure of Colombia," Trans. Amer. Geophys. Union, vol. 33, no. 5, pp. 739-748.

Pierson, W. J., B. B. Scheps, and D. S. Simonett, 1965, "Some Applications of Radar Return Data to the Study of Terrestrial and Oceanic Phenomena," Proc. 3rd Goddard Memorial Symp. on Scientific Experiments for Manned Orbital Flight (March 1965), Washington, D. C., pp. 87-137.

Ray, R. G., 1960, "Aerial Photographs in Geologic Interpretation and Mapping," U. S. Geological Survey Prof. Paper 373, 230 pp.

Roberts, R. J. and E. M. Irving, 1957, "Mineral Deposits of Central America," U.S. Geological Survey Bull. 1034, 205 pp.

Rouse, J. W., Jr., W. P. Waite, and R. L. Walters, 1966, "Use of Orbital Radars for Geoscience Investigations," Proc. 3rd Space Congress, Canaveral Council of Technical Societies, pp. 77-94.

_____, H. C. MacDonald, and W. P. Waite, (in press), "Geoscience Application of Radar Sensors," IEEE Trans. Geoscience Electronics, vol. GE-7, no. 1, January 1969.

Rubinoff, I., 1968, "Central American Sea-Level Canal-Possible Biological Effects," Science, vol. 161, pp. 857-861.

Rydstrom, H. O., 1961, "Geologic Map of an Area in Southeastern Arizona Prepared from Radar Photography," Goodyear Aerospace Corp. Rept. AAP-13730, 6 pp.

Sapper, K., 1937, "Mittelamerika, Handbach der Regionalen Geologie," vol. 8, pt. 4a, Carl Winter, Heidelberg, 160 pp.

Scheps, B. B., 1960, "To Measure is to Know - Geometric Fidelity and Interpretation in Radar Mapping," Photogrammetric Engineering, vol. 26, (4), pp. 637-644.

_____, 1963, "The History of Radar Geology," Proc. 1st Symp. Remote Sensing of Environment (February 1963), University of Michigan, Ann Arbor, pp. 79-81.

Schmidt, W., R. Stewart, and D. Fawcett, 1947, "Geologic Exploration Caledonia Bay Route 10, Geology and Topography," The Panama Canal Isthmian Canal Studies, Memo. 186, Balboa Heights, Canal Zone, 10 pp.

Schuchert, C., 1935, "Historical Geology of the Antillean-Caribbean Region," John Wiley and Sons, Inc. New York, 811 pp.

Shelton, B. J., 1952, "Geology and Petroleum Prospects of Darien, Southeastern Panama," Unpublished Master's Thesis, Oregon State University, 61 pp.

Simons, J. H. and A. D. Beccassio, 1964, "An Evaluation of Geo-Science Applications of Side-Looking Airborne Mapping Radar," Raytheon/Autometric Corp., Alexandria, Virginia, 70 pp.

_____, 1965, "Some Applications of Side-Looking Airborne Radar," Proc. 3rd Symp. Remote Sensing of Environment (October 1964), University of Michigan, Ann Arbor, pp. 563-571.

Skolnik, M. I., 1962, "Introduction to Radar Systems," McGraw-Hill Book Company, Inc., New York, N. Y.

Smith, H. P., Jr., 1948, "Mapping by Radar -- the Procedures and Possibilities of a New and Revolutionary Method of Mapping and Charting," U.S.A.F., Randolph Field, Texas.

Smith, H. T. U., 1943, Aerial Photographs and Their Interpretation, Appleton-Century-Crofts, Inc., 372 pp.

Snavely, P. D., Jr. and H. C. Wagner, 1966, "Geologic Evaluation of Radar Imagery, Oregon Coast," U.S. Geological Survey Unpublished Report, 13 pp.

Taylor, R. C., 1959, "Terrain Return Measurements at X, Ku, and Ka Bands," IRE Nat'l. Conv. Rec., pt. 1, vol. 7, pp. 19-26.

Terr[illegible], R. [illegible], 1956, "A Geological Reconnaissance of Panama," California Acad. Sci. Occasional Paper 23, 91 pp.

Walters, R. L., 1968, "Radar Bibliography for Geoscientists," University of Kansas, Lawrence, CRES Tech. Report 61-30, 28 pp.

West, R. C., 1957, "The Pacific Lowlands of Colombia, Part I. The Physical Milieu," Louisiana State University Press, Baton Rouge, 209 pp.

Westinghouse Electric Corp., 1967, "Side-Look Radar," Westinghouse Electric Corp., Aerospace Div., Baltimore, Maryland, (limited distribution) 45 pp.

Wheeler, G. J., 1967, Radar Fundamentals, Prentice-Hall, Inc., Englewood Cliffs, N. J., 105 pp.

Whitmore, F. C., Jr. and R. H. Stewart, 1965, "Miocene Mammals and Central American Seaways," Science, vol. 148, no. 3667, pp. 180-195.

Wilson, J., H. Nutall, and K. Raimond, 1964, "El Real Environmental Survey Darien Province, Republic of Panama, 1962," TRECOM Tech. Report 63-72, U.S. Army Transp. Research Command, Ft. Eustis, Virginia, 335 pp.

Woakes, E. R., 1923, "The Darien Gold Mine, Panama," Mining Magazine, vol. 29, pp. 270-278.

Wobber, F. J., 1968, "Orbital Photography -- Applied Earth Survey Tool," Photographic Applications in Science and Technology, Summer 1968, pp. 21-29.

Woodring, W. P., 1956, "Caribbean Land and Sea Through the Ages," in Handbook of South American Geology, W. F. Jenks, ed., Geol. Soc. America Mem. 65, pp. 719-732.

_____, 1957, "Geology and Paleontology of Canal Zone and Adjoining Parts of Panama," U. S. Geol. Survey Prof. Paper 306-A, 145 pp.

_____, 1958, "Panama, Outline of Stratigraphy," Lexique Stratigraphique International, vol. 5, Amerique Latine, Fasicile 2a, pp. 309-349.

Wyse, L. N. B., 1877, "L'Exploration de L'Isthme du Darien en 1876-1877," Bull. de la Societe de Geographie, 6th series, vol. 14, Paris, pp. 561-580.

PLATE I

GEOLOGICAL RECONNAISSANCE MAP - DARIEN PROVINCE, PANAMA AND NORTHWESTERN COLOMBIA

LEGEND

STRATIGRAPHIC UNITS

- Holocene
- Pliocene to Upper Miocene
- Upper Middle Miocene
- Lower Middle Miocene
- Lower Miocene
- Miocene - Oligocene (?)
- Upper Oligocene
- Middle Oligocene (?)
- Eocene (?)
- Pre-Tertiary (?)

CONTACTS

- Contact inferred from radar
- Contact inferred from corroborative data
- Contact cannot be determined from radar, no corroborative data available

JOINT SYSTEMS

- Joint systems inferred from radar (dip cannot be determined)

DIP AND STRIKE

- Measured from radar imagery
- 0 - 30° dip - estimated from imagery
- 30° - 60° dip - estimated from imagery
- 60° - 90° dip - estimated from imagery

FAULTS

- Normal fault inferred from radar
- Fault inferred from corroborative data
- High-angle reverse fault, fault trace inferred from radar, movement from corroborative data
- Fault trace inferred from radar, movement cannot be determined
- Strike-slip fault, movement inferred from radar

STRUCTURE

- Anticline inferred from radar
- Syncline inferred from radar
- Anticline from corroborative data
- Syncline from corroborative data